**Title**
Clinical Application of a Novel Three-Dimensional Analysis to Evaluate Temporomandibular Joint Space Changes After Orthognathic Surgery



**Author**
Ikeda, Renie

**Publication Date**
2014

Peer reviewed|Thesis/dissertation

**Clinical Application of a Novel Three-Dimensional Analysis to Evaluate Temporomandibular Joint Space Changes After Orthognathic Surgery**

by

Renie Ikeda, DDS

THESIS

Submitted in partial satisfaction of the requirements for the degree of

MASTER OF SCIENCE

in

Oral and Craniofacial Sciences

in the

GRADUATE DIVISION

of the

[redacted]

## DEDICATION

This thesis is dedicated to my parents, Kazumi and Isayo Ikeda, who have been an incredible source of support throughout my educational career. You have always believed in me and given me the opportunity to strive to become the best that I can be. You are my source of inspiration, and I would not be here today without you. Domo Arigato.

## ACKNOWLEDGEMENTS

I would like to acknowledge the key individuals involved with this project for their invaluable help and support. I wish to thank my committee members who made this project possible. A special thanks to Dr. David Hatcher, who has played a vital role in the development of this project with his innovative vision combined with his expertise in imaging technology. Thank you Dr. Art Miller for being a consistent source of positive encouragement and donating your precious time to work through this ambitious project with me. Dr. Snehlata Oberoi has also offered much support throughout the project and my residency. I would also like to thank Dr. Charles McNeill, who has been my mentor over the last seven years. In addition, I would like to express my appreciation to Dr. David Wiley and Christian Woodhouse for their generous technical support, Dr. Lissa Tallman for her valuable advice and guidance, and Wint Wint Tun for her hard work and important contributions to this project. Finally, I would like to thank my co-residents, Dr. Daniel Hardy, Dr. Seth Lucas, Dr. Emerald Nguyen and Dr. Sachee Parikh for unforgettable seven years together and for helping to keep my sanity during the difficult moments and for sharing many of the happiest memories.

## ABSTRACT

**Introduction:** Positional and morphological changes of the condyles and subsequent changes in the temporomandibular joint (TMJ) space are often observed following orthognathic surgery. The purpose of this study was to present and validate a novel semi-automated method for three-dimensional evaluation of the TMJ space using cone-beam computed tomographic (CBCT) data and clinically apply this method to evaluate the post-operative changes in the TMJ space in orthognathic surgery patients and compare the results to the conventional two-dimensional analysis of the CBCT multiplanar cross-sections.

**Methods:** Three-dimensional TMJ space analysis using Stratovan Checkpoint software (Stratovan Corporation, Sacramento, CA) and two-dimensional TMJ space analysis using Invivo5 software (Anatomage Inc., San Jose, CA) were repeated by an investigator to assess the analyses' reliability. The analyses were further applied to pre-operative, immediate post-operative, and follow-up CBCT scans from nine orthognathic surgery patients to evaluate the joint space change caused by positional and/or morphological changes of the TMJ.

**Results:** For three-dimensional and two-dimensional analyses, the mean intra-observer difference was small and within the clinically accepted margin of error. The two analyses gave concurring results for the majority of the joint spaces when applied to evaluate the longitudinal TMJ space change in orthognathic patients, demonstrating general increase in the joint space

immediately after surgery followed by a decrease in the measurements at follow-up. However, the three-dimensional analysis offered far more morphological information compared to the conventional two-dimensional analysis.

**Conclusions:** This novel semi-automatic method is a reliable tool for the three-dimensional analysis of the TMJ space, allowing longitudinal assessment of the joint changes after orthognathic surgery.

Keywords: three-dimensional analysis, temporomandibular joint space, condylar position, condylar morphology, CBCT, orthognathic surgery

# Table of Contents

# Table of Figures

# Index of Tables

# INTRODUCTION

Orthognathic surgery was first described in 1849 (Steinhäuser, 1996; Aziz, 2004) and has since evolved to become a standard procedure as a way to correct dentofacial disharmonies. Although surgical outcome has become more predictable over time, postsurgical relapse is still an area of major concern. One of the factors related to early skeletal relapse is iatrogenic displacement of the condyles, which is inevitable especially during mandibular surgery. Adaptive capacity of the temporomandibular joint (TMJ) may further lead to long-term change in condylar position and shape. Such postoperative changes can be physiologic as well as pathologic and demands close observation. Accurate positional and morphological assessment of the TMJ after orthognathic surgery is therefore vital to monitor the short- and long-term stability of treatment results. With the advent of cone-beam computed tomography (CBCT), three-dimensional imaging is available for accurate evaluation of condylar displacement during orthognathic surgery as well as any short- and long-term adaptive positional and morphological changes in the TMJ.

## Changes in Temporomandibular Joint Space: Condylar Position

Intraoperative and postoperative alterations in TMJ space can be attributed to two main

components: changes in condylar position and orientation within the glenoid fossa and changes in the shape and size of the condyles.

Numerous studies have reported condylar displacements and resultant alterations in TMJ space both during (Marmulla *et al*., 2007) and shortly after orthognathic surgeries (Alder *et al*., 1999; Angle *et al.*, 2007; Baek *et al.*, 2006; Chen *et al.*, 2013; Ghang *et al.*, 2012; Harris *et al*., 1999; Hwang *et al.*, 2000; Kang *et al.*, 2010; Katsumata *et al.*, 2006; Kawamata *et al*., 1998; Kim *et al.*, 2010; Kim *et al*., 2011; Kim *et al*., 2012; Lee *et al*., 2002; Ueki *et al.*, 2005; Ueki *et al.*, 2012). Contributing factors may include the surgeon's experience, the direction and amount of movement of the distal segment of the mandible, anatomic shape and orientation of the proximal segment, and the fixation method of the osseous segments (Baek *et al.*, 2006; Harris *et al*., 1999; Hwang *et al.*, 2000; Joss *et al.*, 2009; Kang *et al.*, 2010; Lee *et al.*, 2002; Stroster *et al.*, 1994; Van Sickels *et al.*, 1999).

During the early postoperative period, condyle position and joint space may change as a result of short-term adaptive changes such as condyle seating, where iatrogenically displaced condyle reseats within the glenoid fossa (Arnett, 1993; Chen *et al.*, 2013; Kersey *et al*., 2003). Kim *et al.* reported that condylar position within the glenoid fossa moved from its relatively anterior position to a concentric position post-operatively, but tended to return slightly toward the original position (Kim *et al.*, 2010; Kim *et al.*, 2011). Such short-term condylar positional

change can contribute to early skeletal relapse of orthognathic surgery, often manifested as an anterior open bite, increased overjet, and Class II malocclusion within the first few months of the postoperative period (Reyneke *et al*., 2002; Figure 1).

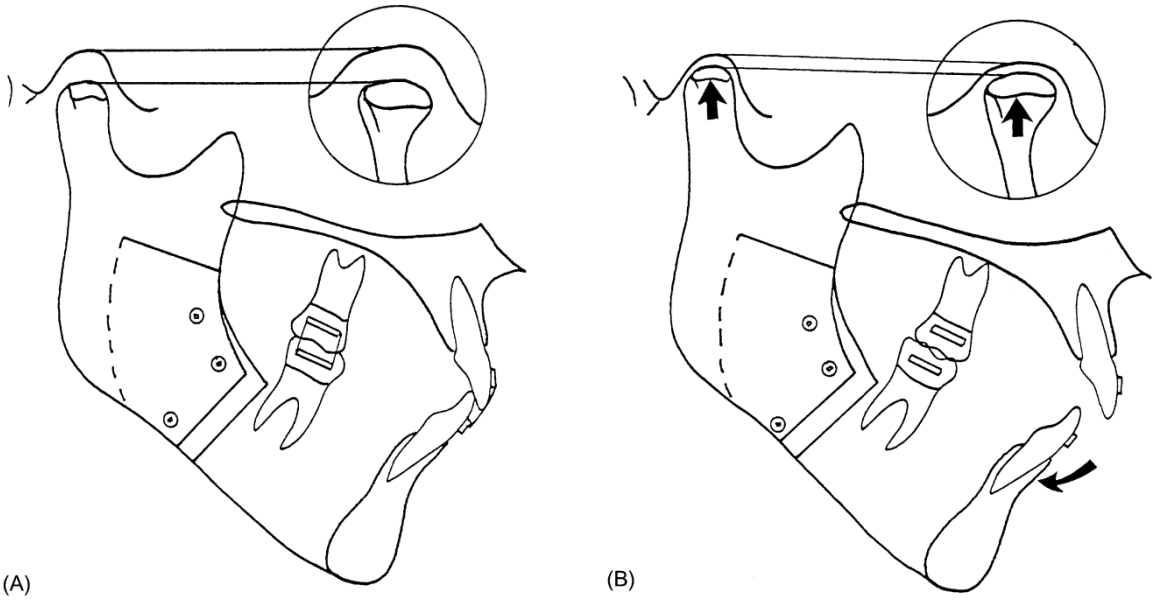


**Figure 1.** An example of early skeletal relapse. (A) The condyle is inferiorly displaced during surgery. (B) After removal of inter-maxillary fixation, condyle seating leads to early skeletal relapse. (From Reyneke *et al.*, 2002)

However, skeletal relapse could occur gradually over time in the late postoperative period, and this may result from the combination of altered condylar morphology and continual condylar position change.

**Changes in Temporomandibular Joint Space: Condylar morphology**

Life-long capacity of TMJs to undergo remodeling has been well-documented. Following orthognathic surgery, shapes of the condyles may be gradually altered due to

physiologic remodeling as a way to adapt to the altered mechanical loading and condylar displacement and contribute to late skeletal relapse more than several months after the surgery (Arnett, 1993; Borstlap *et al.*, 2004; Cutbirth *et al.*, 1998; Ellis *et al.*, 1991; Hwang *et al.*, 2000; Katsumata *et al.*, 2006; Park *et al.*, 2012). For instance, with rigid fixation of the bony segments, condyles can be torqued (rotation of the proximal segment in the axial plane), causing condylar compression against the glenoid fossa, and subsequent remodeling or resorption at the contact area can cause late skeletal relapse as the condyle continues to seat superiorly (Arnett, 1993).

However, the shape change as a result of a pathological phenomenon, such as progressive condylar resorption, can result in severe late skeletal relapse with reduced posterior face height, mandibular retrognathism, and progressive anterior open bite with clockwise rotation of the mandible (Eggensperger *et al.*, 2006; Joss *et al.*, 2009; Kobayashi *et al.*, 2013) and may necessitate re-operation (Borstlap *et al.*, 2004; Hoppenreijs *et al.*, 1998; Hoppenreijs *et al.*, 1999; Huang *et al.*, 1997). Although the etiology and pathogenesis of progressive condylar resorption is not completely clear, some studies suggest that overloading of the condyle either at surgery or, thereafter, is a causative factor (Cutbirth *et al.*, 1998; Ellis *et al.*, 1991). Huang *et al.* evaluated different surgical treatment modalities for patients with progressive condylar resorption and observed that patients treated by a combination of maxillary impaction and

mandibular advancement are more likely to experience further condylar resorption compared to those treated with maxillary impaction alone (Huang *et al.*, 1997). Hoppenreijs *et al*. confirmed this finding in a study with a large sample size (Hoppenreijs *et al*., 1998), and few studies have identified surgical factors that may contribute to post-operative condylar resorption (Hwang *et al.*, 2000).

On the other hand, functional positive remodeling may also occur after orthognathic surgery, perhaps due to a more balanced mechanical loading on the affected condyle after surgical correction of skeletal discrepancy. You *et al*. reported a case of a female patient who, prior to orthognathic surgery, had a unilateral condylar resorption, but gradually showed positive remodeling one to three years after the surgery (You *et al*., 2011).

**Imaging Modalities for Evaluation of the Temporomandibular Joint**

Different radiographic techniques have been used to visualize the TMJ including linear tomography (Cortez *et al.*, 2007; Huang *et al.*, 1997), two-dimensional radiographs such as panoramic radiography (Borstlap *et al.*, 2004; Cutbirth *et al.*, 1998; Hoppenreijis *et al.*, 1998; Hoppenreijis *et al.*, 1999; Hwang *et al.*, 2000; Wohlwender *et al.*, 2011; You *et al.*, 2011), submentovertex radiography (Cortez *et al.*, 2007), lateral and/or antero-posterior cephalometric radiography (Angle *et al.*, 2007; Cortez *et al.*, 2007; Eggensperger *et al.*, 2006; Ellis *et al.*, 1991;

Katsumata *et al.*, 2006; Ueki *et al.*, 2005; Ueki *et al.*, 2007), magnetic resonance imaging (MRI) (Katsumata *et al.*, 2006; Ueki *et al.*, 2007), and computed tomography (CT) (Alder *et al.*, 1999; Harris *et al.*, 1999; Kang *et al.*, 2010; Katsumata *et al.*, 2006; Kawamata *et al.*, 1998; Lee *et al.*, 2002; Ueki *et al., 2012*).

Conventional two-dimensional radiographs present major drawbacks in assessment of condylar position and morphology due to overlapping anatomic structures and inherent distortion in two-dimensional imaging of a three-dimensional structure, as well as magnification error (Barghan *et al.*, 2012). Furthermore, with conventional radiography and tomography, it is difficult to reproduce the x-ray beam projection for follow-up radiography (Athanasiou *et al.*, 1991), which is crucial for long-term evaluation of the TMJ. Condylar position changes should be analyzed in three-dimensions, and in order to achieve this using conventional radiographs, multiple views are required, such as combining submentovertex radiographs and axially corrected sagittal and coronal tomography (Honey *et al.*, 2007; Kersey *et al.*, 2003). CT provides far superior imaging of the hard tissues of the TMJ (Katsumata *et al.*, 2006), and a single imaging sequence provides the necessary information, but the increased radiation exposure and high cost have limited its application (Barghan *et al.*, 2012; Kersey *et al.*, 2003; Schulze *et al.*, 2004; Tsiklakis *et al.*, 2004). While MRI provides images of both soft and hard

tissues without exposing patients to radiation, high cost as well as long scanning time makes it less accessible (Tsiklakis *et al.*, 2004).

The emergence of CBCT has overcome many shortcomings of the aforementioned imaging techniques. Hilgers *et al*. found CBCT images to be highly accurate compared with direct anatomic measurements, whereas measurements made using conventional radiographs were significantly greater than the anatomic truth (Hilgers *et al.*, 2005). Similar finding was reported by Honey *et al*. when comparing diagnostic accuracy of CBCT compared with that of panoramic film and linear tomograms for detection of simulated condylar defects (Honey *et al.*, 2007). CBCT provides accurate three-dimensional imaging of the TMJ using lower radiation dose and at lower cost compared to conventional CT (Barghan *et al.*, 2012; Hilgers *et al.*, 2005; Honda *et al.*, 2001; Hussain *et al.*, 2008; Schulze *et al.*, 2004; Tsiklakis *et al.*, 2004; Zain-Alabdeen *et al.*, 2012). Hence, CBCT has been used extensively as the method of choice to evaluate changes in condylar position and morphology (Kim *et al.*, 2011; Tsiklakis *et al.*, 2004; Zhang *et al.*, 2012).

**Three-Dimensional Temporomandibular Joint Analysis Using CBCT Data**

Although three-dimensional data is readily available with the advent of CBCT, perhaps the most common method of TMJ analysis using CBCT data at the present is to make linear and

angular measurements in the multiplanar cross-sections of the joint (Barghan *et al.*, 2012; Chen *et al.*, 2013; Hilgers *et al.*, 2005; Honda *et al.*, 2001; Ikeda *et al.*, 2009; Ikeda *et al.*, 2011; Kim *et al.*, 2010; Kim *et al.*, 2011; Tsiklakis *et al.*, 2004). This approach, though proven accurate, fails to take full advantage of the CBCT data as it converts the three-dimensional data into a series of two-dimensional cross-sectional images.

Recently, superimpositions of reconstructed images from CBCT data combined with color-mapping techniques have enabled three-dimensional visualization of the skeletal changes after orthognathic surgery, and this technique has been applied to monitor condylar position change (Cevidanes *et al.*, 2007; Ghang *et al.*, 2012; Kim *et al.*, 2012; Motta *et al.*, 2011). Similar method has been used to quantify the amount of resorption in TMJ osteoarthritis (Cevidanes *et al.*, 2010; Paniagua *et al.*, 2011). Other studies have taken an alternative approach and focused on the condylar volume (Tecco *et al.*, 2010; Xi *et al.*, 2013). However, currently there are no methods that allow three-dimensional evaluation of the glenoid fossa and the condyle together as an anatomic unit to determine the relationship between the osseous components of the TMJ.

## PURPOSE

The purpose of this study is to present and validate a novel semi-automated method for three-dimensional evaluation of the TMJ space using CBCT data and apply this method to evaluate the post-operative changes in the TMJ space in orthognathic surgery patients and compare the results to the conventional two-dimensional analysis of the CBCT multiplanar cross-sections.

## SPECIFIC AIMS

1. Introduce the novel semi-automated three-dimensional analysis of the TMJ space using CBCT data and determine its intra-operator reliability.
2. Determine the intra-operator reliability of the two-dimensional analysis of the TMJ space using CBCT multi-planar cross-sections.
3. Apply the two- and three-dimensional analyses to evaluate the immediate and long-term post-operative changes in the TMJ space in patients that underwent orthognathic surgeries.
4. Compare the measurements obtained from three-dimensional analysis to those obtained from the two-dimensional analysis.

## HYPOTHESES

1. The semi-automated three-dimensional analysis of the TMJ space accurately detects spatial and morphological changes in the TMJ and demonstrates high intra-observer reliability.
2. The conventional two-dimensional analysis of the TMJ space using cross-sections demonstrates high intra-observer reliability.
3. The two- and three-dimensional analyses can both be used to evaluate the immediate and long-term post-operative changes in the TMJ space in patients that underwent various orthognathic surgeries.
4. The three-dimensional analysis of the TMJ space offers more information compared to the conventional two-dimensional approach.

# MATERIALS AND METHODS

## Subjects

CBCT images of nine patients (2 males and 7 females between 16.9 years and 52.8 years of age, with an average age of 30.7 years at the time of surgery) were retrospectively selected based on the following selection criteria:

Inclusion criteria:

1. Patients who underwent two-jaw orthognathic surgery in conjunction with orthodontic treatment.
2. CBCT scans were taken on each patient by the same radiographic technician using the same scanner under the same settings and techniques.
3. Scans were available from three time points (pre-operative, immediate post-operative, and follow-up).

Exclusion criteria:

1. Patients whose CBCT scans were not taken in habitual maximum intercuspation with condyle(s) visibly out of the fossa(e).
2. Patients with existing TMJ degenerative conditions and other pathologic joint disease.

**CBCT Imaging**

All scans were taken using the i-CAT Cone Beam 3D Imaging System (Imaging Sciences International Inc., Hatfield, PA) with the subject in an upright sitting position with the patients' Frankfort horizontal plane parallel to the floor (Figure 2).


**Figure 2.** The i-CAT Cone Beam 3D Imaging System.

The scanning settings for the CBCT machine were as follows: 13x13-cm field of view or extended 16x16-cm field of view when a patient's craniofacial structures including Nasion and Menton could not be captured using the smaller field of view, 120-kVp tube voltage, 18.45 to 47.74-mA tube current, and 20-second scan time for 13x13-cm field of view scans and

40-second scan time for 16x16-xm field of view scans. Scans were taken at three time points: pre-operative (T1: 2.8 weeks before surgery on average, SD 0.81 weeks), immediate post-operative (T2: 8.1 days after surgery on average, SD 4.2 days) to assess changes related to surgery, and follow-up (T3: 17.8 months after surgery on average, SD 6.5 months) to assess long-term adaptive changes. Data from the CBCT were exported in DICOM format.

**Semi-automated Three-dimensional Temporomandibular Joint Space Analysis**

Stratovan Checkpoint software (Stratovan Corporation, Sacramento, CA) was used for three-dimensional TMJ space analysis, following a step-by-step protocol as outlined below.

Step 1: Isolation of Region of Interest

Import DICOM data of the patient's head scan (Figure 3). Under the "Volume" tab, crop the right and left condyle-fossa units using the cropping tool  by dragging the cropping lines, which appear as blue dashed lines in each slice window. Hovering over a cropping line with the mouse will highlight it in yellow (Figure 4). Once all crop lines are positioned, save the cropped volume under the "Export" tab (Figure 5).

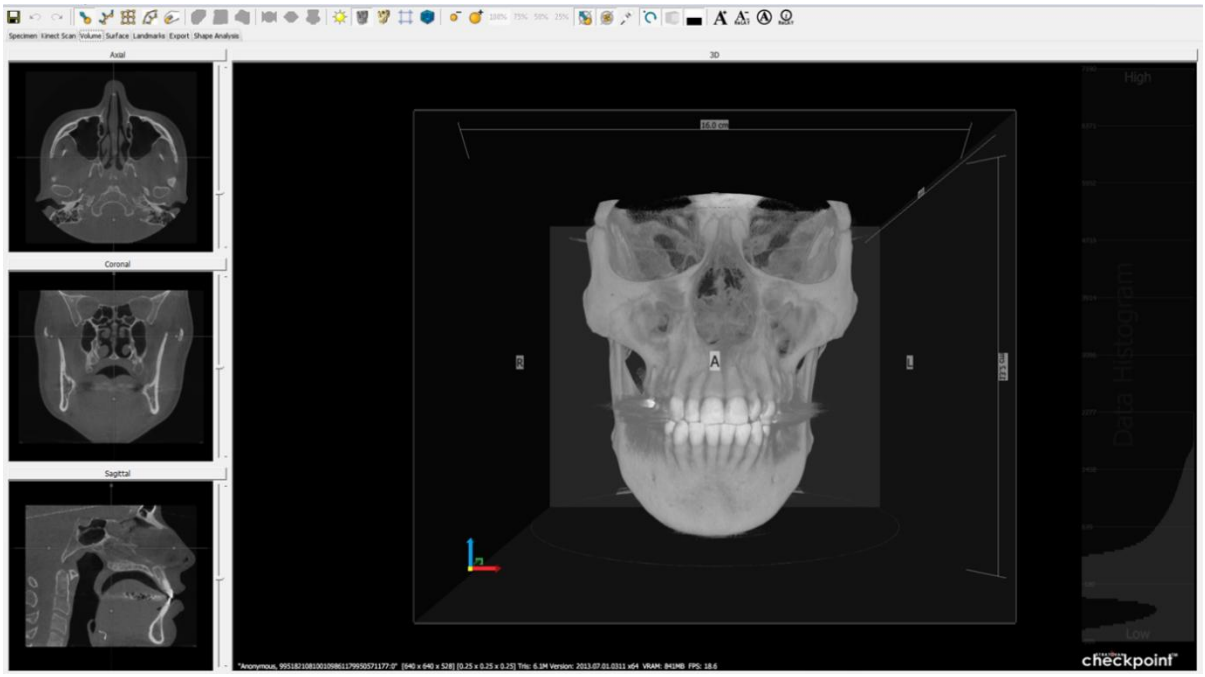


**Figure 3.** Loaded head scan on Stratovan Checkpoint software.

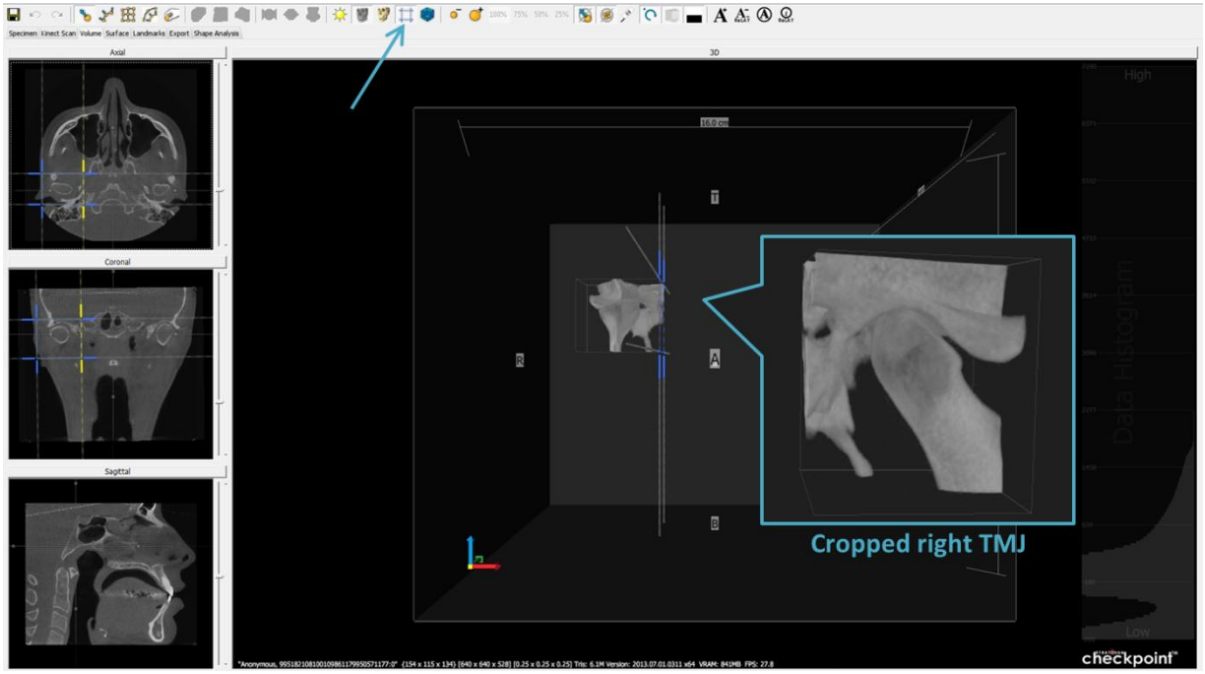


**Figure 4.** Cropped volume isolating the condyle and the fossa.

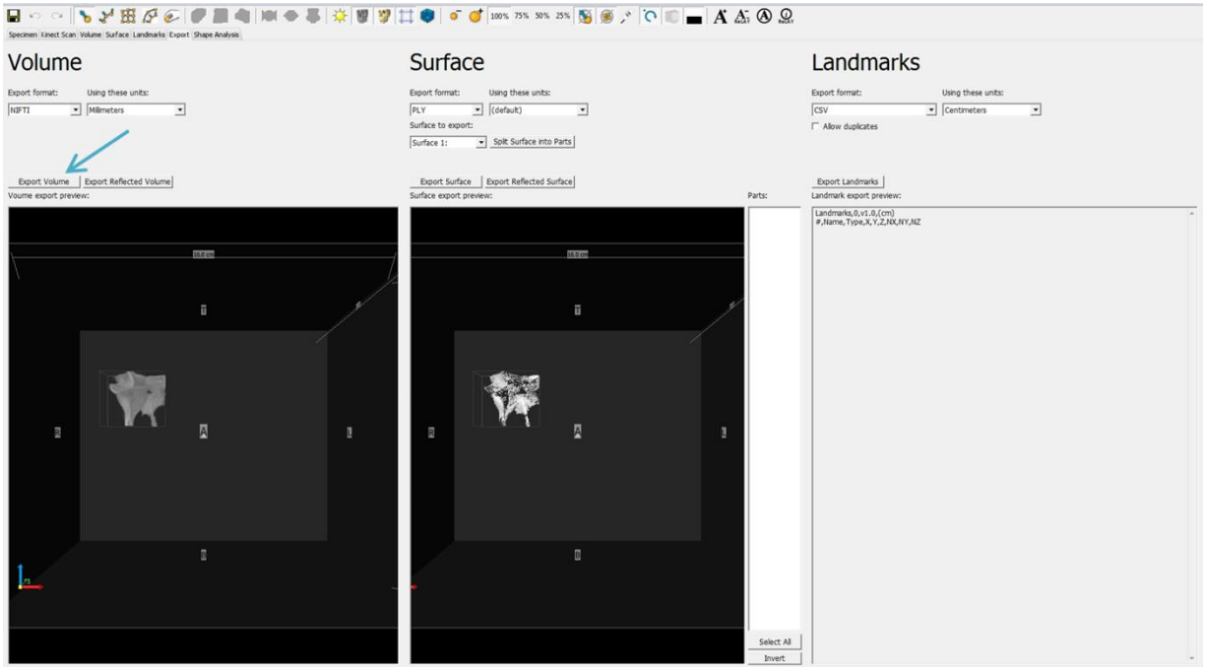


**Figure 5.** Export option for the cropped condyle-fossa unit.

Step 2: Adjustment of Contrast, Brightness, and Isovalue

Load the cropped condyle-fossa unit, and under the "Volume" tab, change the contrast and brightness of the scan by left-clicking and dragging in any of the slice windows up-and-down and left-and-right until the bony structures are well-visualized (Figure 6). Under the "Surface" tab, select a new isovalue on the data histogram on the right side of the 3D window. Hold the Ctrl key and left click to re-compute the isosurface. Select an isosurface—seen in 3D view and as a red outline in the slice windows—that best represents the cortical outlines of the condyle and fossa (Figure 7).

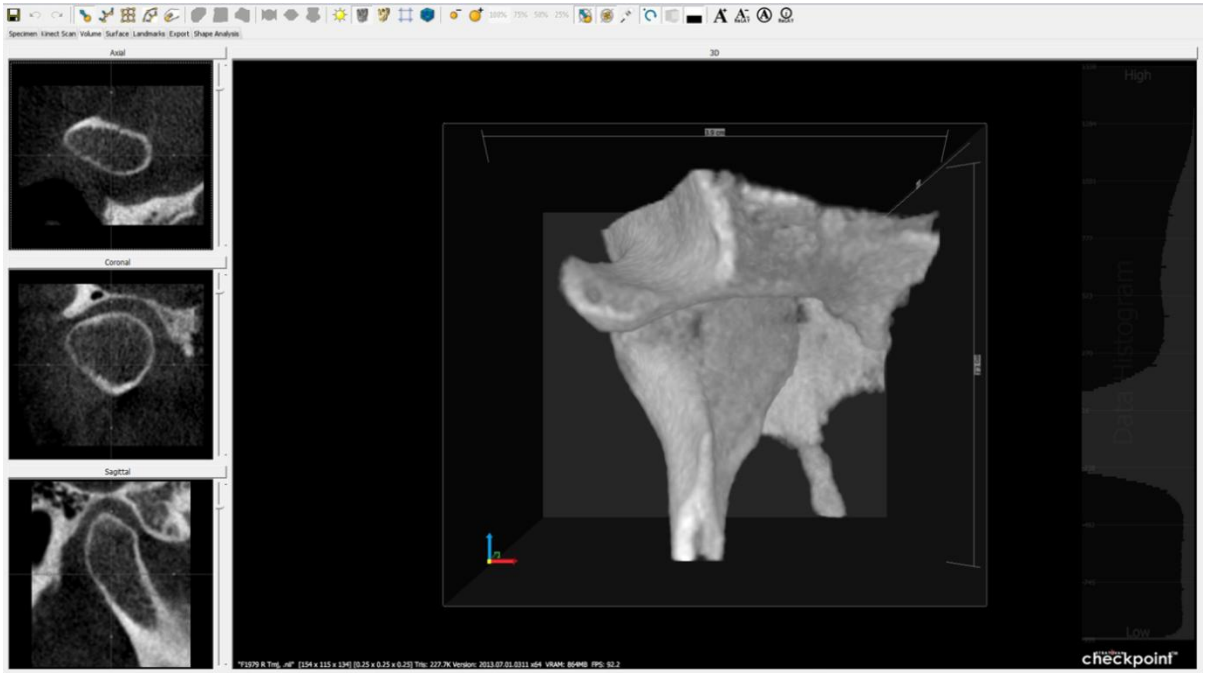


**Figure 6.** Optimized image contrast and brightness on cropped TMJ volume.

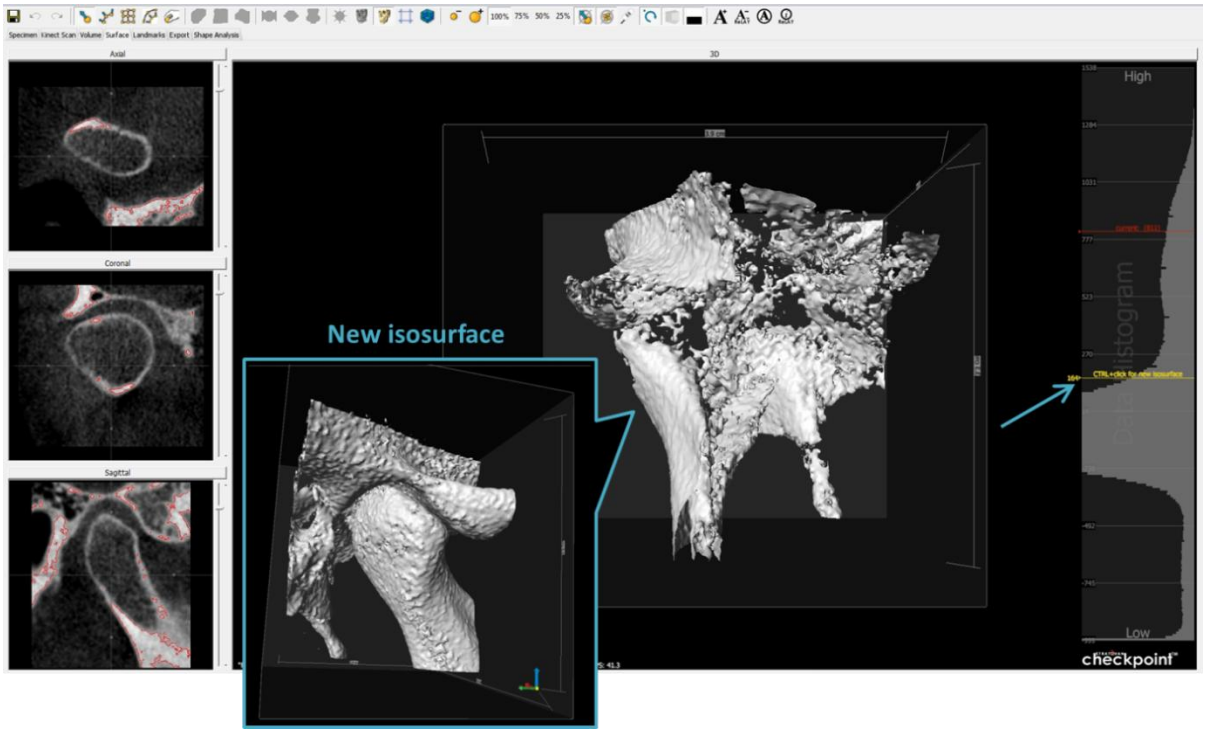


**Figure 7.** Adjusted isovalue to visualize the cortical outlines of articular surfaces.

Step 3: Orientation of TMJ Volume

Under the "Volume" tab, orient the TMJ volume by moving the avatar in the coronal slice where the condyle is widest medio-laterally and by left-clicking and dragging over the slice rotation handles (yellow squares) such that in the axial view, the horizontal line of the avatar equals the long axis of the condyle (Figure 8).

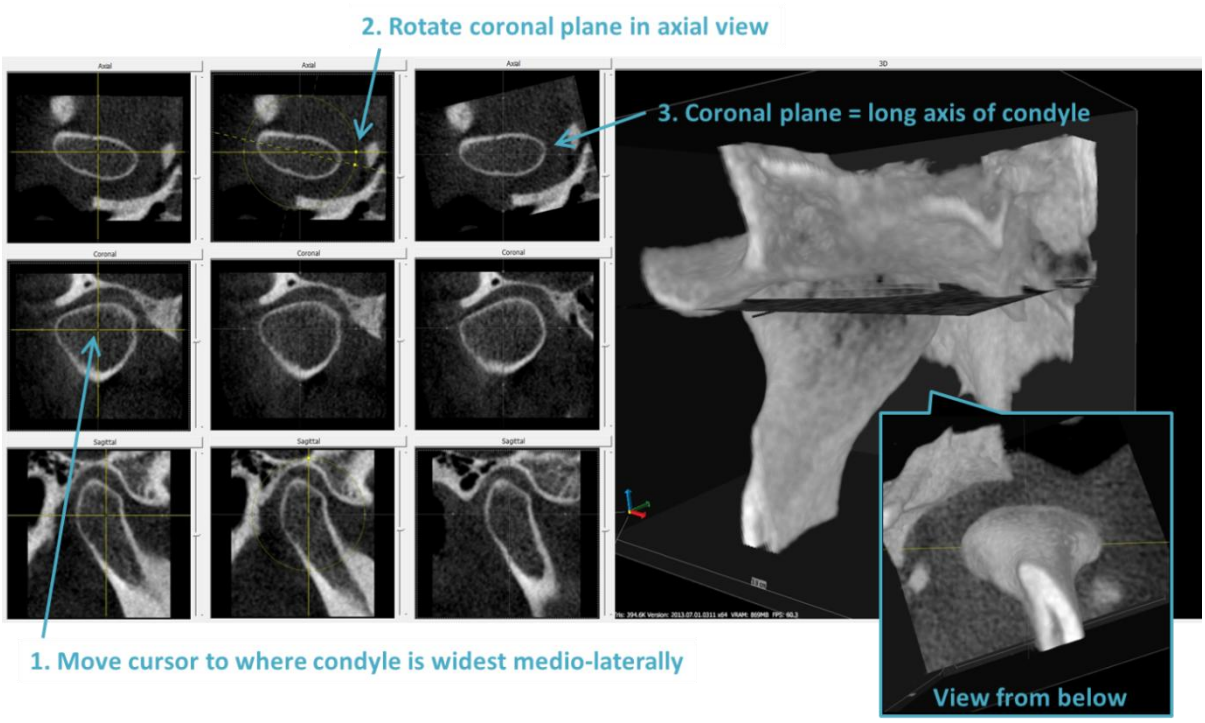


**Figure 8.** Oriented TMJ along the long axis of the condyle.

Step 4: Control Landmarks and Placement

Select the joint tool  and hold the Shift key and left click on the posterior surface of the condyle to add the joint primitive (Figure 9). Joint primitive contains three control landmarks that act as "anchor points" that must be manually placed on the volume

rendering of the condyle. The yellow point is moved to the lateral pole of the condyle, and the sagittal plane can be used to assist in identifying the most prominent lateral contour of the condyle (Figure 10, Table 1). The red point is moved to the medial pole of the condyle, and the sagittal plane can similarly be used to confirm the most prominent medial contour of the condyle (Figure 11, Table 1). The white point is on the sagittal plane that is equidistant from the lateral and medial poles. To achieve this, select the "Align Avatar to Joint" option from the pop up menu and subsequently select the "Snap condyle white landmark to sagittal slice" option (Figure 12). Finally, using the sagittal slice window, white point is moved to the posterior aspect of the condyle where the cortication tapers off to an even thickness (Figure 12, Table 1).

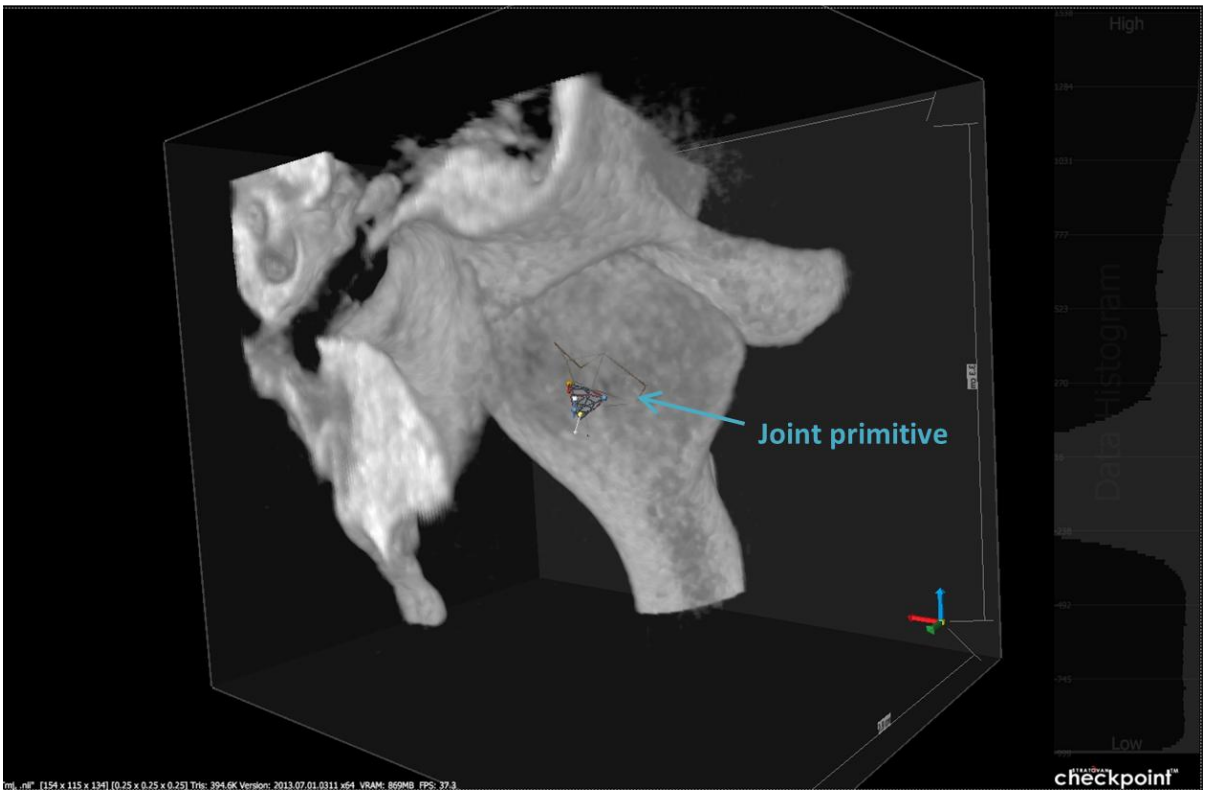


**Figure 9.** Joint primitive added to the condyle.

**Table 1.** Definition of the three condylar "anchor points."

| Anchor point | Landmark | Description |
|---|---|---|
| **Yellow** | Lateral pole | Most prominent point on the lateral contour of mandibular condyle |
| **Red** | Medial pole | Most prominent point on the medial contour of mandibular condyle |
| **White** | Posterior point | Point on the posterior contour of the condyle where the cortication tapers off to an even thickness |

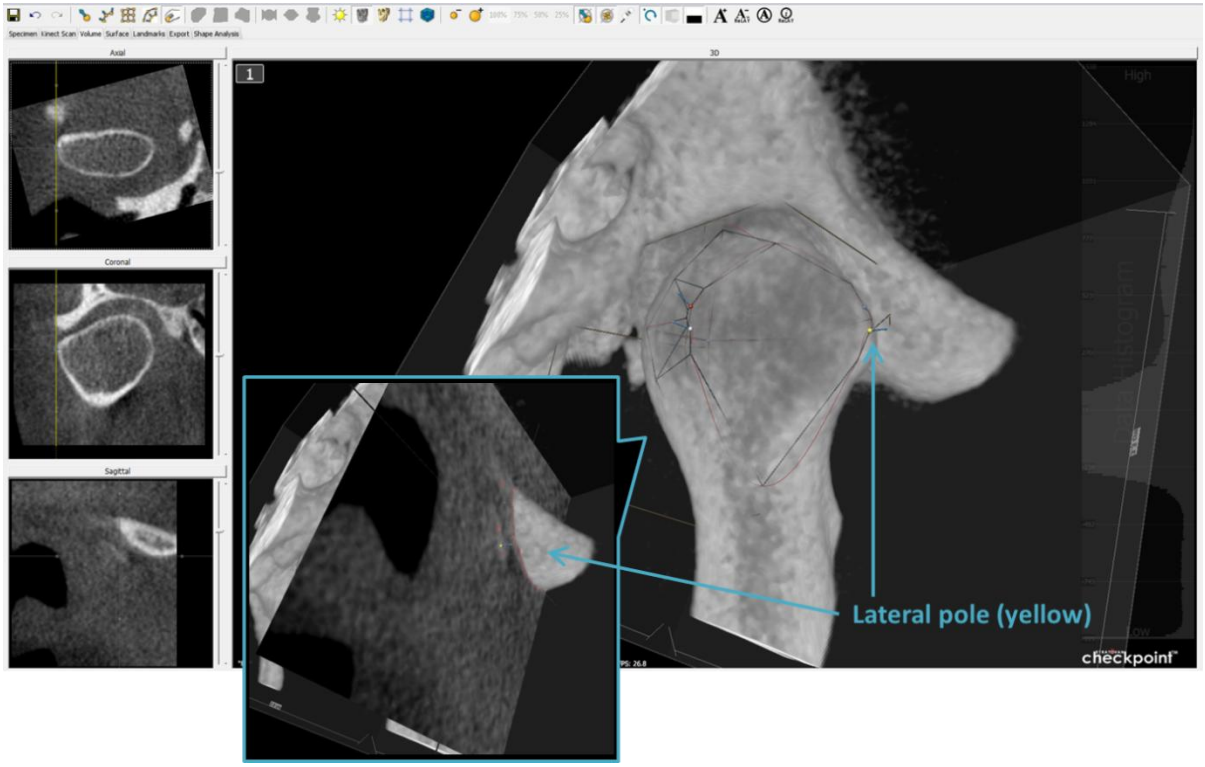


**Figure 10.** Yellow point placed on the lateral pole of the condyle.


**Figure 11.** Red point placed on the medial pole of the condyle.

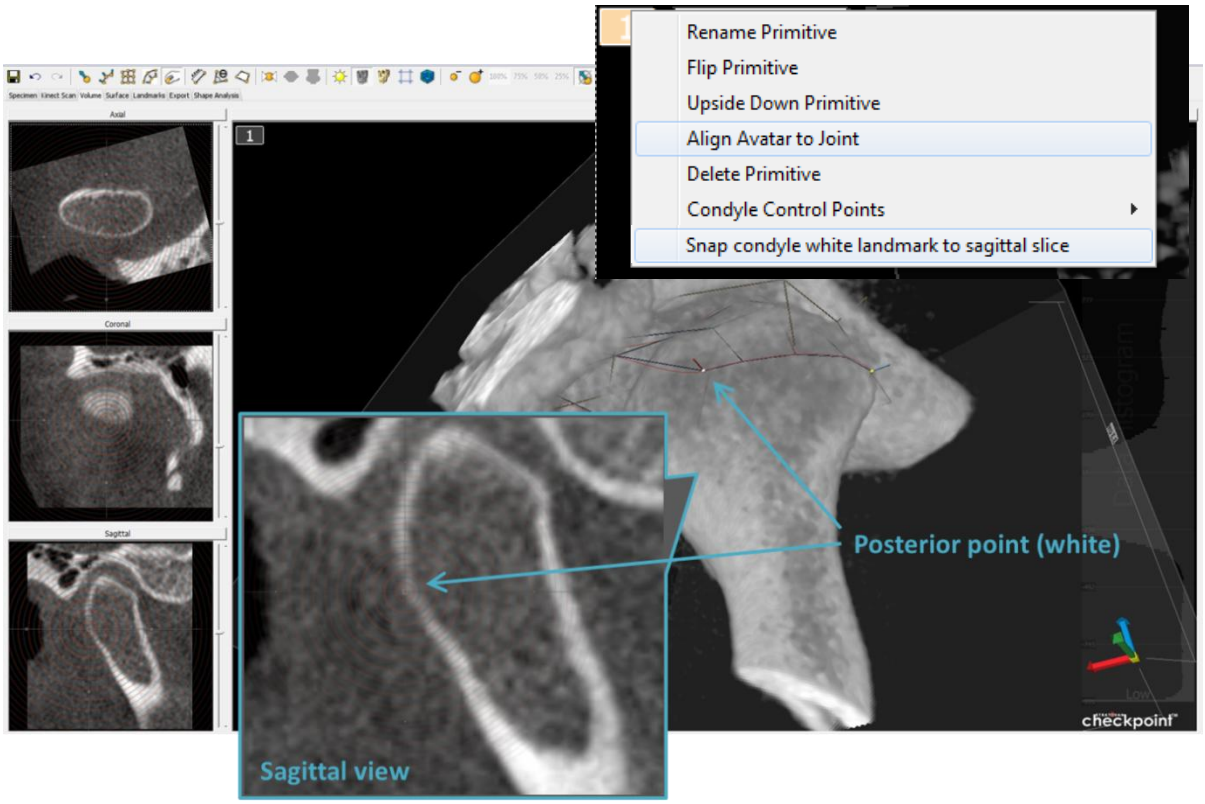


**Figure 12.** White point placed on the posterior contour of the condyle.

Step 5: Adjustment of Semi-Landmarks

The aforementioned three control points together constitute an "equator" around the condylar head and serve as the foundation for the remaining semi-landmarks. Semi-landmarks of a chosen density (5x5, 7x7, 9x9, etc.) are then automatically placed along the isosurface previously chosen in Step 2 (Figure 13). First, placement of each semi-landmark on the condyle is reviewed one by one and adjusted if needed by dragging the point in a slice window. The semi-landmark's movement is restricted to the long dotted line (Figure 14) until all of the semi-landmarks are correctly placed on the condyle (Figure 15).

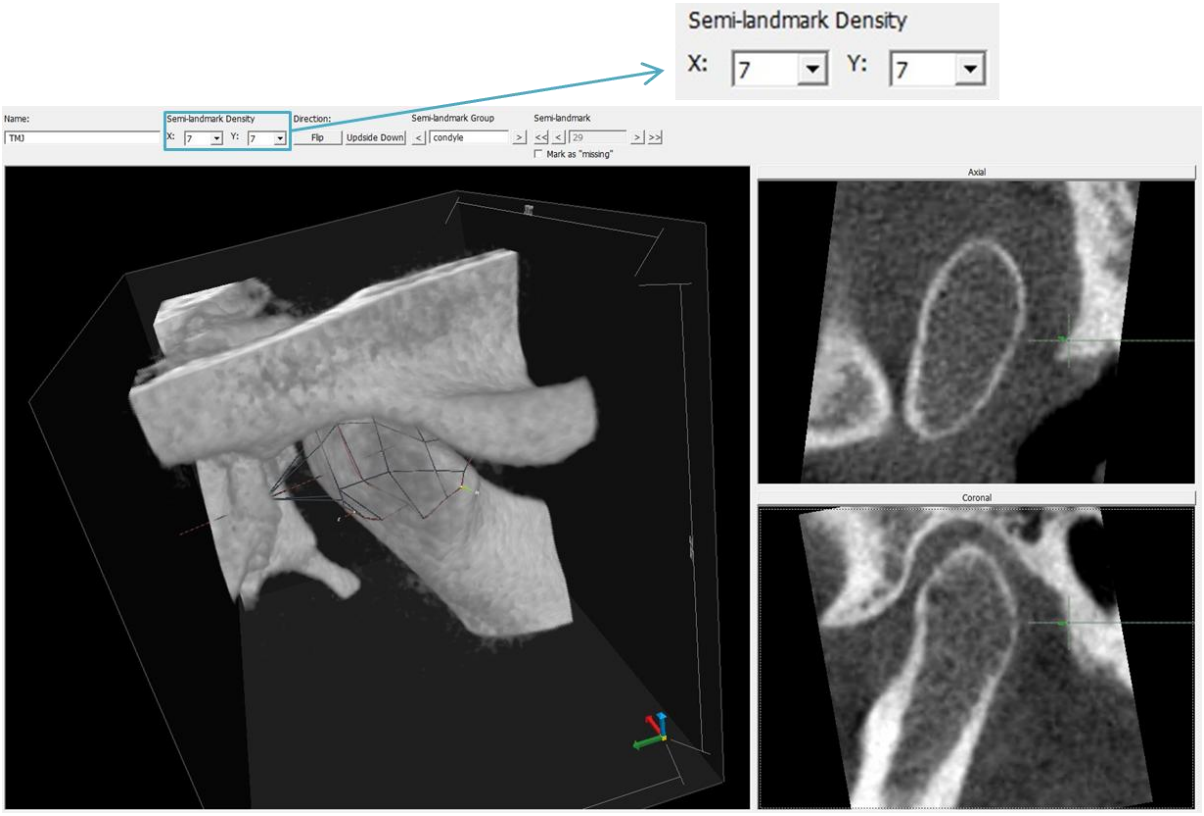


**Figure 13.** Automatically placed semi-landmarks (density of 7x7) on the condyle.

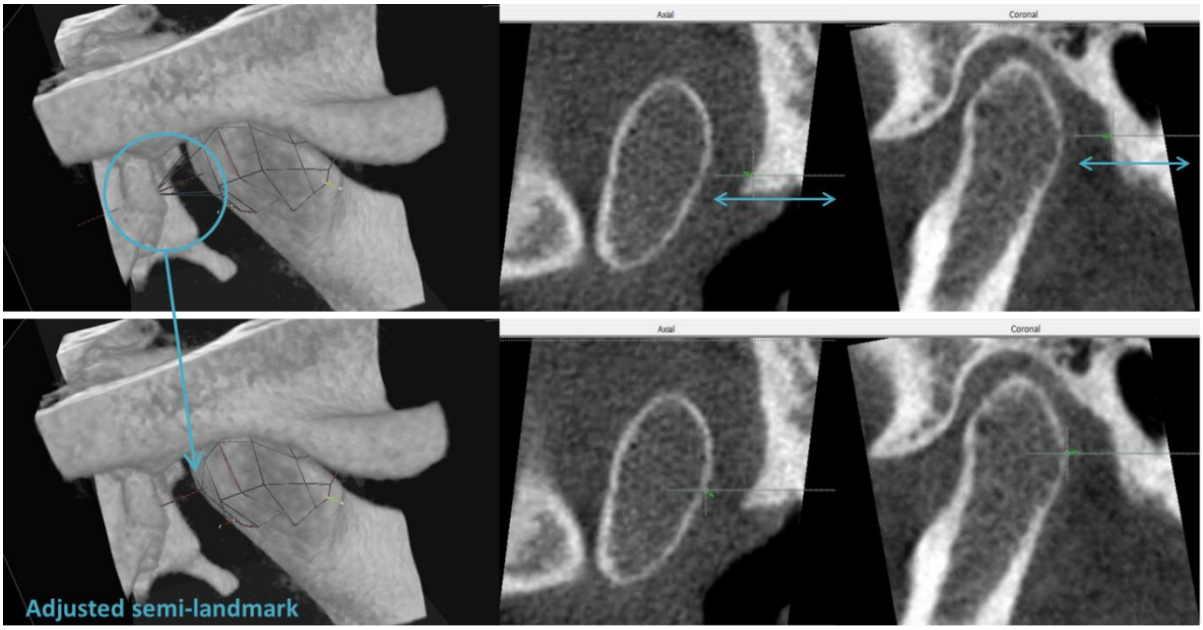


**Figure 14.** Example of how an incorrectly placed semi-landmark can be adjusted.

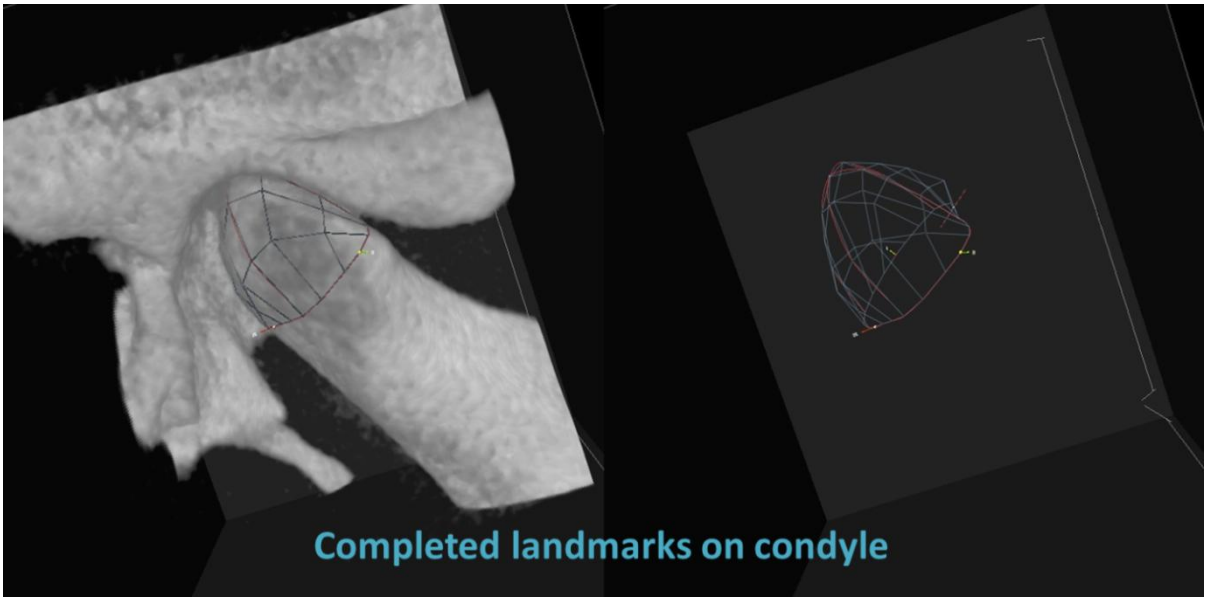


**Figure 15.** Completed condyle semi-landmarks.

Subsequently, semi-landmarks that are automatically placed on the opposing fossa surface (Figure 16) are reviewed and adjusted. Any fossa semi-landmarks that are non-existent due to

the absence of an opposing fossa wall (Figure 17A) or highly variable from being placed directly over orifices (Figure 17B), for example, should be marked as "missing" and excluded from the analysis. Finalized fossa semi-landmarks (Figure 18) and all of the landmarks on the condyle-fossa (Figure 19) can be reviewed in the volumetric view before proceeding with data analysis.

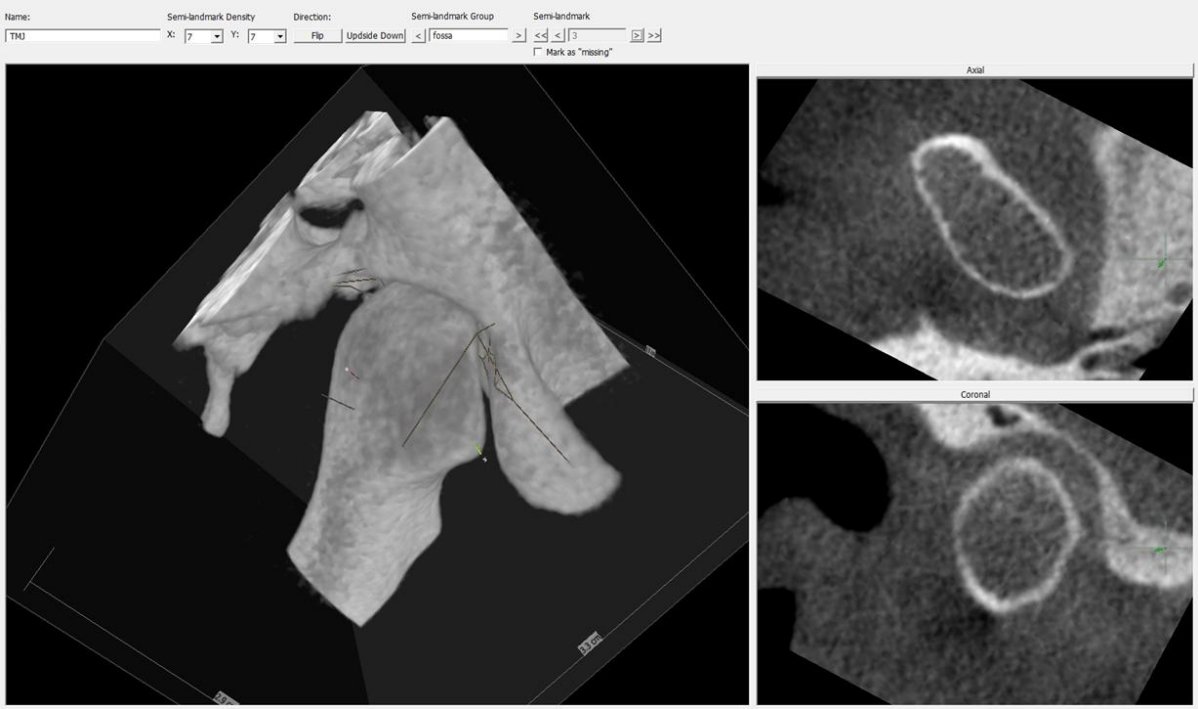


**Figure 16.** Automatically placed semi-landmarks on the fossa.

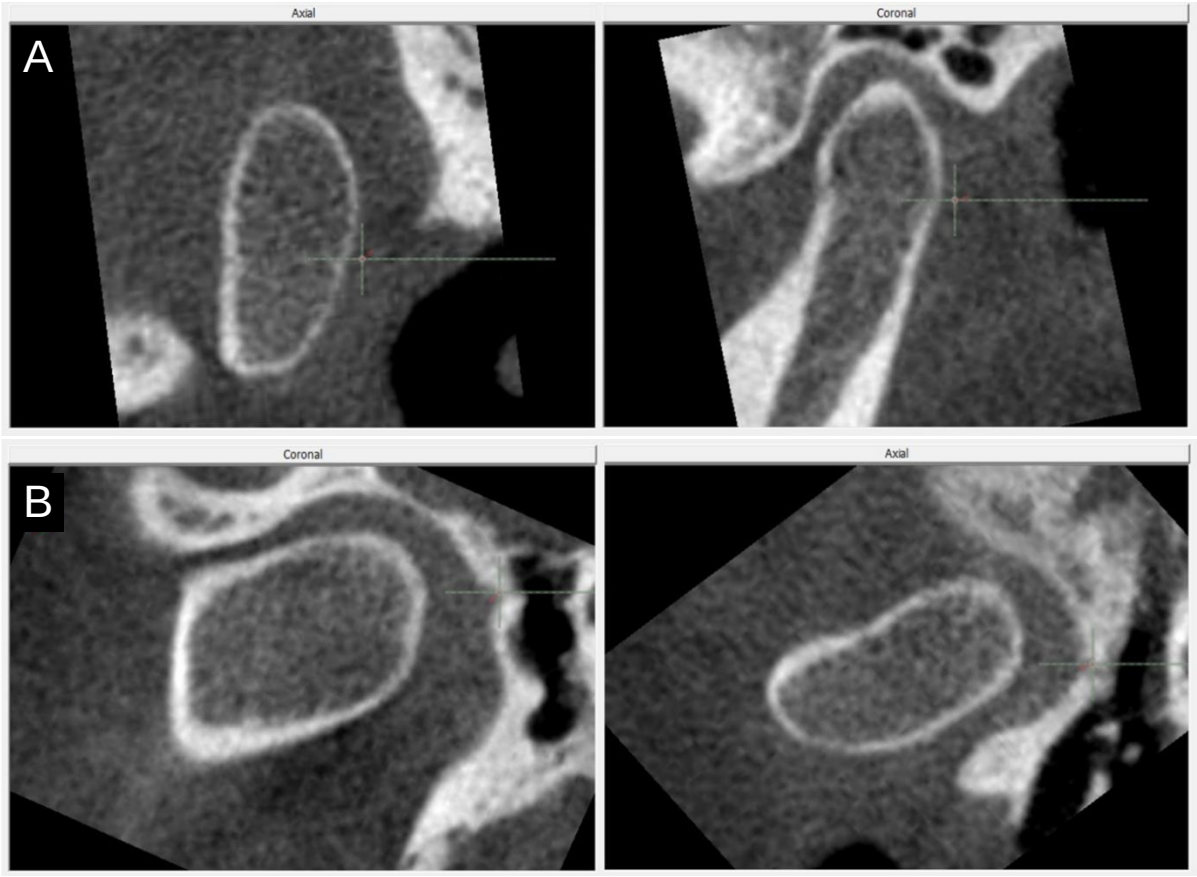


**Figure 17.** Examples of "missing" fossa points. (A) No opposing fossa wall. (B) Highly variable location such as around orifices.

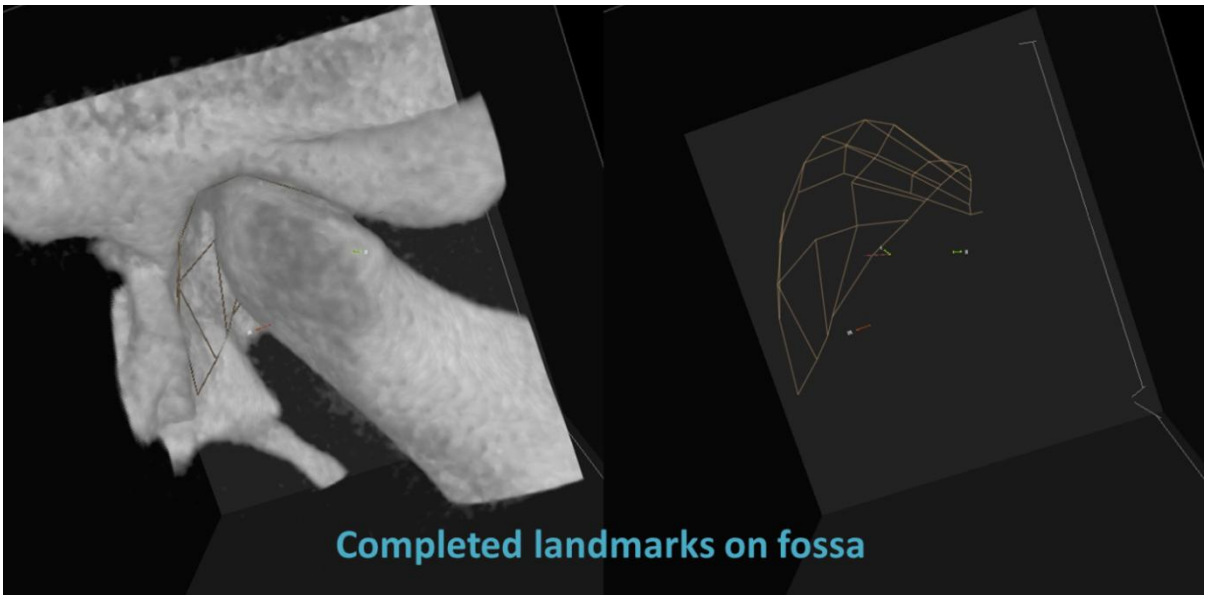


**Figure 18.** Completed fossa semi-landmarks.

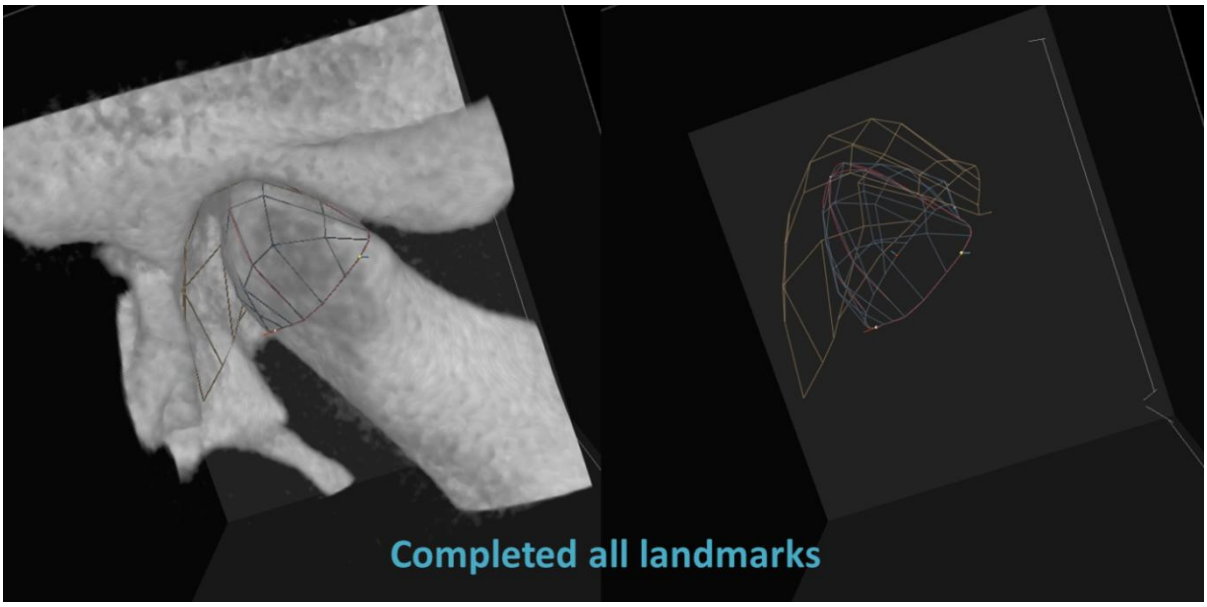


**Figure 19.** Completed condyle and fossa semi-landmarks.

**Optimal Patch Density**

Stratovan Checkpoint software allows the user to select different patch densities (number of landmarks), ranging from 5x5 up to 103x103, to place over the structure of interest to capture its shape. In general, lower patch densities will capture less shape variations, but there will be a point where adding more landmarks will not provide any additional morphological information. To determine which patch density most effectively captures the shapes of the TMJ condyles and fossae—and therefore the joint space, fifteen TMJs representing a range of TMJ shape changes that might be expected were selected (Hatcher, 2013; Figure 20). However, one of the fifteen TMJs was excluded since the condyle was noticeably out of the fossa (Figure 21).

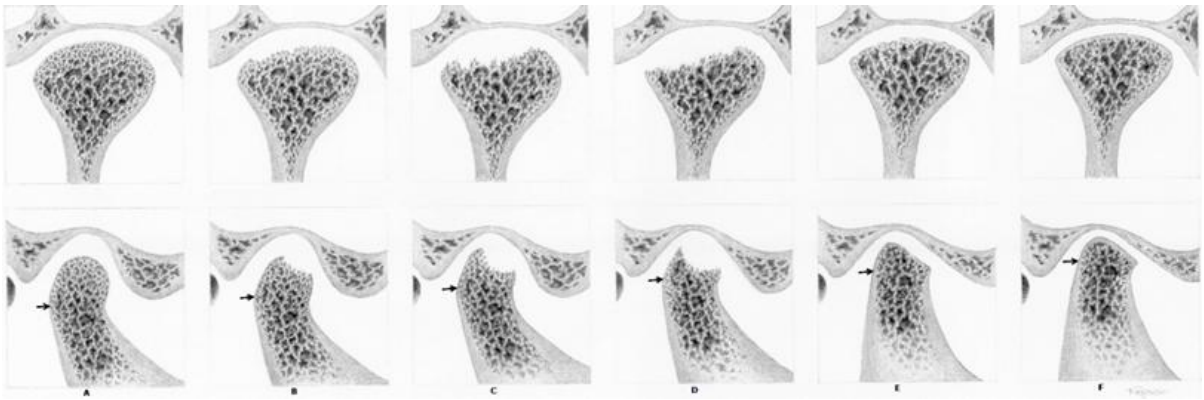

**Figure 20.** Possible range of TMJ shape changes (From Hatcher, 2013).

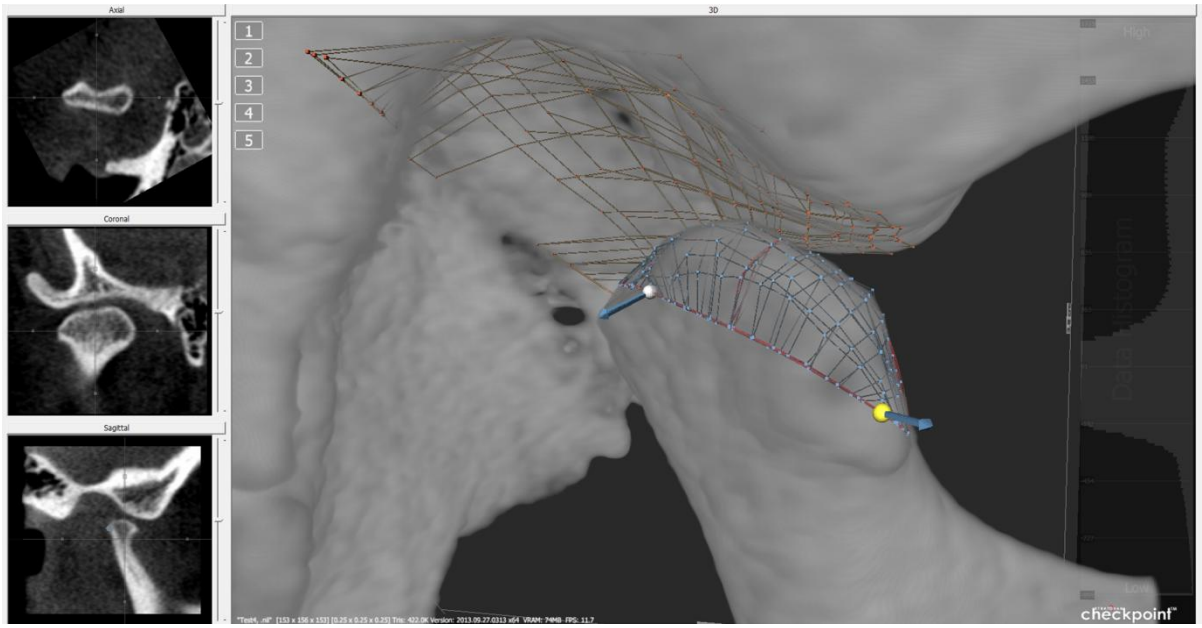


**Figure 21.** Excluded TMJ due to noticeably unseated condyle.

Each of the remaining fourteen TMJs was analyzed by the steps previously described using the following densities: 1) 5x5 or 25 landmarks, 2) 7x7 or 49 landmarks, 3) 9x9 or 81 landmarks, 4) 11x11 or 121 landmarks, and 5) 13x13 or 169 landmarks, and all five patches for a given TMJ were placed directly over one another by aligning each patch at the three "anchor points" (Figure 22).

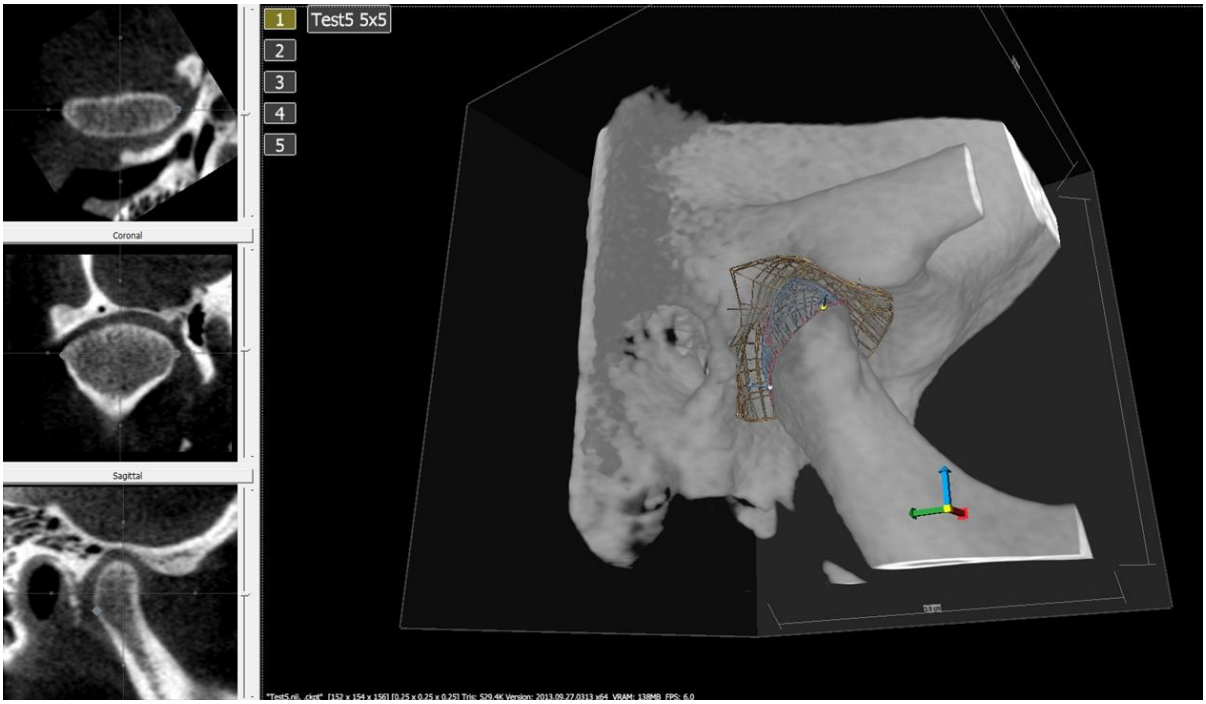


**Figure 22.** One TMJ with five patches of different landmark densities.

**Reliability of the Three-dimensional Joint Space Analysis**

To evaluate the intra-observer reliability of the novel semi-automated three-dimensional analysis of the TMJ space, five TMJs were analyzed by the same investigator three times using the optimal patch density, one to two weeks apart.

**Conventional Two-dimensional Temporomandibular Joint Space Analysis**

Invivo5 (Anatomage Inc., San Jose, CA) was used for two-dimensional TMJ space

analysis using the multiplanar view as described by Ikeda *et al.* (Ikeda *et al.*, 2009; Ikeda *et al.*, 2011), following a step-by-step protocol as outlined below.

Step 1: Orientation of TMJ

After opening the DICOM data of the patient's head scan, the TMJ orientation is adjusted until the following conditions are met: 1) in axial view, the horizontal line of cursor (blue) equates the long axis of the condyle; and 2) in axial and coronal views, the vertical line of cursor (green) bisects the long axis of the condyle (Figure 23). Subsequently, in the sagittal view, the horizontal line of cursor (orange) is moved superiorly or inferiorly until it passes through the anterior-most point of convexity of the condylar head (Figure 24).

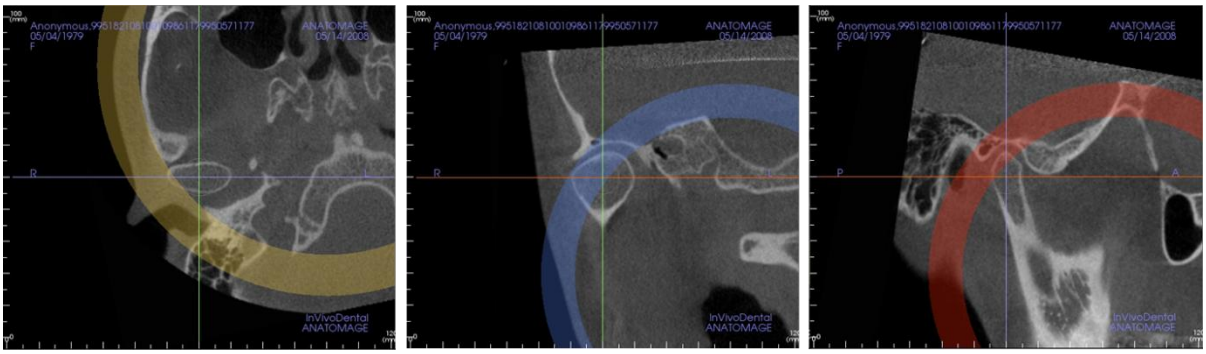

**Figure 23.** TMJ oriented to the long axis of the condyle.

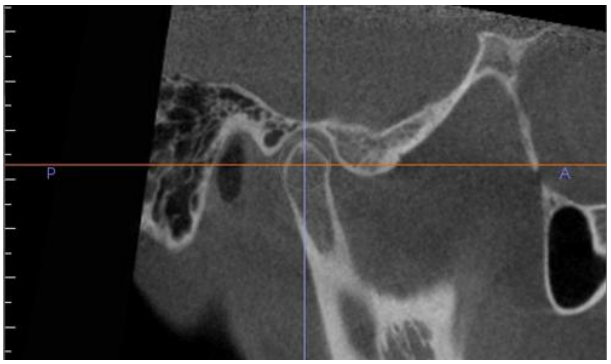

**Figure 24.** Adjusted horizontal plane (orange).

Step 2: Measurements in the Sagittal Slice

In the sagittal view, three joint space measurements are made (Figure 25). Superior space (SS) is measured from the most superior point along the condylar surface to the opposing fossa surface. For the anterior (AS) and posterior (PS) spaces, tangent lines from the superior point on the fossa to most prominent anterior and posterior surfaces of the condyle are drawn, then AS and PS are measured perpendicularly to the respective tangent lines to the opposing fossa surface.

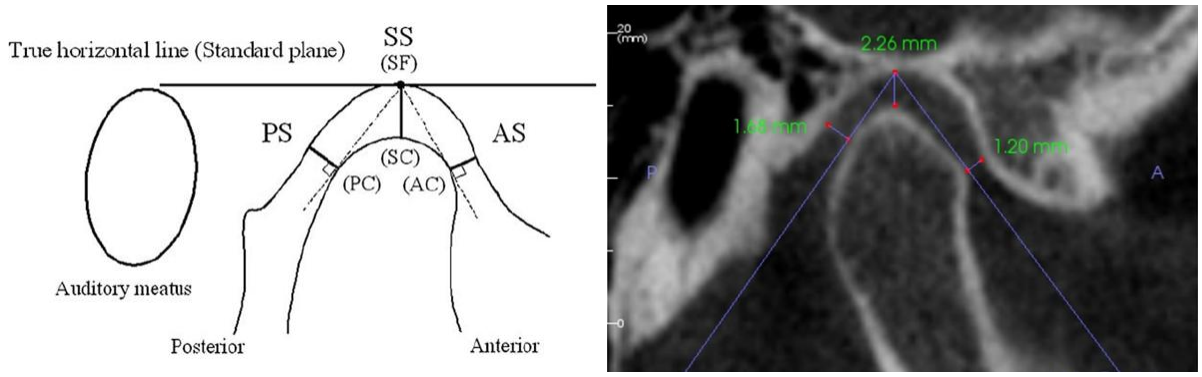


**Figure 25.** Three joint space measurements taken in the sagittal view.

Step 3: Measurements in the Coronal Slice

In the coronal view, three joint space measurements are made (Figure 26). Mediolateral width of the condyle is divided into sextants. Coronal central space (CCS) is measured as the shortest distance from the mid-point of the total width on the condyle surface to the opposing fossa wall superiorly. Coronal medial space (CMS) is measured as the shortest

distance from the junction of the medial first and second sextants of the condyle to the opposing fossa wall. Coronal lateral space (CLS) is similarly measured on the lateral aspect of the TMJ.

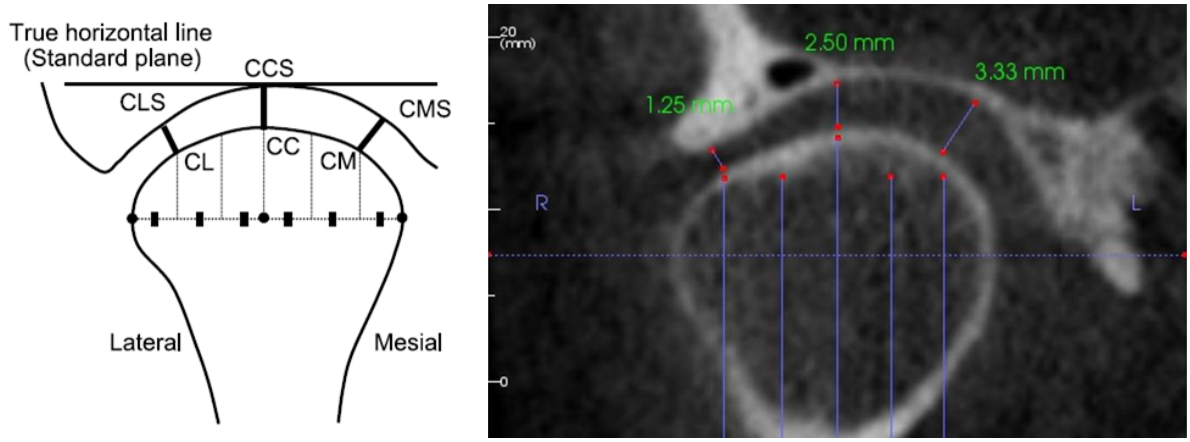


**Figure 26.** Three joint space measurements taken in the coronal view.

Step 4: Measurements in the Axial Slice

In the axial view, two joint space measurements are made (Figure 27). Axial medial space (AMS) and axial lateral space (ALS) are measured from the medial and lateral poles of the condyle to the medial and lateral walls of the fossa along an imaginary line extending from the long axis of the condyle.

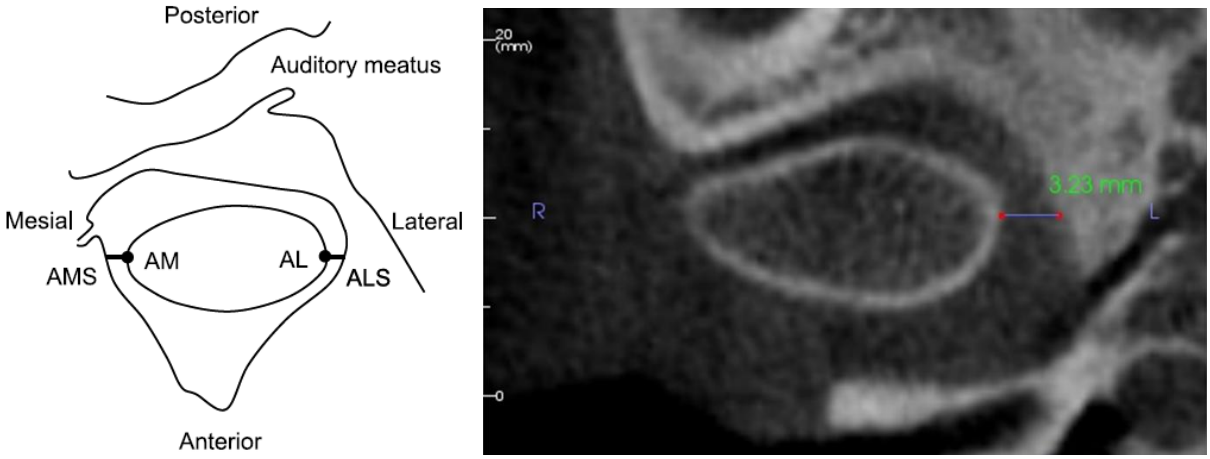


**Figure 27.** Three joint space measurements taken in the axial view.

**Reliability of the Two-dimensional Joint Space Analysis**

To evaluate the intra-observer reliability of the conventional two-dimensional analysis of the TMJ space, five TMJs were analyzed by the same investigator three times, one to two weeks apart.

**Statistical Analysis**

Optimal Patch Density

To determine the optimal patch density for the semi-automated three-dimensional analysis of the TMJ space, Principal Components Analysis (PCA) was applied to the condyle landmark coordinates for the five groups of different patch densities (5x5, 7x7, 9x9, 11x11, 13x13). Each group consisted of landmark data from the same fourteen TMJs that represent the range of shape variation one may expect in a condyle. Using the "Generalized Procrustes Analysis" function under the "Shape Analysis" tab on the Stratovan Checkpoint software (Figure 28), the landmark data for each of the five groups was first subjected to Procrustes superimposition, which translates, rotates, and scales all landmark configurations to remove the size, position, and orientation data so that only shape information remains (Adams *et al.*, 2004; Terhune, 2013).

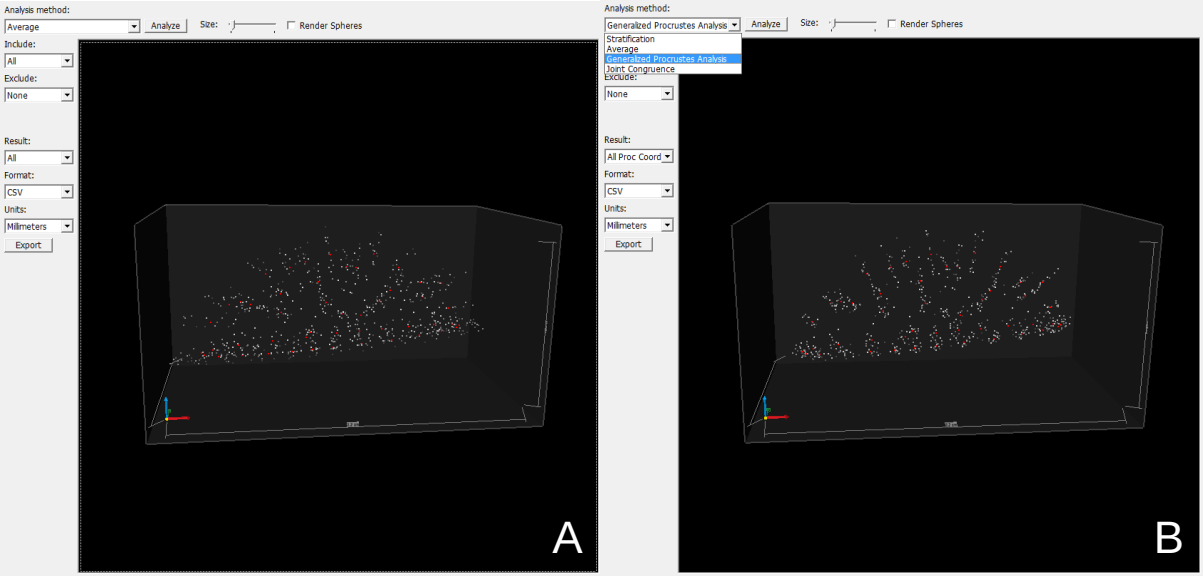


**Figure 28.** 7x7 patch density group containing landmarks of the fourteen TMJs. (A) Unscaled, average superimposition. (B) Procrustes superimposition.

Subsequently, MorphoJ program (Klingenberg, 2011) was used to perform the PCA, which analyzes the shape variance within a set of data—in this case, three-dimensional coordinates of condyle landmarks—and reduce the dataset to a few dimensions that represent most of the variation in the dataset (Mitteroecker *et al.*, 2009, Terhune, 2013). Applying PCA to each group helps identify the lowest patch density that demonstrates similar shape variance as the higher densities. In PCA, shape variance is described in terms of principal component vectors, where first principal component accounts for the largest possible shape variance, and each succeeding component has the highest variability possible under the constraint that it is orthogonal to—and therefore unrelated with—the preceding component (Abdi *et al*, 2010).

Focus was placed on principal components that explained at least 5% of the total shape variance, as principal components associated with shape variance below 5% were considered to be inconsequential. To visualize the shape variations along the major principal component axes, Morphologika software was used.

Reliability

To assess the reliability of the novel semi-automated three-dimensional analysis of the TMJ space, variance for the placement of each condylar landmark was calculated by obtaining the % error using the coordinate data (x, y, z) within each specimen for the repeated trials. This method compares the landmark position for each trial to its average within a specimen. An average % error greater than or equal to 5% was considered to be significant. For the reliability of the conventional two-dimensional analysis of the TMJ space, Pearson product-moment correlation coefficient was calculated to quantify the agreement between the repeated trials.

Three-dimensional Analysis

To evaluate the immediate and long-term post-operative changes in the TMJ space in the nine subjects using the data from the three-dimensional analysis, eight joint space measurements approximating (but not identical to) those from the two-dimensional analysis were extracted (Figure 29). Paired t-test was used after observing the normal distribution of data to compare the joint space measurements between different time points (T1 vs. T2, T2 vs. T3, and

T1 vs. T3). *P*-values less than 0.025 were considered to be statistically significant to account for the repeated comparison using the same group of data.

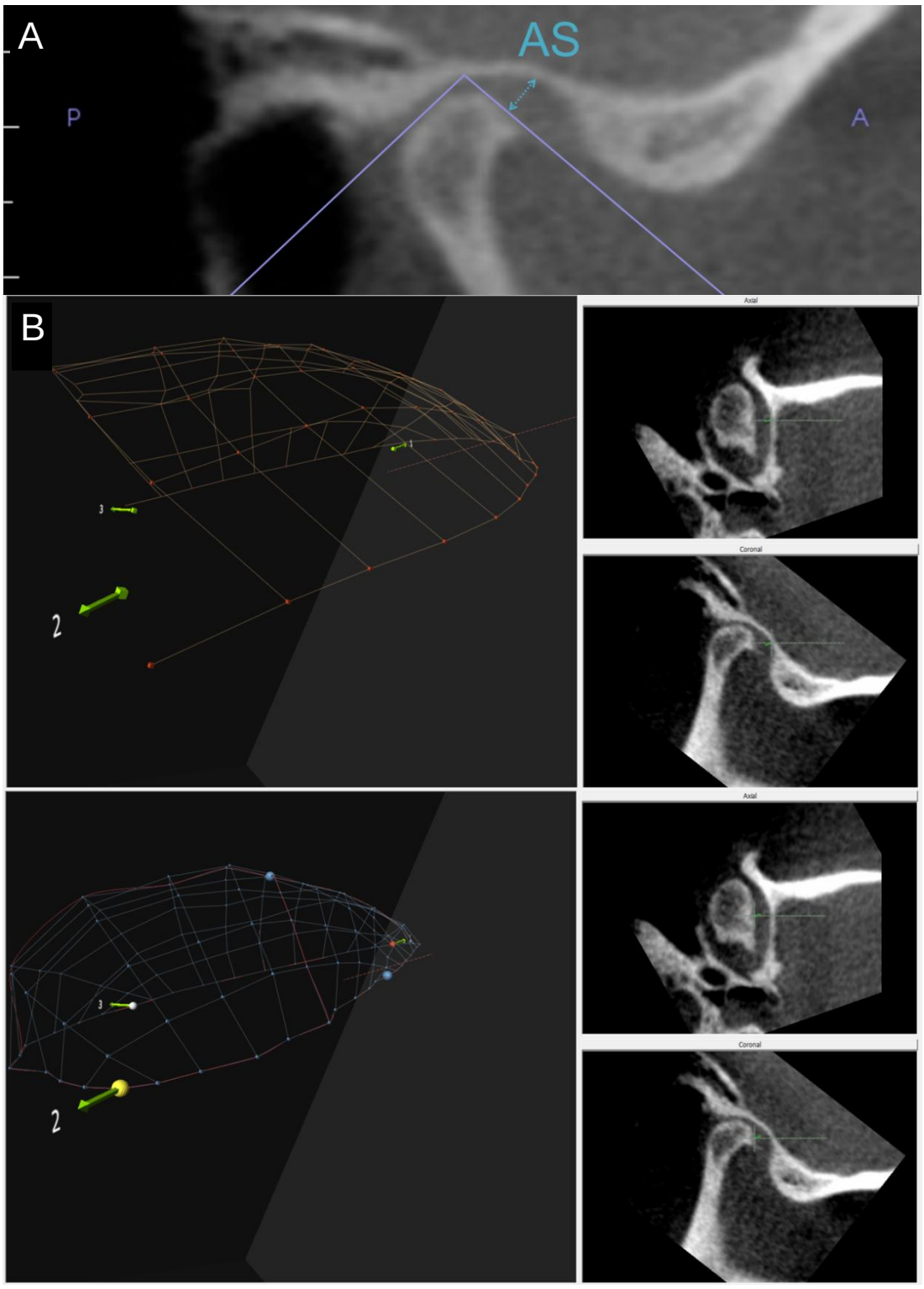


**Figure 29.** Example of corresponding 2D and 3D measurements. (A) Anterior Space (AS) defined by two-dimensional analysis. (B) Approximated joint space measurement (between the condyle and fossa patches along the dashed line) in the three-dimensional analysis of the same specimen.

Two-dimensional Analysis

Similarly, after observing the normal distribution of data from the conventional two-dimensional analysis of TMJ space, paired t-test was used to evaluate the significance in the changes of the joint space over the three different time points (T1 vs. T2, T2 vs. T3, and T1 vs. T3). *P*-values less than 0.025 were considered to be statistically significant to account for the repeated comparison using the same group of data.

# RESULTS

## Optimal Patch Density

As number of landmarks increased from patch density of 5x5 to 13x13, the higher density patches visually captured more detailed outline of the condyle (Figure 30).

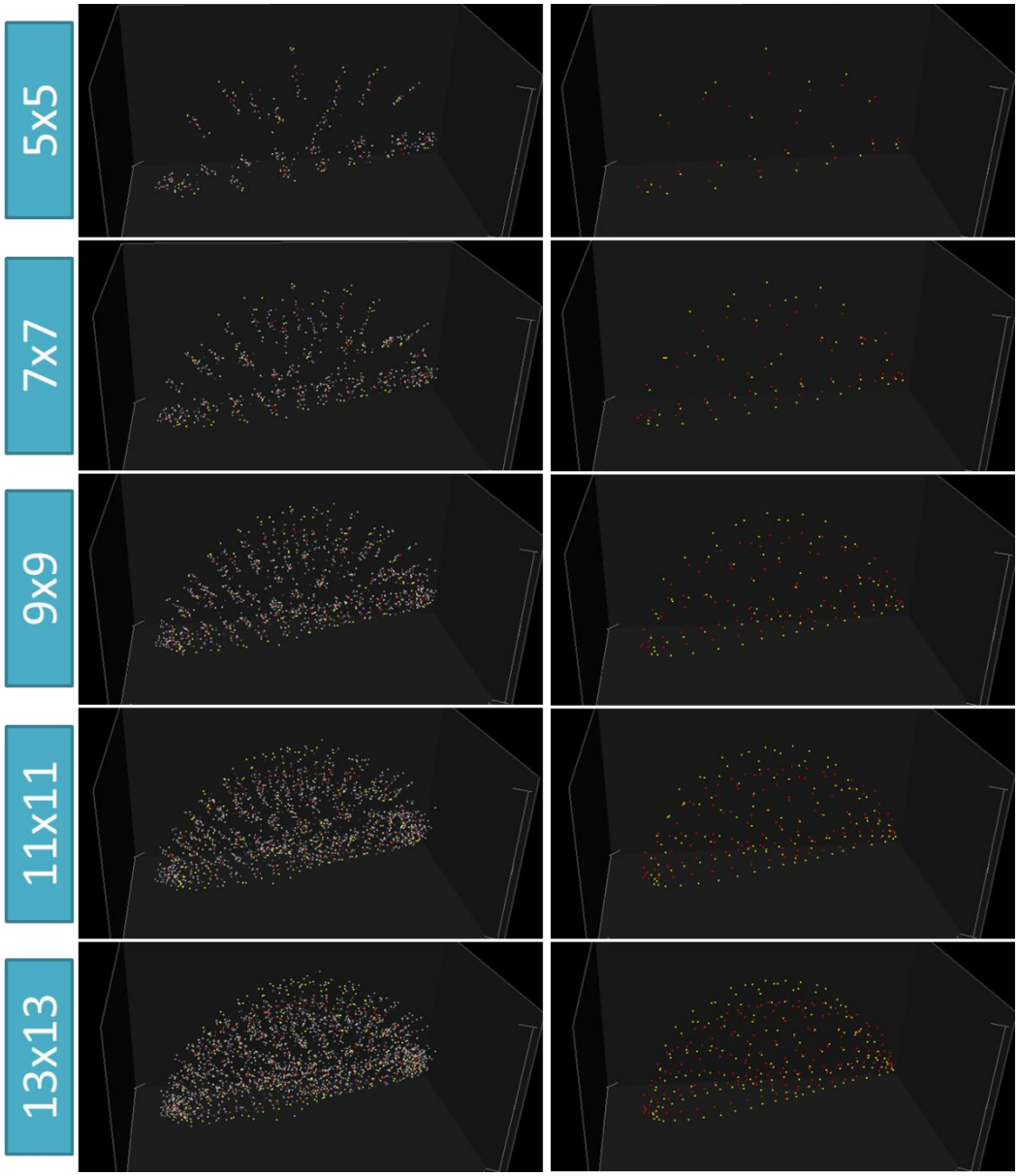


**Figure 30.** Condyle landmarks of fourteen TMJs with various patch densities. Landmarks of the fourteen TMJs are grey with one of them highlighted in yellow, and their average is indicated in red.

For the fourteen condyles representing the range of expected condylar shape variation, PCA revealed that first four principal components (PC) were responsible for at least 5% of the total shape variance (Table 2 and Figure 31). PC 1 represented 40.2% of the total shape variance, while PC 2, PC 3, and PC 4 represented 20.1%, 15.5%, and 7.1%, respectively (Table 2).

**Table 2.** Principal components and % variance.

| PC | % Variance | Cumulative % | PC | % Variance | Cumulative % |
|---|---|---|---|---|---|
| 1 | 40.223 | 40.223 | 8 | 2.024 | 96.071 |
| 2 | 20.123 | 60.345 | 9 | 1.471 | 97.542 |
| 3 | 15.458 | 75.804 | 10 | 1.070 | 98.613 |
| 4 | 7.132 | 82.936 | 11 | 0.679 | 99.292 |
| 5 | 4.818 | 87.754 | 12 | 0.540 | 99.831 |
| 6 | 3.347 | 91.100 | 13 | 0.169 | 100.000 |
| 7 | 2.947 | 94.047 | | | |

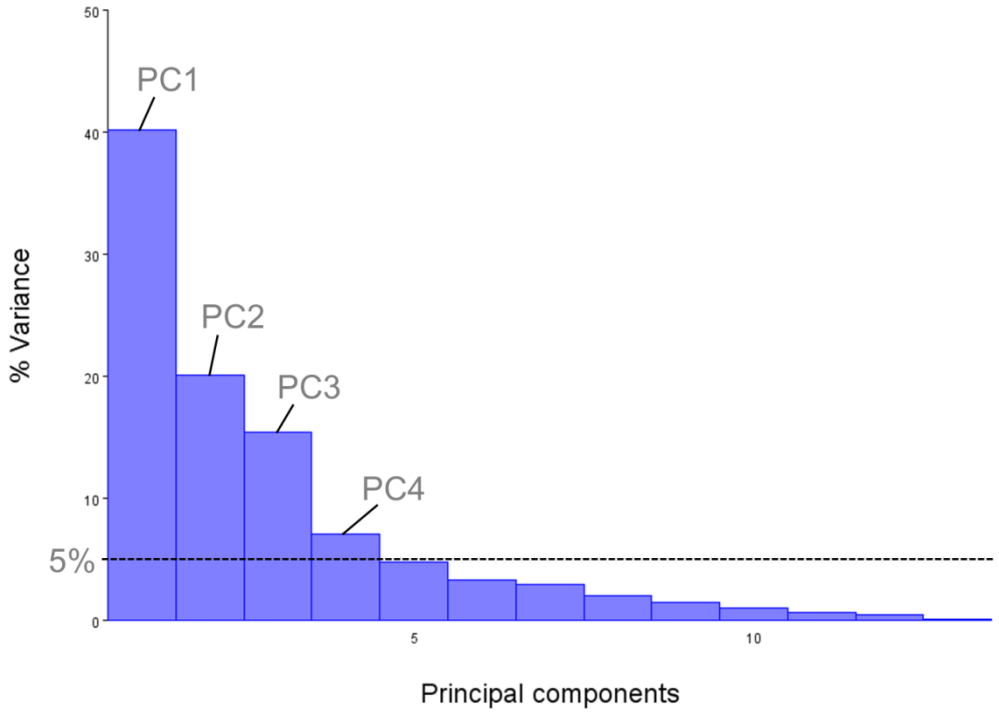


**Figure 31.** Percentage of total variance represented by each principal component.

The Procrustes average shape, which is at zero on the PC axes, is shown in Figure 32. Shape variation along PC 1 (which explains 40.2% of variance) is associated with the vertical dimension of the condyle as well as the mediolateral location of the anterior convexity; at the negative end of the PC 1 axis, the condylar head is tall and the convexity is located anteriorly at the lateral aspect of the condyle, while at the positive end of the axis, condyle has a very vertically compressed shape with anterior convexity at the medial aspect (Figure 33).

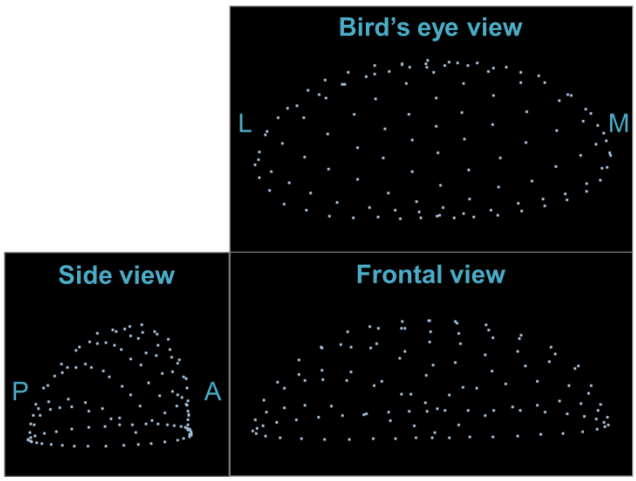


**Figure 32.** Procrustes average condyle shape.

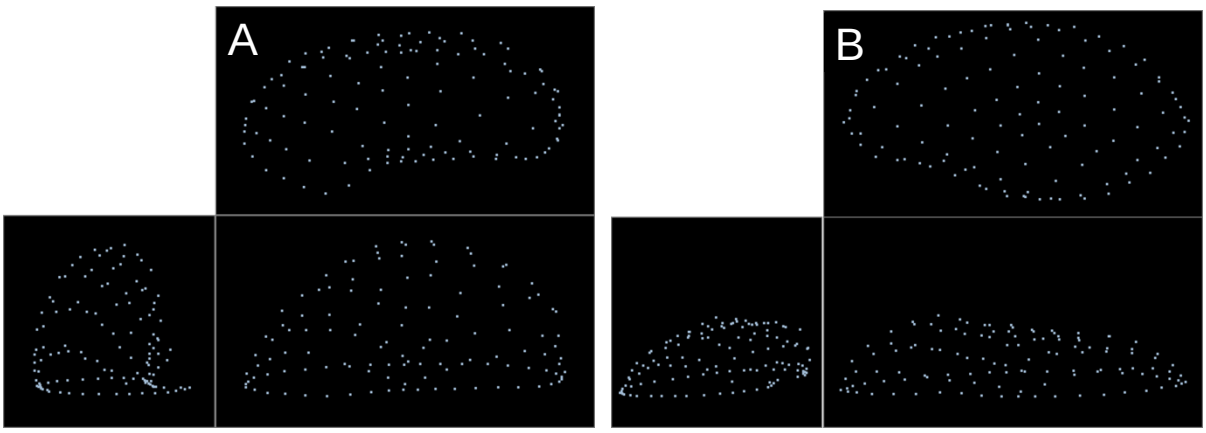


**Figure 33.** Shape variations along PC 1. (A) Shape at the negative extreme displaying tall condylar head with convexity at the anterolateral aspect. (B) Shape at the positive extreme showing vertically compressed condyle with convexity at the anteromedial part.

Shape variation along PC 2 (which explains 20.1% of variance) is associated with the relative anteroposterior and mediolateral dimensions of the condyle; at the negative end of the PC 2 axis, the condylar head is elongated mediolaterally and is narrowed in the anteroposterior dimension, while at the positive end of the axis, condyle has a rounded appearance in the bird's eye view with increased anteroposterior dimension to mediolateral dimension ratio (Figure 34).

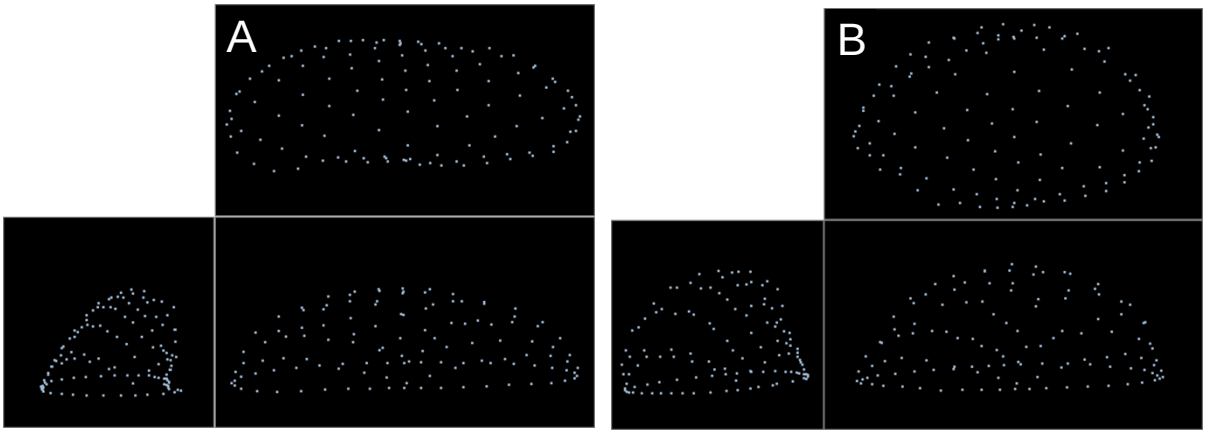


**Figure 34.** Shape variations along PC 2. (A) Shape at the negative extreme with a condylar head that is wide mediolaterally while narrow anteroposteriorly. (B) Shape at the positive extreme with a more rounded shape.

When plotting the fourteen TMJs with PC 1 as the x-axis and PC 2 as the y-axis, the spread of the points—each representing a condyle with a specific degree of shape variance for the first two principal component vectors—differed dramatically between 5x5 patch density group and the remaining groups (Figure 35).

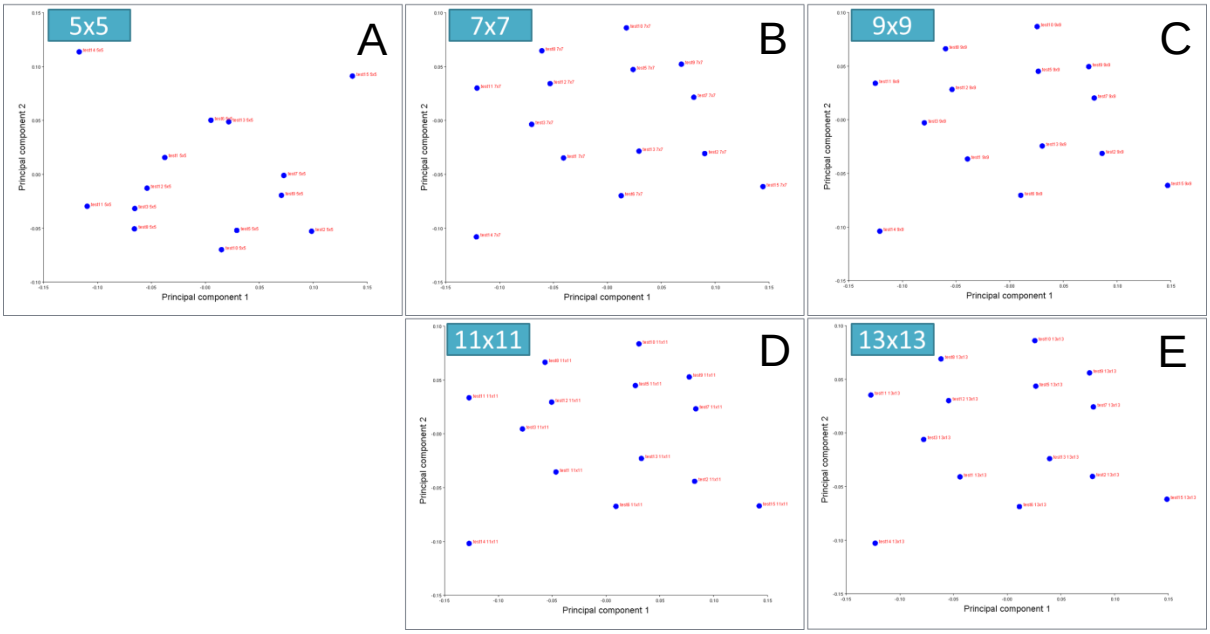


**Figure 35.** Comparison of the spread on PC 1 vs. PC 2 plot between groups. Spread of points when using: (A) 5x5 patch density, (B) 7x7 patch density, (C) 9x9 patch density, (D) 11x11 patch density, and (E) 13x13 patch density.

Shape variation along PC 3 (which explains 15.5% of variance) is associated with whether or not the condyle "leans" anteriorly and whether the superior aspect is leveled or conical in shape; at the negative end of the PC 3 axis, the condylar head is centered in the side view and flattened at the top, while at the positive end of the axis, condyle appears to "lean" forward and has a conical shape (Figure 36).

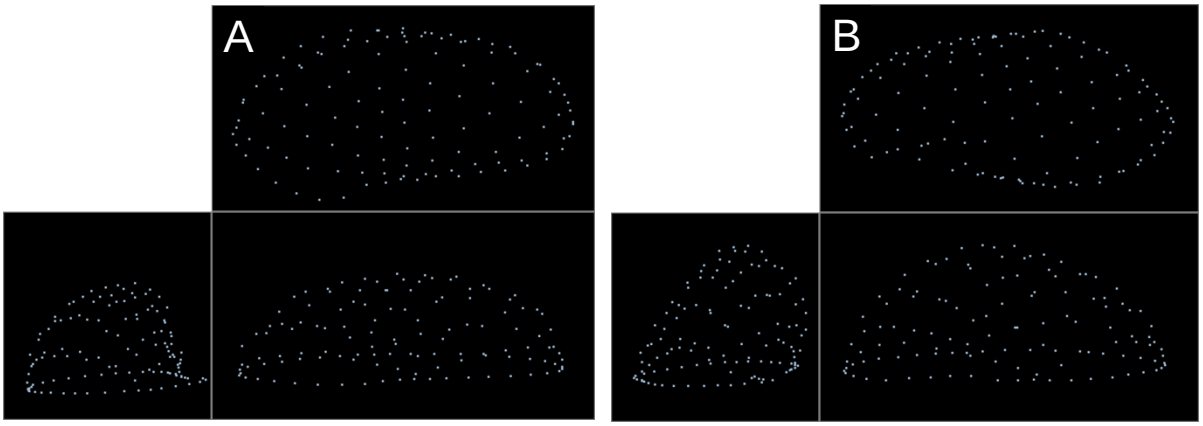


**Figure 36.** Shape variations along PC 3. (A) Shape at the negative extreme with a condylar head that is centered anteroposteriorly with a flattened superior contour. (B) Shape at the positive extreme with a condyle that appears to "lean" forward with a more conical shape.

Shape variation along PC 4 (which explains 7.1% of variance) is associated with absence of presence of "bending" of the condylar head; at the negative end of the PC 4 axis, the condylar head appears to "bend" as the medial and lateral aspects of the condyle come forward, while at the positive end of the axis, there is no such tendency (Figure 37).

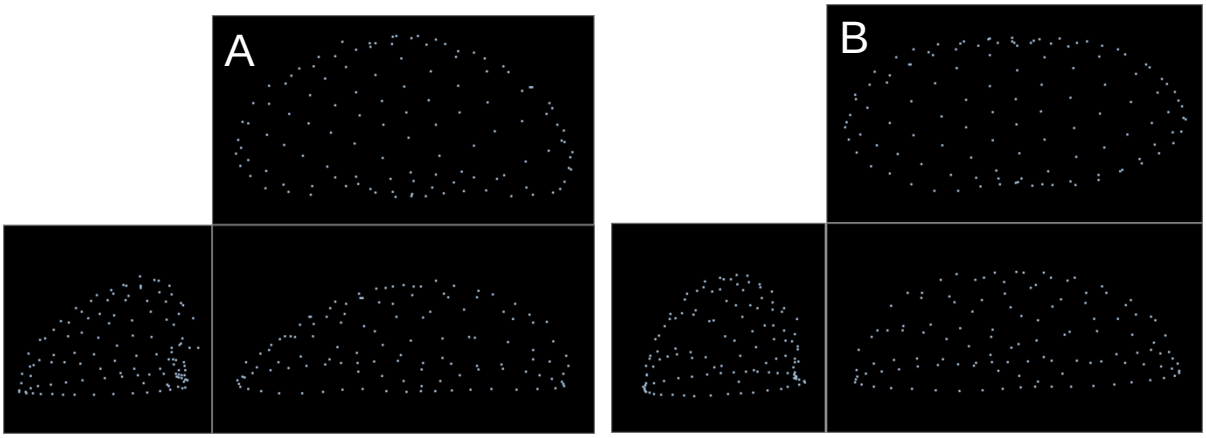


**Figure 37.** Shape variations along PC 4. (A) Shape at the negative extreme with a condylar head that appears to "bend." (B) Shape at the positive end shows no "bending."

When plotting the fourteen TMJs with PC 3 as the x-axis and PC 4 as the y-axis, the difference in the pattern of the spread of the points was not as obvious (Figure 38). Once again, however, 5x5 patch density group showed the most deviation from the general trend. Within the remaining four groups, 9x9, 11x11, and 13x13 were quite similar with few subtle variations.

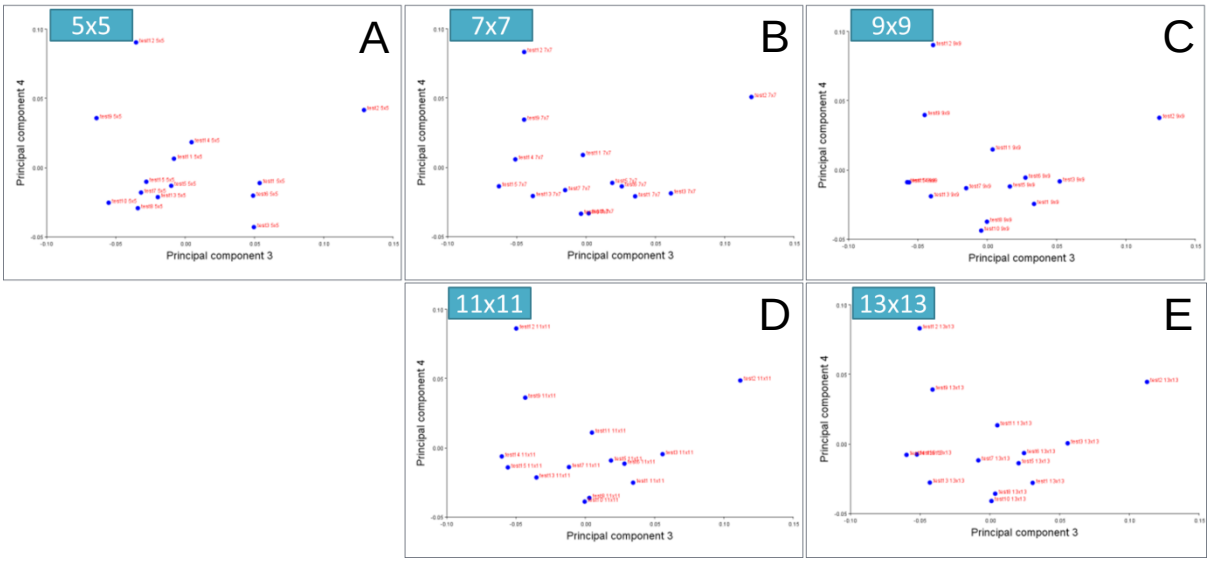


**Figure 38.** Comparison of the spread on PC 3 vs. PC 4 plot between groups. Spread of points when using: (A) 5x5 patch density, (B) 7x7 patch density, (C) 9x9 patch density, (D) 11x11 patch density, and (E) 13x13 patch density.

**Reliability**

Five TMJs were analyzed by the same investigator three times using the optimal patch density of 11x11, one to two weeks apart (Figure 39). To assess the reliability of the novel semi-automated three-dimensional analysis of the TMJ space, variance for the placement of each condylar landmark was calculated by obtaining the % error using the coordinate data (x, y, z) for the repeated trials for each specimen (Table 3). Average % error ranged from 1.15% to 3.65%,

and none of the 121 landmarks showed significant average % error equal to or greater than 5% (Table 3).

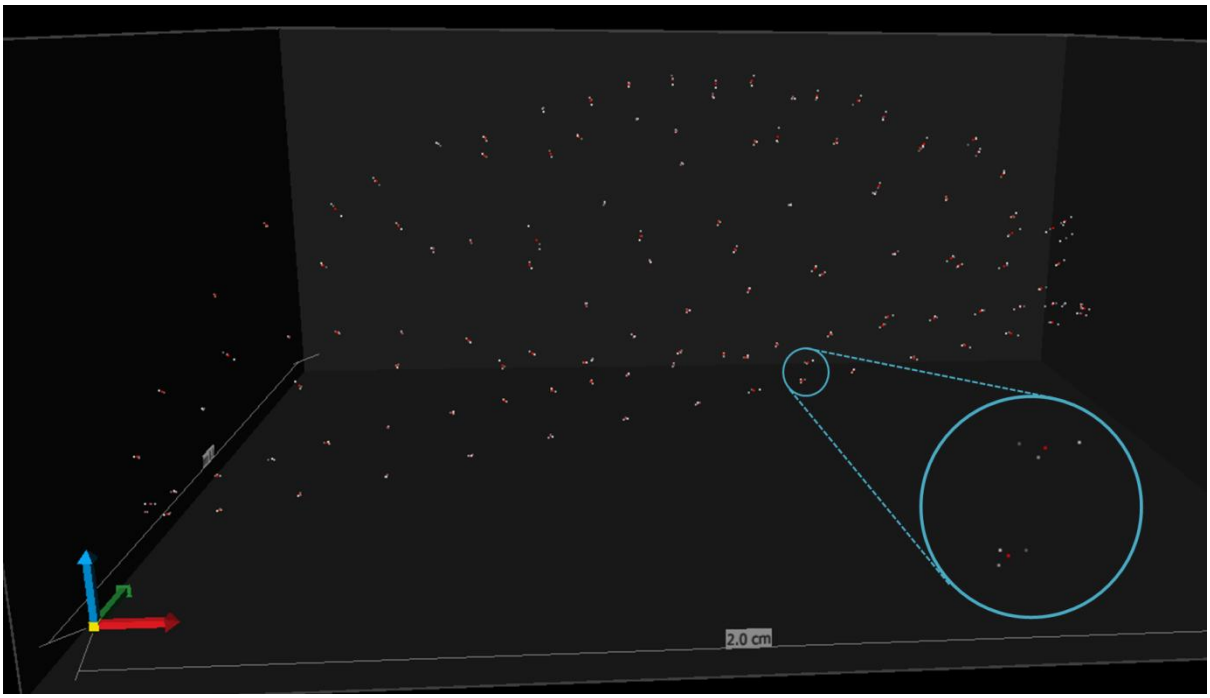


**Figure 39.** Condylar points from repeated trials. Landmarks from each of the three repeated trials are shown in different shades of grey, while the red landmarks denote their average location.

**Table 3.** Reliability data for the three-dimensional analysis (% error).

| Landmark | TMJ 1 % Error | TMJ 2 % Error | TMJ 3 % Error | TMJ 4 % Error | TMJ 5 % Error | Average % Error |
|---|---|---|---|---|---|---|
| 1 | 2.6798 | 2.1856 | 3.4851 | 1.8125 | 1.1207 | **2.2567** |
| 2 | 1.9537 | 2.7435 | 1.9062 | 2.9556 | 1.9652 | **2.3049** |
| 3 | 2.4743 | 2.2695 | 2.3268 | 2.6660 | 2.4424 | **2.4358** |
| 4 | 2.9924 | 1.8161 | 4.2478 | 1.5235 | 1.4228 | **2.4005** |
| 5 | 3.8388 | 3.4564 | 4.1306 | 3.0673 | 1.9048 | **3.2796** |
| 6 | 2.7074 | 3.1312 | 4.0210 | 2.7301 | 1.4832 | **2.8146** |
| 7 | 1.7103 | 1.7680 | 4.1975 | 2.2467 | 1.7125 | **2.3270** |
| 8 | 2.4804 | 1.1882 | 3.6747 | 1.9571 | 1.9352 | **2.2471** |

**Table 3 cont'd.** Reliability data for the three-dimensional analysis (% error).

| Landmark | TMJ 1 % Error | TMJ 2 % Error | TMJ 3 % Error | TMJ 4 % Error | TMJ 5 % Error | Average % Error |
|---|---|---|---|---|---|---|
| 9 | 1.5666 | 1.9228 | 2.9470 | 1.7343 | 1.0734 | **1.8488** |
| 10 | 1.4148 | 1.8575 | 1.1965 | 1.0521 | 1.0242 | **1.3090** |
| 11 | 1.7881 | 2.0543 | 1.5026 | 1.7088 | 1.1678 | **1.6443** |
| 12 | 1.2427 | 2.4651 | 3.3380 | 1.7688 | 2.7475 | **2.3124** |
| 13 | 3.2282 | 2.1445 | 2.7787 | 1.9481 | 2.1039 | **2.4407** |
| 14 | 2.6806 | 1.9871 | 3.2795 | 2.2294 | 0.9785 | **2.2310** |
| 15 | 2.4731 | 1.4084 | 2.9769 | 2.7549 | 0.8539 | **2.0934** |
| 16 | 2.5064 | 0.9390 | 3.0912 | 3.3950 | 1.6345 | **2.3132** |
| 17 | 2.5238 | 3.0438 | 4.4563 | 1.5975 | 1.1138 | **2.5470** |
| 18 | 2.1383 | 2.0369 | 3.0401 | 3.0556 | 0.9388 | **2.2420** |
| 19 | 1.2174 | 2.2633 | 1.9908 | 2.4537 | 1.0323 | **1.7915** |
| 20 | 1.2536 | 1.5831 | 2.6372 | 2.0474 | 1.5316 | **1.8106** |
| 21 | 1.3394 | 2.3412 | 2.3670 | 1.7150 | 1.3412 | **1.8208** |
| 22 | 2.0447 | 1.9753 | 3.2075 | 2.2187 | 1.5526 | **2.1998** |
| 23 | 2.2336 | 2.1668 | 3.9198 | 1.6466 | 1.8175 | **2.3569** |
| 24 | 2.7381 | 2.8430 | 3.0002 | 1.3969 | 2.0839 | **2.4124** |
| 25 | 0.9356 | 1.6143 | 2.1046 | 0.9992 | 1.3782 | **1.4064** |
| 26 | 1.7983 | 1.2220 | 1.4361 | 1.3675 | 0.7313 | **1.3111** |
| 27 | 2.1113 | 2.2549 | 1.4838 | 2.2564 | 0.7377 | **1.7688** |
| 28 | 2.0705 | 2.4565 | 2.5487 | 2.2333 | 0.6778 | **1.9974** |
| 29 | 3.1315 | 1.9620 | 2.2097 | 0.9068 | 1.6711 | **1.9762** |
| 30 | 1.3730 | 1.7197 | 1.8440 | 1.1376 | 1.9611 | **1.6071** |
| 31 | 3.9258 | 1.7415 | 1.0762 | 1.5065 | 2.2229 | **2.0946** |
| 32 | 2.4914 | 1.4815 | 1.7753 | 1.0316 | 2.1596 | **1.7879** |
| 33 | 2.4579 | 1.7519 | 1.2164 | 1.6225 | 1.5552 | **1.7208** |
| 34 | 1.2956 | 1.9179 | 3.1314 | 1.0844 | 3.9064 | **2.2671** |
| 35 | 1.9130 | 2.3211 | 2.5986 | 1.5738 | 1.2843 | **1.9382** |
| 36 | 1.0880 | 1.5433 | 1.6835 | 0.5467 | 1.9801 | **1.3683** |
| 37 | 1.3250 | 1.8835 | 1.6203 | 0.8898 | 1.2226 | **1.3882** |
| 38 | 2.0196 | 1.8887 | 2.2021 | 1.2307 | 1.3487 | **1.7379** |

**Table 3 cont'd.** Reliability data for the three-dimensional analysis (% error).

| Landmark | TMJ 1 % Error | TMJ 2 % Error | TMJ 3 % Error | TMJ 4 % Error | TMJ 5 % Error | Average % Error |
|---|---|---|---|---|---|---|
| **39** | 2.2907 | 2.1253 | 2.0983 | 1.7857 | 1.2411 | **1.9082** |
| **40** | 1.6700 | 1.7706 | 2.8937 | 1.2467 | 1.4049 | **1.7972** |
| **41** | 1.9108 | 2.3087 | 3.6844 | 1.2971 | 2.0633 | **2.2529** |
| **42** | 2.4650 | 1.4147 | 1.8396 | 1.1630 | 3.1757 | **2.0116** |
| **43** | 2.9653 | 1.7950 | 1.6078 | 1.9595 | 2.4925 | **2.1640** |
| **44** | 2.8767 | 2.6739 | 1.7848 | 2.4379 | 1.6928 | **2.2932** |
| **45** | 1.9152 | 2.1550 | 2.5173 | 1.2074 | 2.4821 | **2.0554** |
| **46** | 1.9278 | 2.0610 | 2.1908 | 2.0095 | 1.6398 | **1.9658** |
| **47** | 1.6910 | 1.4547 | 1.6410 | 1.6987 | 1.6972 | **1.6365** |
| **48** | 1.3957 | 1.9251 | 2.0106 | 1.2700 | 1.3356 | **1.5874** |
| **49** | 2.0785 | 2.4829 | 2.1676 | 1.2146 | 1.4444 | **1.8776** |
| **50** | 2.4680 | 2.4037 | 2.8560 | 1.4104 | 0.7720 | **1.9820** |
| **51** | 3.9982 | 1.9450 | 2.2585 | 1.4667 | 3.2780 | **2.5893** |
| **52** | 2.2865 | 1.4505 | 1.8005 | 1.4026 | 2.9627 | **1.9806** |
| **53** | 2.1796 | 2.2207 | 2.7116 | 1.2826 | 2.6515 | **2.2092** |
| **54** | 2.5958 | 1.6557 | 0.9889 | 1.8427 | 2.4039 | **1.8974** |
| **55** | 3.1419 | 2.1742 | 1.8625 | 1.5170 | 2.0075 | **2.1406** |
| **56** | 2.0735 | 1.9293 | 2.0329 | 1.3566 | 2.7258 | **2.0236** |
| **57** | 0.8393 | 1.4808 | 1.0030 | 1.3298 | 1.0837 | **1.1473** |
| **58** | 1.0230 | 1.4776 | 1.9030 | 2.0854 | 1.1319 | **1.5242** |
| **59** | 2.4286 | 2.3628 | 1.9857 | 1.0901 | 1.4168 | **1.8568** |
| **60** | 4.5034 | 2.3122 | 2.1193 | 1.9285 | 1.8080 | **2.5343** |
| **61** | 2.7532 | 3.0502 | 3.0068 | 1.5770 | 1.5816 | **2.3938** |
| **62** | 5.6241 | 2.9096 | 1.8621 | 1.7361 | 2.6211 | **2.9506** |
| **63** | 4.6211 | 2.6118 | 2.9382 | 1.5935 | 2.6233 | **2.8776** |
| **64** | 3.2468 | 2.5054 | 5.7709 | 1.6162 | 2.4609 | **3.1200** |
| **65** | 2.4092 | 2.6475 | 3.3058 | 1.2922 | 3.2735 | **2.5856** |
| **66** | 3.4147 | 2.1603 | 2.0681 | 3.0409 | 2.2126 | **2.5793** |
| **67** | 1.9841 | 1.9382 | 1.0687 | 1.9797 | 2.4456 | **1.8833** |
| **68** | 1.1203 | 0.8087 | 1.8613 | 1.2737 | 1.4918 | **1.3112** |

**Table 3 cont'd.** Reliability data for the three-dimensional analysis (% error).

| Landmark | TMJ 1 % Error | TMJ 2 % Error | TMJ 3 % Error | TMJ 4 % Error | TMJ 5 % Error | Average % Error |
|---|---|---|---|---|---|---|
| **69** | 1.2066 | 1.4403 | 2.1278 | 1.9557 | 0.8004 | **1.5061** |
| **70** | 3.2956 | 1.9028 | 1.3044 | 1.7483 | 1.5384 | **1.9579** |
| **71** | 4.9021 | 3.5512 | 0.7395 | 2.1655 | 2.3374 | **2.7392** |
| **72** | 2.5049 | 2.7828 | 2.5521 | 3.0484 | 1.2047 | **2.4186** |
| **73** | 2.7705 | 3.5631 | 1.8704 | 2.5290 | 3.5395 | **2.8545** |
| **74** | 5.3389 | 1.9432 | 2.4438 | 1.4258 | 3.8922 | **3.0088** |
| **75** | 4.7527 | 2.9584 | 1.9789 | 2.4825 | 3.4981 | **3.1341** |
| **76** | 4.6205 | 2.6089 | 1.5776 | 1.7549 | 3.3949 | **2.7914** |
| **77** | 3.3840 | 2.3390 | 0.8778 | 2.1306 | 2.6260 | **2.2715** |
| **78** | 2.1360 | 2.1240 | 1.6289 | 2.1802 | 2.1295 | **2.0397** |
| **79** | 1.7685 | 1.4938 | 2.4672 | 2.3432 | 1.2861 | **1.8718** |
| **80** | 1.1740 | 1.9083 | 2.2877 | 3.5508 | 0.9362 | **1.9714** |
| **81** | 3.2846 | 2.0905 | 1.6982 | 2.0624 | 1.3155 | **2.0903** |
| **82** | 4.2774 | 2.5219 | 2.6406 | 2.0346 | 1.2946 | **2.5538** |
| **83** | 5.3475 | 2.1685 | 2.8397 | 2.0283 | 2.6482 | **3.0064** |
| **84** | 1.4840 | 2.2170 | 2.4249 | 2.3442 | 2.0211 | **2.0982** |
| **85** | 2.4407 | 4.4237 | 3.4564 | 0.9200 | 2.9497 | **2.8381** |
| **86** | 3.6207 | 3.6041 | 2.7952 | 3.3259 | 3.4595 | **3.3611** |
| **87** | 2.7170 | 2.3104 | 3.2222 | 2.0590 | 3.1028 | **2.6823** |
| **89** | 3.3933 | 2.3985 | 0.4858 | 2.4390 | 2.3712 | **2.2176** |
| **90** | 2.1634 | 1.9864 | 1.2892 | 2.3410 | 1.6618 | **1.8884** |
| **91** | 2.1479 | 1.5404 | 3.1817 | 1.4184 | 0.8680 | **1.8313** |
| **92** | 1.8094 | 2.5110 | 1.7855 | 1.5316 | 1.6675 | **1.8610** |
| **93** | 3.0065 | 3.7502 | 3.0860 | 2.7750 | 2.1379 | **2.9511** |
| **94** | 4.6712 | 3.2759 | 2.2526 | 2.2581 | 2.0801 | **2.9076** |
| **95** | 5.1753 | 1.7216 | 3.3816 | 3.7931 | 4.1513 | **3.6446** |
| **96** | 5.1550 | 3.3054 | 4.6974 | 2.1524 | 2.4379 | **3.5496** |
| **97** | 4.9601 | 2.2808 | 2.1605 | 2.6022 | 3.7408 | **3.1489** |
| **98** | 3.0809 | 2.2348 | 1.2782 | 1.4798 | 2.2459 | **2.0639** |
| **99** | 2.5954 | 2.1756 | 1.4848 | 1.7579 | 2.2932 | **2.0614** |

**Table 3 cont'd.** Reliability data for the three-dimensional analysis (% error).

| Landmark | TMJ 1 % Error | TMJ 2 % Error | TMJ 3 % Error | TMJ 4 % Error | TMJ 5 % Error | Average % Error |
|---|---|---|---|---|---|---|
| **100** | 1.6388 | 2.4260 | 1.2751 | 2.5671 | 2.5386 | **2.0891** |
| **101** | 2.5500 | 2.2728 | 1.3820 | 1.9549 | 1.0829 | **1.8485** |
| **102** | 2.4473 | 2.3354 | 1.8610 | 1.3911 | 1.6408 | **1.9351** |
| **103** | 0.5151 | 2.3927 | 3.2336 | 2.2826 | 2.7063 | **2.2261** |
| **104** | 2.6425 | 3.0962 | 3.0746 | 2.6020 | 2.4555 | **2.7742** |
| **105** | 2.4508 | 3.7042 | 1.6649 | 2.2946 | 4.2335 | **2.8696** |
| **106** | 3.4584 | 3.2781 | 2.9546 | 3.2697 | 2.9901 | **3.1902** |
| **107** | 4.3987 | 3.1872 | 1.9178 | 2.2423 | 3.6793 | **3.0850** |
| **108** | 3.3513 | 3.1392 | 4.2944 | 4.0072 | 2.9682 | **3.5521** |
| **109** | 5.0467 | 1.5465 | 2.9653 | 2.4671 | 2.1983 | **2.8448** |
| **110** | 3.7056 | 2.7847 | 2.4897 | 2.3690 | 3.7773 | **3.0253** |
| **111** | 2.4452 | 2.1179 | 1.7913 | 2.3027 | 3.1088 | **2.3532** |
| **112** | 2.6780 | 2.9700 | 2.5334 | 2.7911 | 1.0136 | **2.3972** |
| **113** | 2.4917 | 2.3395 | 3.3252 | 2.4784 | 1.0359 | **2.3341** |
| **114** | 2.7673 | 3.2792 | 2.8653 | 1.6406 | 1.5678 | **2.4240** |
| **115** | 2.9837 | 2.5200 | 2.3635 | 0.9062 | 1.9567 | **2.1460** |
| **116** | 3.0126 | 2.4733 | 1.4341 | 1.6430 | 2.9257 | **2.2977** |
| **117** | 3.2534 | 2.0076 | 2.9788 | 2.1834 | 0.9895 | **2.2825** |
| **118** | 2.3176 | 1.9033 | 2.6939 | 2.6500 | 2.1961 | **2.3522** |
| **119** | 3.3830 | 2.5653 | 2.4206 | 4.1341 | 2.1694 | **2.9345** |
| **120** | 2.6489 | 2.4422 | 1.9826 | 1.3202 | 1.0239 | **1.8836** |
| **121** | 3.4866 | 1.0420 | 3.2806 | 3.3260 | 1.9632 | **2.6197** |

Similarly, to assess the reliability of the conventional two-dimensional analysis of the TMJ space, the same five TMJs were analyzed by one investigator three times, one to two weeks apart, and

Pearson product-moment correlation coefficient was computed (Table 4, Figure 40). The correlation coefficient ranged from 0.9875 to 0.9888.

**Table 4.** Reliability data for the two-dimensional analysis (correlation coefficient).

| | Correlation Coefficient (r) |
|---|---|
| Trial 1 vs. 2 | 0.9860 |
| Trial 2 vs. 3 | 0.9875 |
| Trial 1 vs. 3 | 0.9888 |

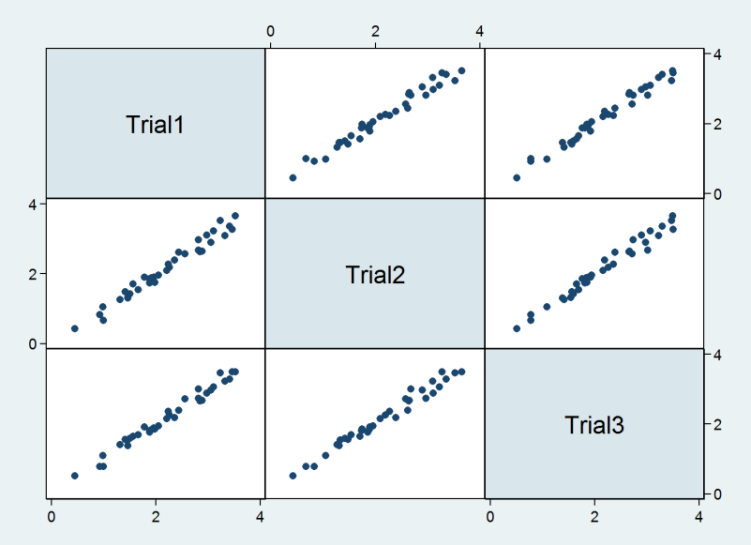


**Figure 40.** Scatter plot of repeated measurements from two-dimensional analysis.

**TMJ Space Changes in Orthognathic Surgery Patients**

All of the joint space data from the two- and three-dimensional analyses had a normal distribution, and hence paired t-test was considered appropriate to analyze the joint space difference between different time points. Anterior Space (AS) data from the two-dimensional analysis and corresponding approximated joint space measurement from the three-dimensional analysis for the three time points is shown in Table 5 and Figure 41.

**Table 5.** Anterior Space (AS) measurements from 2D and 3D analyses.

| | 2D Analysis | | | 3D Analysis | | |
|---|---|---|---|---|---|---|
| | T1 (pre-op) | T2 (post-op) | T3 (follow-up) | T1 (pre-op) | T2 (post-op) | T3 (follow-up) |
| **BS right** | 2.21 | 5.33 | 3.60 | 3.08 | 4.71 | 4.00 |
| **BS left** | 2.80 | 4.54 | 4.18 | 3.30 | 4.57 | 2.88 |
| **DK right** | 2.10 | 2.36 | 2.75 | 2.57 | 3.19 | 2.51 |
| **DK left** | 2.09 | 3.46 | 2.28 | 2.40 | 3.66 | 2.24 |
| **DC right** | 2.03 | 4.14 | 2.93 | 2.08 | 4.76 | 4.26 |
| **DC left** | 2.60 | 3.63 | 3.61 | 3.01 | 3.40 | 3.92 |
| **KW right** | 3.14 | 3.35 | 3.33 | 3.96 | 3.07 | 3.33 |
| **KW left** | 4.26 | 3.98 | 3.79 | 3.06 | 2.07 | 2.22 |
| **LS right** | 1.03 | 0.83 | 1.04 | 1.45 | 0.77 | 1.08 |
| **LS left** | 1.03 | 0.79 | 0.89 | 1.11 | 0.76 | 0.86 |
| **PB right** | 3.15 | 3.84 | 3.34 | 3.24 | 3.93 | 2.72 |
| **PB left** | 2.29 | 2.78 | 1.63 | 2.54 | 2.84 | 2.09 |
| **VA right** | 1.13 | 2.80 | 1.34 | 0.85 | 2.96 | 1.91 |
| **VA left** | 1.40 | 0.76 | 0.88 | 1.46 | 0.89 | 1.00 |
| **VN right** | 2.40 | 2.85 | 2.19 | 2.81 | 2.98 | 2.49 |
| **VN left** | 1.28 | 1.78 | 1.15 | 1.80 | 2.82 | 1.86 |
| **WT right** | 1.53 | 2.51 | 1.63 | 1.41 | 2.51 | 1.82 |
| **WT left** | 1.90 | 2.58 | 2.21 | 2.70 | 3.55 | 3.14 |
| **Average** | **2.13** | **2.91** | **2.38** | **2.38** | **2.97** | **2.46** |

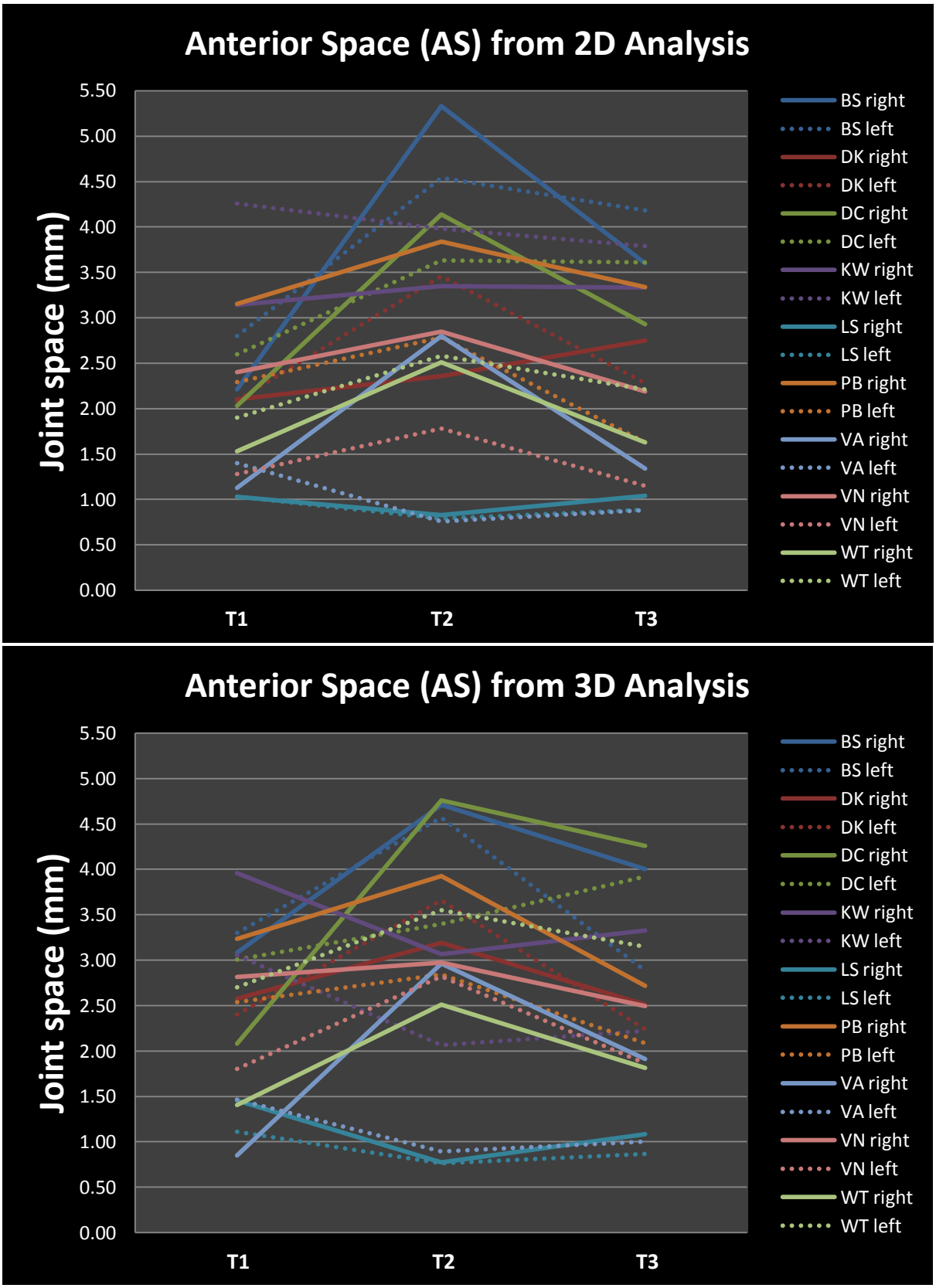


**Figure 41.** Anterior Space (AS) measurements from 2D (top) and 3D (bottom) analyses.

In both analyses, while majority of the sample showed a temporary increase in the AS from T1 to T2 followed by a decrease from T2 to T3, some displayed an opposite pattern. For two-dimensional analysis, on average, the AS significantly increased from 2.13mm at T1 to 2.91mm at T2 with *p*-value of 0.0015 and significantly decreased from T2 to 2.38mm at T3 with *p*-value of 0.0011. When comparing the measurements between T1 and T3, the difference was not statistically significant with *p*-value of 0.0531 (Figure 42). For three-dimensional analysis, on average, the AS significantly increased from 2.38mm at T1 to 2.97mm at T2 with *p*-value of 0.0133 and significantly decreased from T2 to 2.46mm at T3 with *p*-value of 0.0018. When comparing the measurements between T1 and T3, the difference was not statistically significant with *p*-value of 0.3457 (Figure 42).

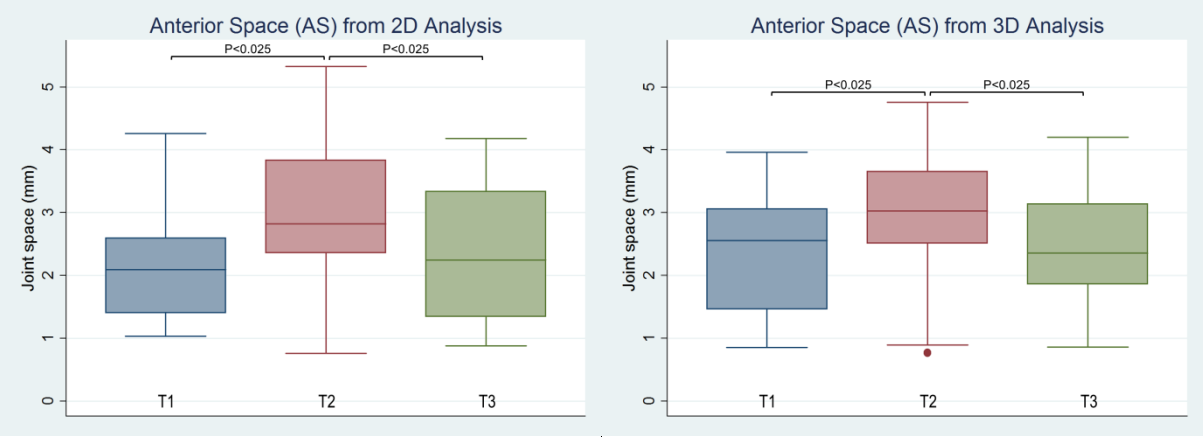


**Figure 42.** Box plots of AS measurements from 2D (left) and 3D (right) analyses.

Superior Space (SS) data from the two-dimensional analysis and corresponding approximated joint space measurement from the three-dimensional analysis for the three time points is shown in Table 6 and Figure 43.

**Table 6.** Superior Space (SS) measurements from 2D and 3D analyses.

| | 2D Analysis | | | 3D Analysis | | |
|---|---|---|---|---|---|---|
| | T1 (pre-op) | T2 (post-op) | T3 (follow-up) | T1 (pre-op) | T2 (post-op) | T3 (follow-up) |
| BS right | 1.06 | 2.29 | 1.48 | 3.08 | 4.71 | 4.00 |
| BS left | 1.34 | 2.30 | 2.66 | 3.30 | 4.57 | 2.88 |
| DK right | 2.18 | 2.04 | 2.03 | 2.57 | 3.19 | 2.51 |
| DK left | 0.70 | 2.31 | 1.25 | 2.40 | 3.66 | 2.24 |
| DC right | 1.17 | 1.89 | 1.63 | 2.08 | 4.76 | 4.26 |
| DC left | 2.06 | 2.93 | 3.04 | 3.01 | 3.40 | 3.92 |
| KW right | 1.91 | 1.16 | 2.15 | 3.96 | 3.07 | 3.33 |
| KW left | 2.57 | 1.80 | 3.29 | 3.06 | 2.07 | 2.22 |
| LS right | 2.55 | 3.34 | 2.61 | 1.45 | 0.77 | 1.08 |
| LS left | 2.02 | 1.74 | 2.61 | 1.11 | 0.76 | 0.86 |
| PB right | 1.88 | 1.25 | 1.53 | 3.24 | 3.93 | 2.72 |
| PB left | 1.25 | 1.17 | 1.67 | 2.54 | 2.84 | 2.09 |
| VA right | 1.06 | 1.88 | 1.13 | 0.85 | 2.96 | 1.91 |
| VA left | 0.85 | 0.74 | 0.78 | 1.46 | 0.89 | 1.00 |
| VN right | 1.84 | 1.41 | 2.65 | 2.81 | 2.98 | 2.49 |
| VN left | 1.02 | 1.30 | 0.95 | 1.80 | 2.82 | 1.86 |
| WT right | 1.24 | 2.32 | 1.13 | 1.41 | 2.51 | 1.82 |
| WT left | 1.27 | 2.40 | 1.75 | 2.70 | 3.55 | 3.14 |
| Average | **1.55** | **1.90** | **1.91** | **2.38** | **2.97** | **2.46** |

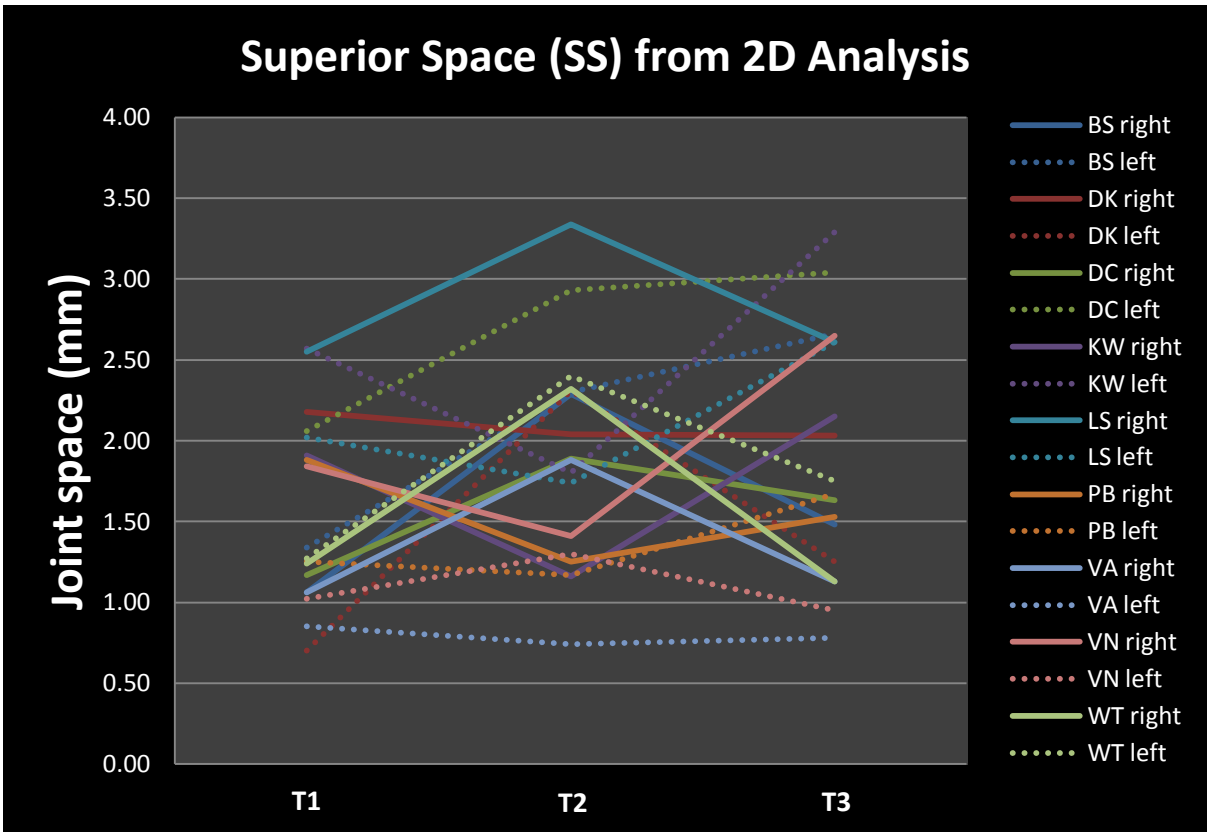


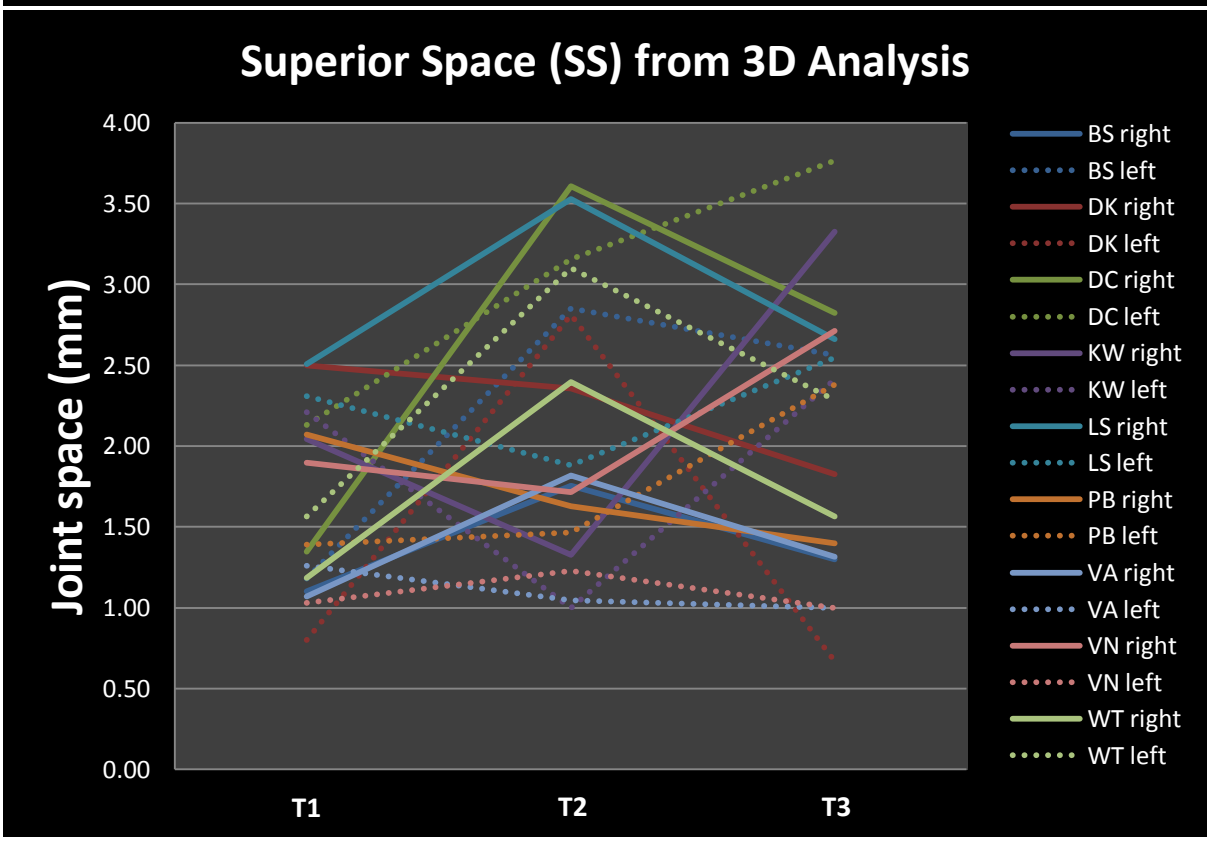


**Figure 43.** Superior Space (SS) measurements from 2D (top) and 3D (bottom) analyses.

In both analyses, many of the sample showed a temporary increase in the SS from T1 to T2 followed by a decrease from T2 to T3, some displayed an opposite pattern, and others showed continual increase. For two-dimensional analysis, on average, the SS had a tendency to increase from 1.55mm at T1 to 1.90mm at T2, which was not statistically significant with *p*-value of 0.0334, and no difference was seen from T2 to 1.91mm at T3 with *p*-value of 0.4919. However, there was a significant increase when comparing T1 to T3 with *p*-value of 0.0017 (Figure 44). For three-dimensional analysis, on average, the SS significantly increased from 2.38mm at T1 to 2.97mm at T2 with *p*-value of 0.0133 and significantly decreased from T2 to 2.46mm at T3 with *p*-value of 0.0018. When comparing the measurements between T1 and T3, the difference was not statistically significant with *p*-value of 0.3457 (Figure 44).

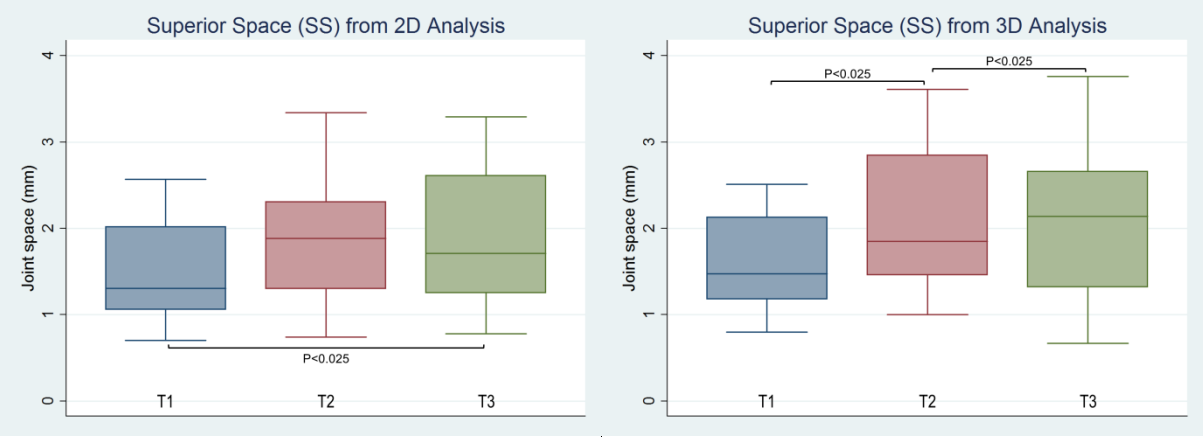


**Figure 44.** Box plots of SS measurements from 2D (left) and 3D (right) analyses.

Posterior Space (PS) data from the two-dimensional analysis and corresponding approximated joint space measurement from the three-dimensional analysis for the three time points is shown in Table 7 and Figure 45.

**Table 7.** Posterior Space (PS) measurements from 2D and 3D analyses.

| | 2D Analysis | | | 3D Analysis | | |
|---|---|---|---|---|---|---|
| | T1 (pre-op) | T2 (post-op) | T3 (follow-up) | T1 (pre-op) | T2 (post-op) | T3 (follow-up) |
| **BS right** | 0.70 | 1.25 | 1.43 | 0.81 | 1.16 | 1.81 |
| **BS left** | 1.25 | 1.96 | 1.38 | 1.51 | 2.12 | 1.59 |
| **DK right** | 1.21 | 0.87 | 0.73 | 1.60 | 0.91 | 0.91 |
| **DK left** | 0.79 | 1.99 | 1.10 | 1.21 | 2.28 | 1.25 |
| **DC right** | 1.28 | 0.96 | 0.85 | 1.88 | 1.25 | 0.67 |
| **DC left** | 1.67 | 5.22 | 2.45 | 2.02 | 4.48 | 3.37 |
| **KW right** | 1.21 | 0.65 | 1.64 | 1.00 | 0.90 | 2.09 |
| **KW left** | 1.12 | 0.46 | 1.67 | 1.28 | 0.50 | 1.88 |
| **LS right** | 1.68 | 3.67 | 1.61 | 1.69 | 3.79 | 1.66 |
| **LS left** | 1.44 | 1.39 | 1.27 | 1.24 | 1.35 | 1.39 |
| **PB right** | 1.34 | 0.58 | 1.87 | 1.14 | 0.84 | 0.87 |
| **PB left** | 0.95 | 0.48 | 1.88 | 1.00 | 0.60 | 1.67 |
| **VA right** | 1.15 | 0.75 | 0.60 | 1.36 | 1.60 | 1.16 |
| **VA left** | 0.69 | 0.66 | 0.66 | 1.52 | 1.14 | 1.53 |
| **VN right** | 1.20 | 0.92 | 2.32 | 1.32 | 0.72 | 2.90 |
| **VN left** | 0.67 | 0.86 | 0.83 | 1.25 | 1.59 | 1.61 |
| **WT right** | 1.05 | 1.20 | 1.24 | 1.50 | 1.50 | 1.97 |
| **WT left** | 0.98 | 0.69 | 0.95 | 1.11 | 0.80 | 1.50 |
| **Average** | **1.13** | **1.36** | **1.36** | **1.36** | **1.53** | **1.66** |

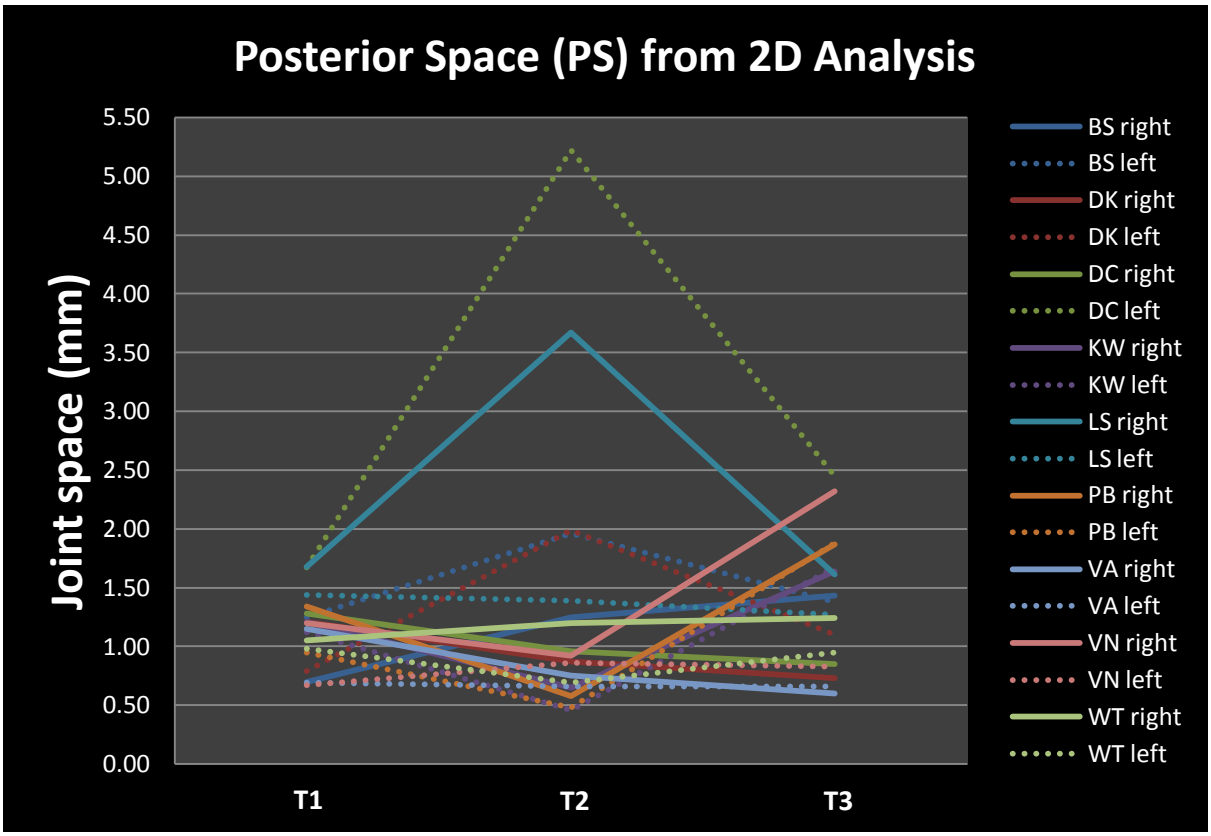


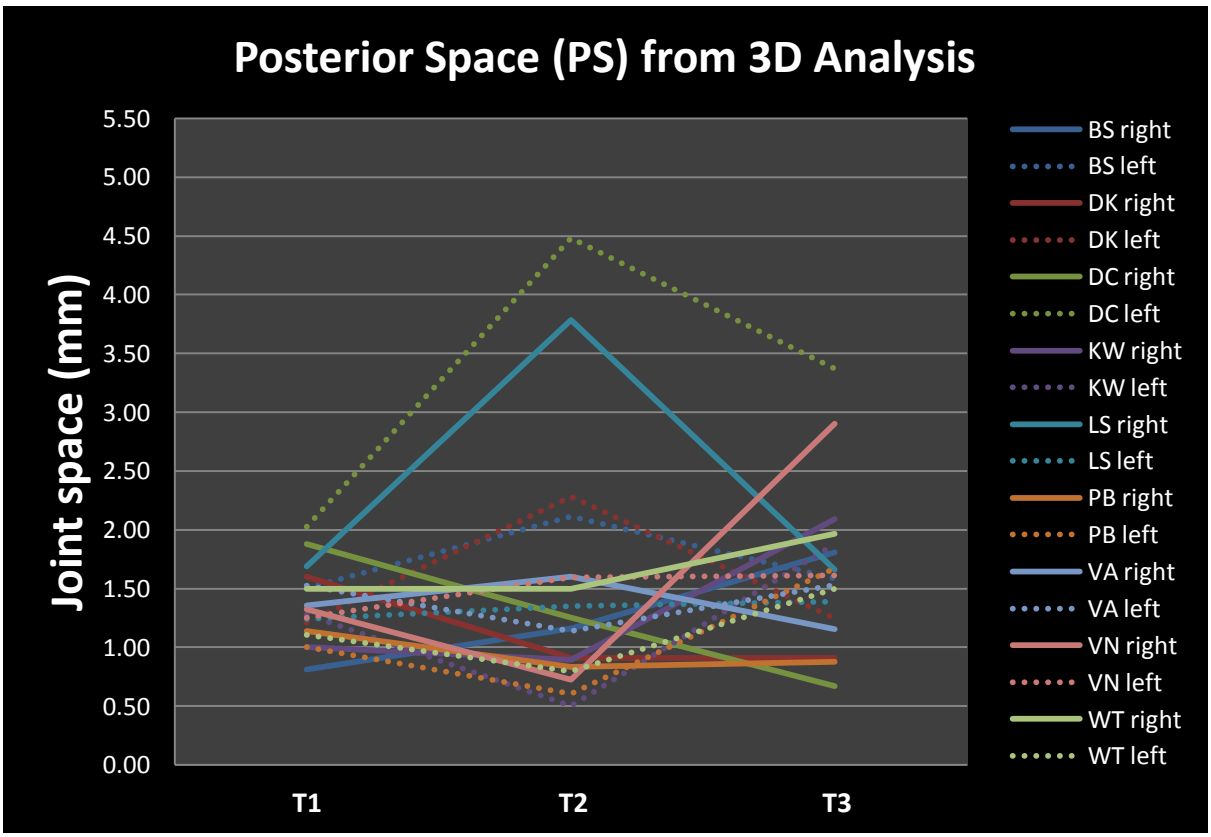


**Figure 45.** Posterior Space (SS) measurements from 2D (top) and 3D (bottom) analyses.

In both analyses, two of the sample showed a dramatic increase in PS from T1 to T2 followed by a decrease from T2 to T3, while many of the sample showed smaller magnitude of change in various patterns. For both analyses, none of the differences between the time points was significant. For two-dimensional analysis, on average, the PS very slightly increased from 1.13mm at T1 to 1.36mm at T2 with *p*-value of 0.1881 and remained the same from T2 to 1.36mm at T3 with *p*-value of 0.4934. The *p*-value of the small difference between T1 and T3 was 0.0317 (Figure 46). Similarly, for three-dimensional analysis, the PS very slightly increased from 1.36mm at T1 to 1.53mm at T2 with *p*-value of 0.2174 and increased even less from T2 to T3 with *p*-value of 0.4899. The *p*-value of the difference between T1 and T3 was 0.2025 (Figure 46).

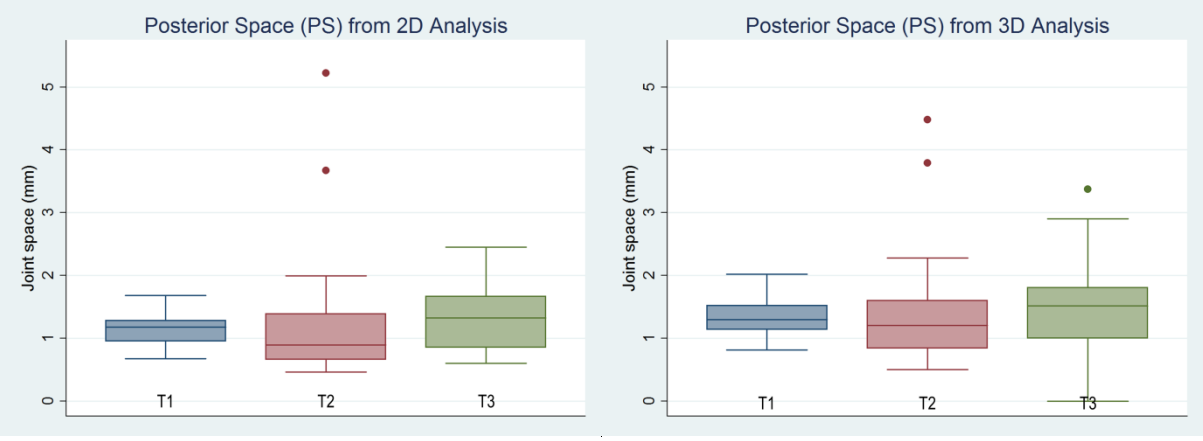


**Figure 46.** Box plots of PS measurements from 2D (left) and 3D (right) analyses.

Coronal Lateral Space (CLS) data from the two-dimensional analysis and corresponding approximated joint space measurement from the three-dimensional analysis for the three time points is shown in Table 8 and Figure 47. Samples with missing data for different time points were excluded from the respective paired t-test.

**Table 8.** Coronal Lateral Space (CLS) measurements from 2D and 3D analyses.

| | 2D Analysis | | | 3D Analysis | | |
|---|---|---|---|---|---|---|
| | T1 (pre-op) | T2 (post-op) | T3 (follow-up) | T1 (pre-op) | T2 (post-op) | T3 (follow-up) |
| BS right | 0.63 | 0.70 | 0.52 | 1.02 | 0.79 | 1.16 |
| BS left | 0.89 | 1.14 | 1.18 | 1.35 | 2.32 | 1.68 |
| DK right | 2.79 | 1.64 | 2.00 | 2.77 | 1.64 | 1.89 |
| DK left | 0.79 | 2.07 | 1.16 | 0.80 | 2.20 | 0.99 |
| DC right | 1.72 | 2.19 | 2.17 | 1.70 | 2.10 | 2.60 |
| DC left | 2.49 | | 1.87 | 2.91 | | |
| KW right | 0.67 | 0.50 | 1.10 | 1.00 | 0.84 | 1.50 |
| KW left | 1.38 | 0.61 | 1.21 | 1.71 | 0.81 | 1.63 |
| LS right | 1.58 | 2.57 | 2.95 | 1.87 | 2.43 | 2.33 |
| LS left | 2.21 | 1.50 | 1.85 | 1.25 | 1.46 | 1.93 |
| PB right | 2.12 | 1.83 | 1.82 | 2.89 | 1.92 | 1.80 |
| PB left | 1.28 | 1.26 | 2.24 | 1.18 | 1.30 | 1.50 |
| VA right | 0.81 | 0.72 | 0.47 | 0.86 | 1.06 | 0.68 |
| VA left | 0.87 | 0.82 | 0.77 | 0.95 | 0.65 | 0.73 |
| VN right | 1.84 | 0.71 | 2.56 | 2.23 | 1.00 | 4.11 |
| VN left | 0.82 | 1.49 | 1.02 | 0.81 | 0.82 | 1.74 |
| WT right | 1.08 | 0.95 | 1.03 | 1.27 | 1.05 | 1.30 |
| WT left | 2.14 | 3.86 | 2.18 | 1.64 | 0.95 | 1.18 |
| **Average** | **1.45** | **1.44** | **1.56** | **1.57** | **1.37** | **1.69** |

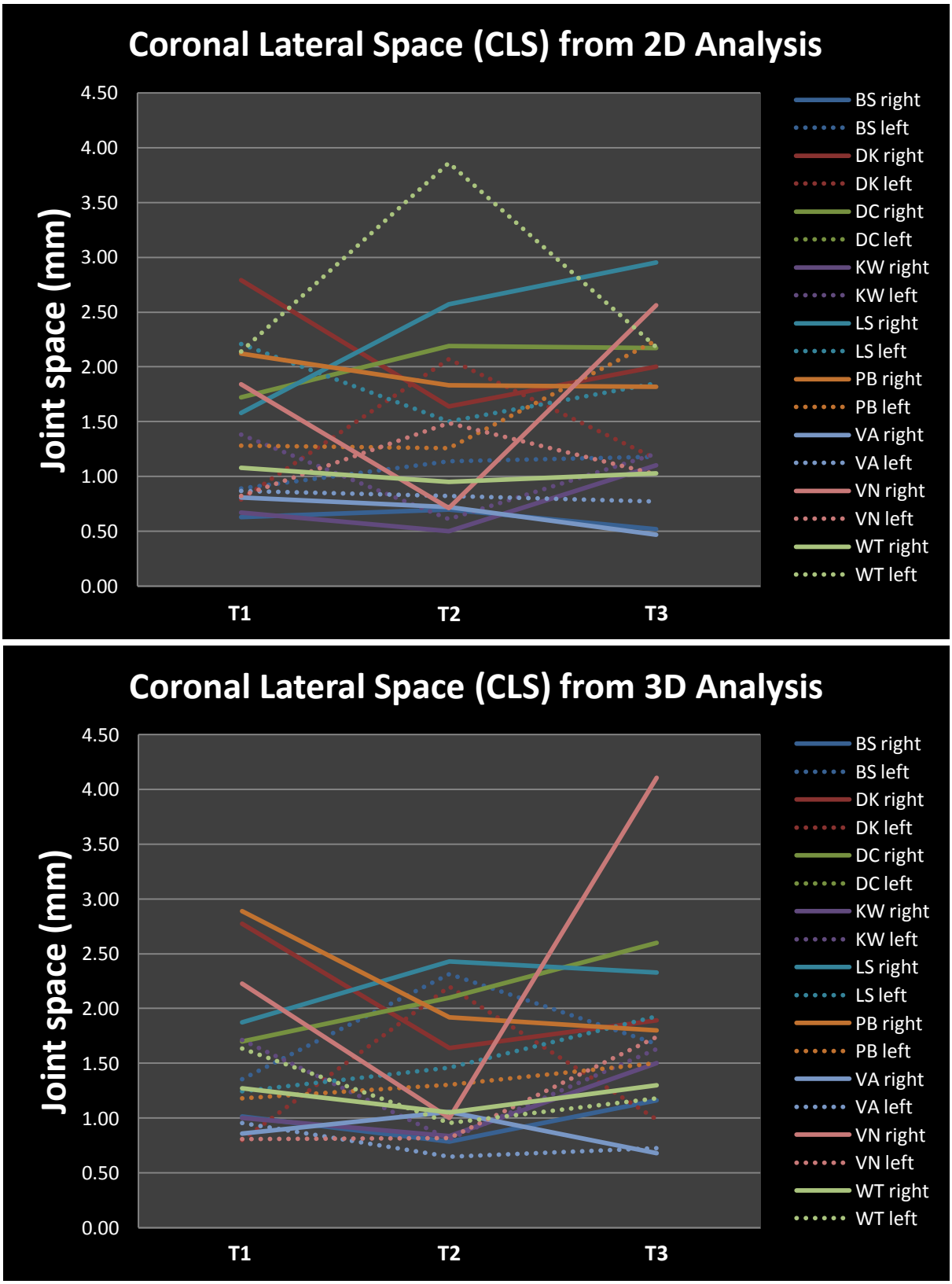


**Figure 47.** Coronal Lateral Space (CLS) measurements from 2D (top) and 3D (bottom) analyses.

In both analyses, there was no evident pattern in the change of CLS, and none of the differences between the time points was significant. For two-dimensional analysis, on average, the CLS very slightly increased from 1.39mm (adjusted average after removing the pair with missing data for paired comparison) at T1 to 1.44mm at T2 with *p*-value of 0.3889 and very slightly increased from T2 to 1.54mm (adjusted average) at T3 with *p*-value of 0.3014. The *p*-value of the small increase from 1.45mm at T1 to T3 was 0.2028 (Figure 48). For three-dimensional analysis, the CLS very slightly decreased from 1.49mm (adjusted average) at T1 to 1.37mm at T2 with *p*-value of 0.2615 and slightly increased from T2 to 1.69mm at T3 with *p*-value of 0. 0807. The *p*-value of the difference between T1 and T3 was 0.1264 (Figure 48).

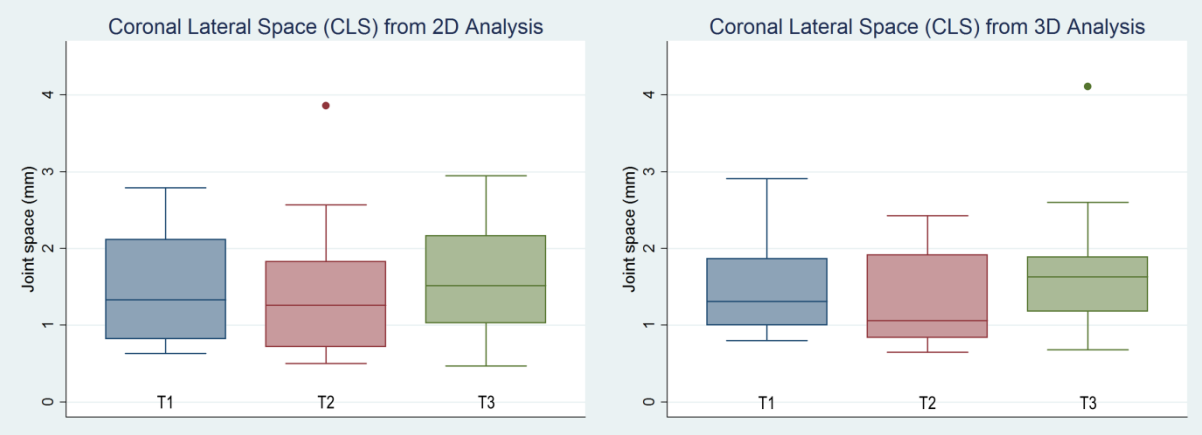


**Figure 48.** Box plots of CLS measurements from 2D (left) and 3D (right) analyses.

Coronal Central Space (CCS) data from the two-dimensional analysis and corresponding approximated joint space measurement from the three-dimensional analysis for the three time points is shown in Table 9 and Figure 49.

**Table 9.** Coronal Central Space (CCS) measurements from 2D and 3D analyses.

| | 2D Analysis | | | 3D Analysis | | |
|---|---|---|---|---|---|---|
| | T1 (pre-op) | T2 (post-op) | T3 (follow-up) | T1 (pre-op) | T2 (post-op) | T3 (follow-up) |
| BS right | 1.13 | 2.19 | 1.59 | 1.30 | 2.30 | 1.80 |
| BS left | 1.02 | 2.09 | 2.39 | 1.22 | 2.25 | 2.27 |
| DK right | 2.29 | 2.01 | 1.92 | 2.40 | 2.05 | 1.75 |
| DK left | 1.02 | 2.72 | 1.41 | 1.20 | 3.39 | 1.27 |
| DC right | 1.94 | 3.97 | 2.50 | 2.10 | 4.76 | 3.10 |
| DC left | 2.80 | 3.57 | 3.20 | 2.30 | 3.50 | 4.39 |
| KW right | 1.87 | 1.13 | 2.36 | 1.43 | 1.00 | 2.61 |
| KW left | 2.51 | 1.66 | 2.97 | 2.57 | 1.50 | 2.50 |
| LS right | 2.63 | 3.91 | 2.94 | 2.31 | 3.79 | 2.33 |
| LS left | 1.86 | 1.50 | 2.26 | 1.69 | 1.53 | 2.13 |
| PB right | 2.00 | 2.56 | 2.20 | 2.01 | 1.99 | 2.01 |
| PB left | 1.30 | 1.56 | 1.16 | 0.94 | 1.34 | 1.13 |
| VA right | 1.13 | 1.56 | 1.06 | 1.00 | 2.27 | 1.46 |
| VA left | 0.92 | 0.78 | 0.49 | 0.95 | 0.89 | 0.89 |
| VN right | 1.48 | 1.37 | 2.27 | 1.53 | 1.60 | 2.42 |
| VN left | 0.70 | 1.27 | 1.13 | 1.10 | 1.41 | 1.54 |
| WT right | 1.03 | 3.09 | 1.17 | 1.46 | 3.09 | 1.32 |
| WT left | 1.07 | 1.92 | 1.49 | 0.85 | 2.20 | 1.87 |
| Average | **1.59** | **2.16** | **1.92** | **1.58** | **2.27** | **2.04** |

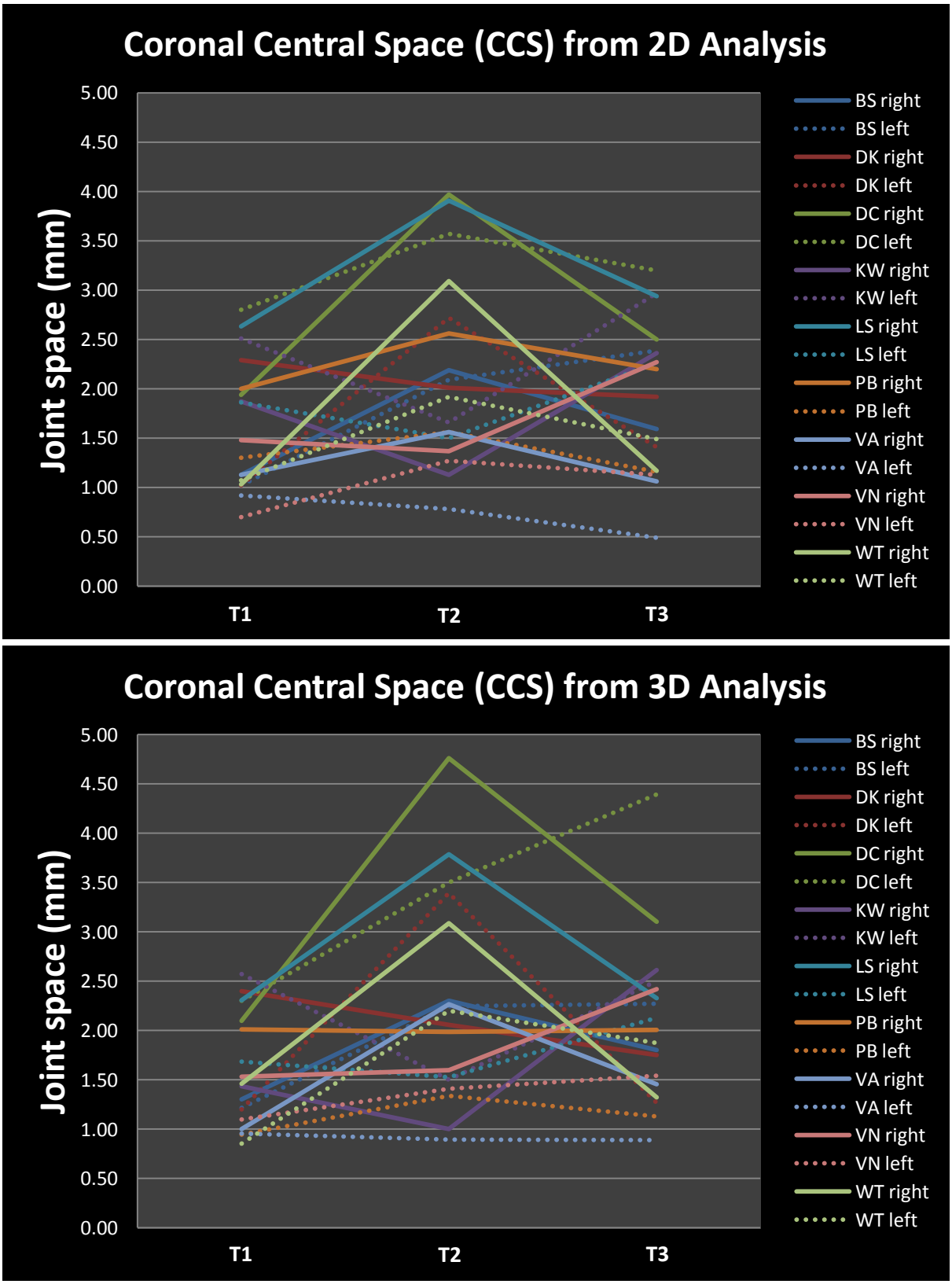


**Figure 49.** Coronal Central Space (CCS) measurements from 2D (top) and 3D (bottom) analyses.

In both analyses, majority of the sample showed a temporary increase in the CCS from T1 to T2 followed by a decrease from T2 to T3, a few displayed an opposite pattern, and few others showed continual increase/decrease. For two-dimensional analysis, on average, the CCS significantly increased from 1.59mm at T1 to 2.16mm at T2 with *p*-value of 0.0072 and slightly decreased from T2 to 1.92mm at T3 with *p*-value of 0.1329. Furthermore, there was a significant increase when comparing T1 to T3 with *p*-value of 0.0021 (Figure 50). Similarly, for three-dimensional analysis, on average, the SS significantly increased from 1.58mm at T1 to 2.27mm at T2 with *p*-value of 0.0097 and slightly decreased from T2 to 2.04mm at T3 with *p*-value of 0.3213. When comparing the measurements between T1 and T3, CCS at T3 was significantly larger with *p*-value of 0.0022 (Figure 50).

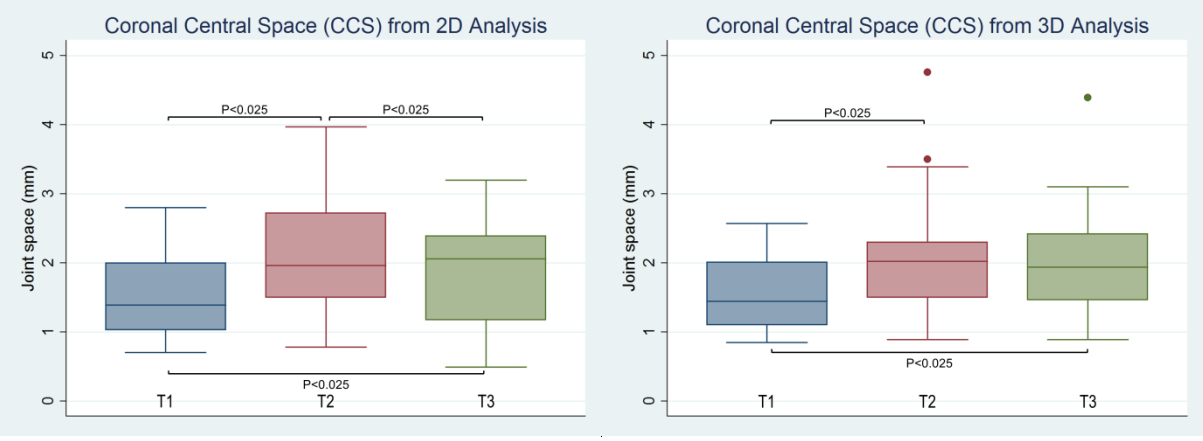


**Figure 50.** Box plots of CCS measurements from 2D (left) and 3D (right) analyses.

Coronal Medial Space (CMS) data from the two-dimensional analysis and corresponding approximated joint space measurement from the three-dimensional analysis for the three time points is shown in Table 10 and Figure 51.

**Table 10.** Coronal Medial Space (CMS) measurements from 2D and 3D analyses.

| | 2D Analysis | | | 3D Analysis | | |
|---|---|---|---|---|---|---|
| | T1 (pre-op) | T2 (post-op) | T3 (follow-up) | T1 (pre-op) | T2 (post-op) | T3 (follow-up) |
| BS right | 1.14 | 2.74 | 1.91 | 1.22 | 2.97 | 2.32 |
| BS left | 1.21 | 3.21 | 2.04 | 1.70 | 4.57 | 1.51 |
| DK right | 1.17 | 2.08 | 1.60 | 1.60 | 2.30 | 1.88 |
| DK left | 1.13 | 3.12 | 1.66 | 1.20 | 3.44 | 1.34 |
| DC right | 0.92 | 4.83 | 3.49 | 1.40 | 5.30 | 3.32 |
| DC left | 1.61 | 5.57 | 2.67 | 1.61 | 5.88 | 2.59 |
| KW right | 2.32 | 1.47 | 2.79 | 2.38 | 1.21 | 4.54 |
| KW left | 2.48 | 2.06 | 3.09 | 2.43 | 1.65 | 3.40 |
| LS right | 2.23 | 2.07 | 2.23 | 3.37 | 3.73 | 2.99 |
| LS left | 1.51 | 1.41 | 2.12 | 2.62 | 1.75 | 2.27 |
| PB right | 2.03 | 2.40 | 0.58 | 2.34 | 2.32 | 1.00 |
| PB left | 2.15 | 1.59 | 1.41 | 1.99 | 2.07 | 2.26 |
| VA right | 0.96 | 1.80 | 1.21 | 1.30 | 1.90 | 1.72 |
| VA left | 0.70 | 0.55 | 0.64 | 1.15 | 1.06 | 0.90 |
| VN right | 0.64 | 1.59 | 1.83 | 1.22 | 2.20 | 2.66 |
| VN left | 0.54 | 0.56 | 0.70 | 1.25 | 1.84 | 1.50 |
| WT right | 1.45 | 3.76 | 1.20 | 1.80 | 3.27 | 1.50 |
| WT left | 1.00 | 0.95 | 0.75 | 1.98 | 3.60 | 2.28 |
| **Average** | **1.40** | **2.32** | **1.77** | **1.81** | **2.84** | **2.22** |

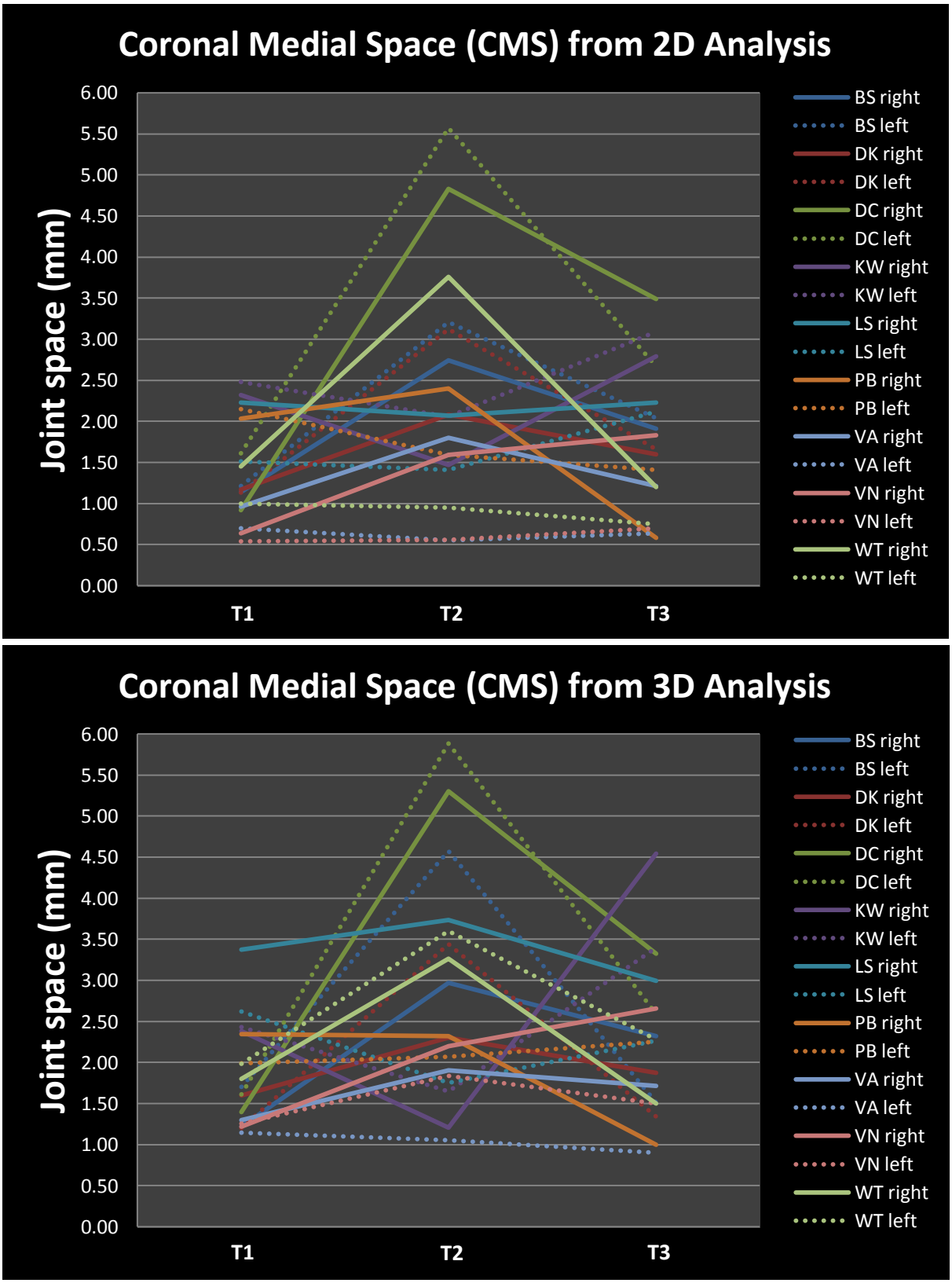


**Figure 51.** Coronal Medial Space (CMS) measurements from 2D (top) and 3D (bottom) analyses.

In both analyses, majority of the sample showed a temporary increase in the CMS from T1 to T2 followed by a decrease from T2 to T3, a few displayed an opposite pattern, and few others showed continual increase/decrease. For two-dimensional analysis, on average, the CMS significantly increased from 1.40mm at T1 to 2.32mm at T2 with *p*-value of 0.0075 and decreased from T2 to 1.77mm at T3 with *p*-value of 0.0311. There was a non-significant increase when comparing T1 to T3 with *p*-value of 0.0393 (Figure 52). Similarly, for three-dimensional analysis, on average, the CMS significantly increased from 1.81mm at T1 to 2.84mm at T2 with *p*-value of 0.0059 and decreased from T2 to 2.22mm at T3 with *p*-value of 0.0621. There was a non-significant increase when comparing T1 to T3 with *p*-value of 0.0319 (Figure 52).

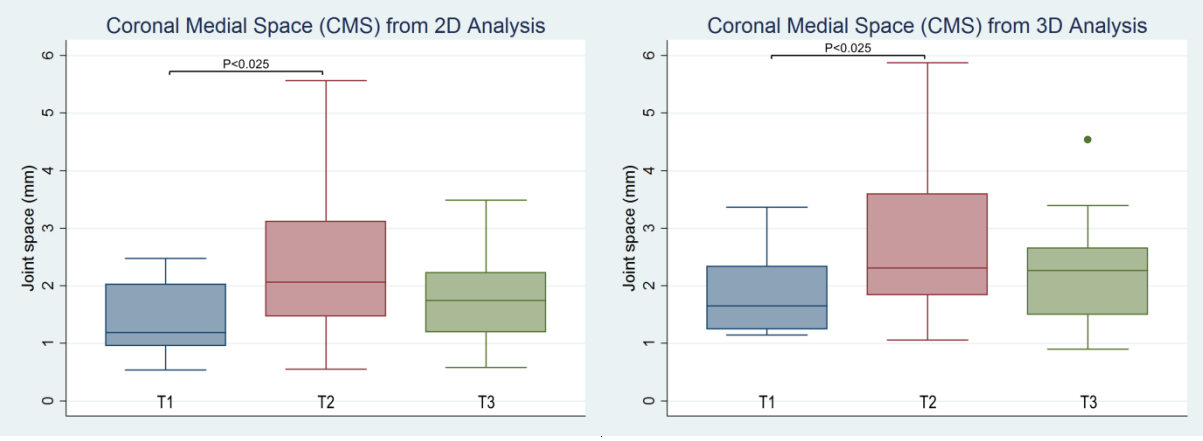


**Figure 52.** Box plots of CMS measurements from 2D (left) and 3D (right) analyses.

Axial Lateral Space (ALS) data from the two-dimensional analysis and corresponding approximated joint space measurement from the three-dimensional analysis for the three time points is shown in Table 11 and Figure 53. Samples with missing data for different time points were excluded from the respective paired t-test.

**Table 11.** Axial Lateral Space (ALS) measurements from 2D and 3D analyses.

| | 2D Analysis | | | 3D Analysis | | |
|---|---|---|---|---|---|---|
| | T1 (pre-op) | T2 (post-op) | T3 (follow-up) | T1 (pre-op) | T2 (post-op) | T3 (follow-up) |
| BS right | 2.23 | | 2.57 | 2.96 | | 1.40 |
| BS left | 1.80 | | | 2.00 | | |
| DK right | 4.82 | 3.50 | 3.42 | 5.01 | 3.00 | 3.35 |
| DK left | 2.11 | | 1.62 | 2.16 | 2.70 | 2.06 |
| DC right | 2.05 | | | 1.70 | 1.63 | |
| DC left | | | | | | |
| KW right | | 1.41 | | 1.92 | 1.10 | 1.80 |
| KW left | | 1.27 | 1.98 | | 1.27 | 1.09 |
| LS right | | | | 3.26 | | 3.07 |
| LS left | | | | 1.75 | 1.75 | 2.70 |
| PB right | | | 3.33 | | 2.72 | 2.17 |
| PB left | 1.54 | 1.89 | 1.48 | 2.23 | | 2.51 |
| VA right | 0.75 | 0.85 | 0.78 | 0.56 | 0.85 | 0.84 |
| VA left | 0.81 | 0.64 | 0.80 | 0.84 | 0.65 | 0.77 |
| VN right | 2.52 | 1.91 | 2.62 | 2.78 | 0.98 | 3.01 |
| VN left | 0.84 | 0.52 | 0.77 | 1.92 | 1.22 | 1.34 |
| WT right | 1.56 | 1.06 | 1.33 | 1.00 | 0.58 | 1.00 |
| WT left | 1.19 | 0.56 | 0.85 | 1.10 | 0.59 | 0.95 |
| **Average** | **1.85** | **1.36** | **1.80** | **2.08** | **1.46** | **1.87** |

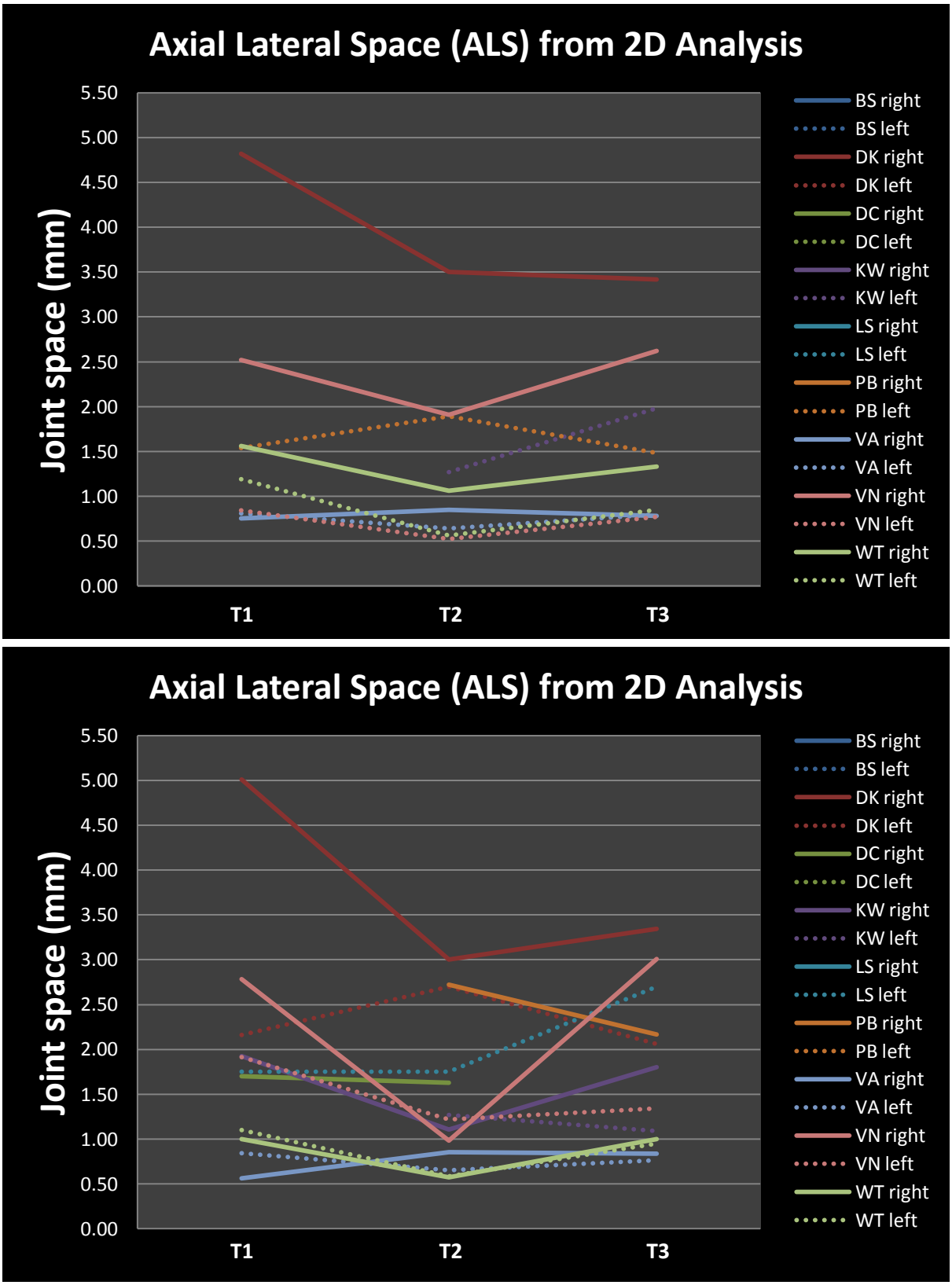


**Figure 53.** Axial Lateral Space (ALS) measurements from 2D (top) and 3D (bottom) analyses.

In both analyses, many joint space measurements were unavailable, and none of the differences between the time points was significant due to the small amount of data. Majority of the available data showed a temporary decrease in the ALS from T1 to T2 followed by an increase from T2 to T3. For two-dimensional analysis, on average, the ALS decreased from 1.75mm (adjusted average) at T1 to 1.37mm (adjusted average) at T2 with *p*-value of 0.0345 and increased from 1.36mm (adjusted average) at T2 to 1.56mm (adjusted average) at T3 with *p*-value of 0.0662. There was a slight decrease in ALS from 1.84mm (adjusted average) at T1 to 1.62mm (adjusted average) at T3 with *p*-value of 0.0959 (Figure 54). Similarly, for three-dimensional analysis, on average, the ALS decreased from 1.89mm (adjusted average) at T1 to 1.37mm (adjusted average) at T2 with *p*-value of 0.00284 and increased from 1.45mm (adjusted average) at T2 to 1.76mm (adjusted average) at T3 with *p*-value of 0.0827. ALS increased from 2.11mm (adjusted average) at T1 to 1.91mm (adjusted average) at T3 with *p*-value of 0.1593 (Figure 54).

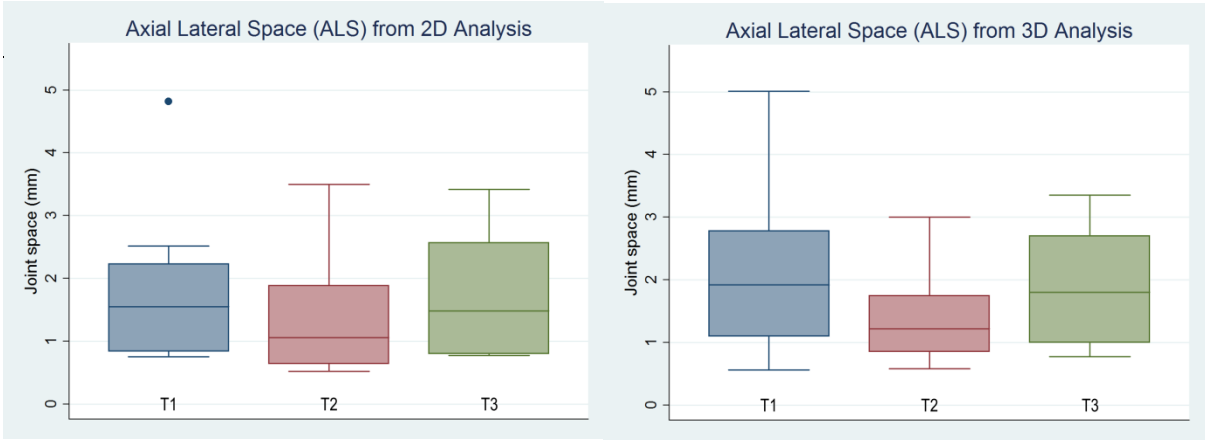


**Figure 54.** Box plots of ALS measurements from 2D (left) and 3D (right) analyses.

Axial Medial Space (AMS) data from the two-dimensional analysis and corresponding approximated joint space measurement from the three-dimensional analysis for the three time points is shown in Table 12 and Figure 55.

**Table 12.** Axial Medial Space (AMS) measurements from 2D and 3D analyses.

| | 2D Analysis | | | 3D Analysis | | |
|---|---|---|---|---|---|---|
| | T1 (pre-op) | T2 (post-op) | T3 (follow-up) | T1 (pre-op) | T2 (post-op) | T3 (follow-up) |
| BS right | 2.83 | 2.53 | 2.94 | 1.84 | 2.00 | 3.50 |
| BS left | 2.93 | 3.12 | 4.25 | 3.52 | 4.23 | 3.41 |
| DK right | 1.91 | 2.90 | 2.48 | 3.14 | 5.70 | 4.10 |
| DK left | 2.55 | 3.57 | 1.79 | 2.65 | 5.20 | 3.50 |
| DC right | 1.75 | 6.30 | 5.45 | 3.12 | 6.41 | 5.99 |
| DC left | 1.70 | 8.35 | 4.77 | 2.34 | 7.46 | 5.18 |
| KW right | 7.26 | 5.13 | 7.27 | 3.93 | 1.85 | 3.96 |
| KW left | 5.76 | 4.54 | 5.01 | 3.93 | 2.52 | 2.14 |
| LS right | 2.26 | 2.25 | 2.27 | 3.51 | 5.42 | 2.54 |
| LS left | 2.42 | 1.82 | 2.67 | 2.75 | 2.11 | 2.68 |
| PB right | 2.77 | 2.24 | 1.75 | 2.67 | 2.38 | 1.41 |
| PB left | 4.47 | 4.50 | 3.71 | 3.93 | 3.71 | 1.46 |
| VA right | 0.63 | 1.56 | 0.95 | 0.79 | 1.56 | 1.00 |
| VA left | 0.93 | 0.82 | 1.13 | 0.83 | 1.00 | 0.73 |
| VN right | 1.41 | 3.77 | 4.33 | 1.46 | 2.40 | 2.89 |
| VN left | 1.03 | 1.59 | 1.66 | 2.73 | 2.32 | 2.55 |
| WT right | 0.99 | 3.76 | 1.30 | 0.82 | 2.52 | 1.25 |
| WT left | 2.65 | 3.52 | 3.05 | 2.42 | 3.80 | 3.10 |
| **Average** | **2.57** | **3.46** | **3.15** | **2.58** | **3.48** | **2.86** |

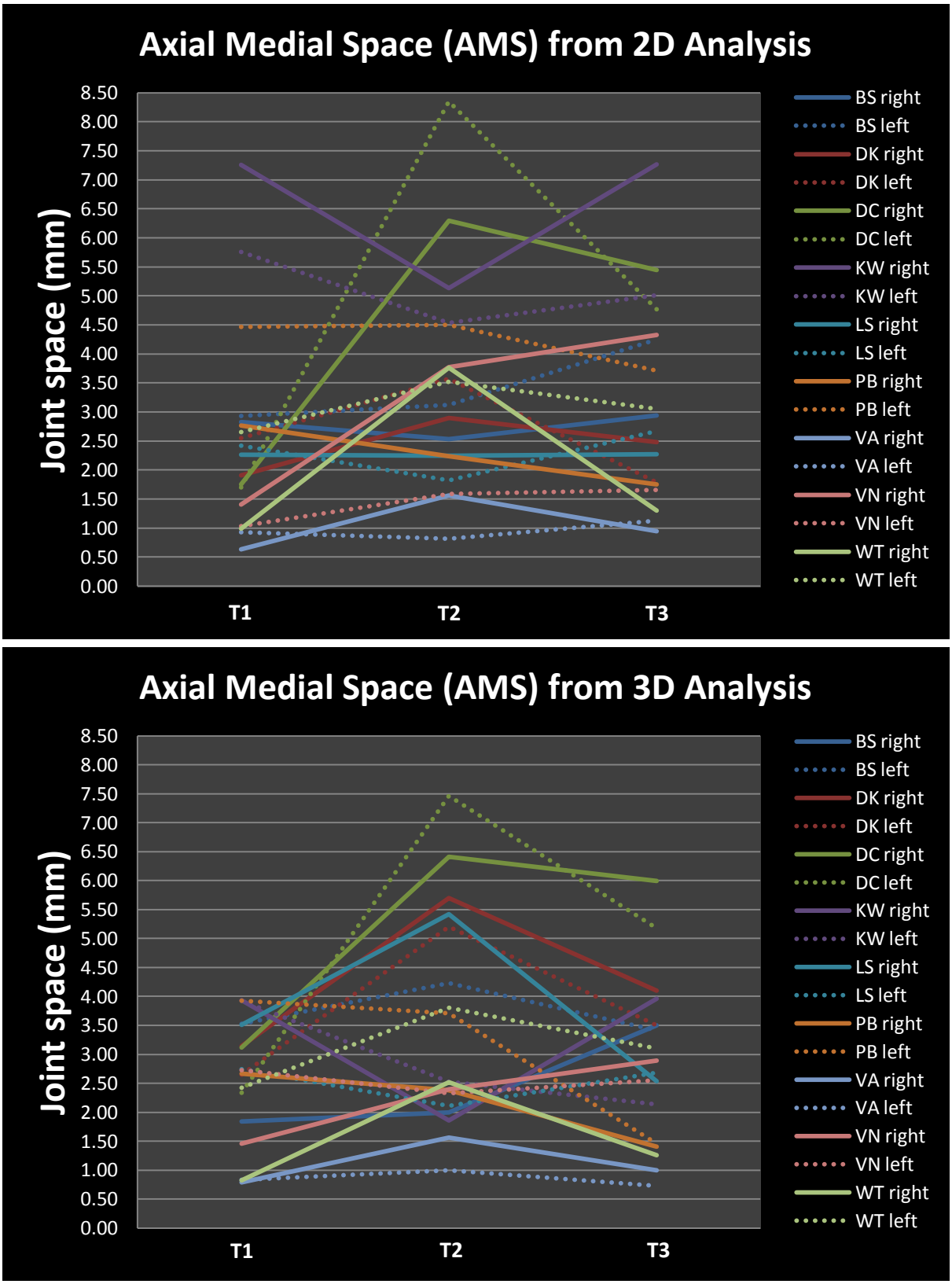


**Figure 55.** Axial Medial Space (AMS) measurements from 2D (top) and 3D (bottom) analyses.

In both analyses, majority of the sample showed a temporary increase in the AMS from T1 to T2 followed by a decrease from T2 to T3, while some displayed an opposite pattern. For two-dimensional analysis, none of the differences between the time points was statistically significant. On average, the AMS increased from 2.57mm at T1 to 3.46mm at T2 with *p*-value of 0.0447 and decreased from T2 to 3.15mm at T3 with *p*-value of 0.0292. There was an increase in AMS from T1 to T3, but the difference was non-significant with *p*-value of 0.0422 (Figure 56). For three-dimensional analysis, the only significant difference in AMS was the increase from 2.58mm at T1 to 3.48mm at T2 with *p*-value of 0.0225. AMS then decreased from T2 to 2.86mm at T3 with *p*-value of 0.0292. There was a non-significant increase when comparing T1 to T3 with *p*-value of 0.2074 (Figure 56).

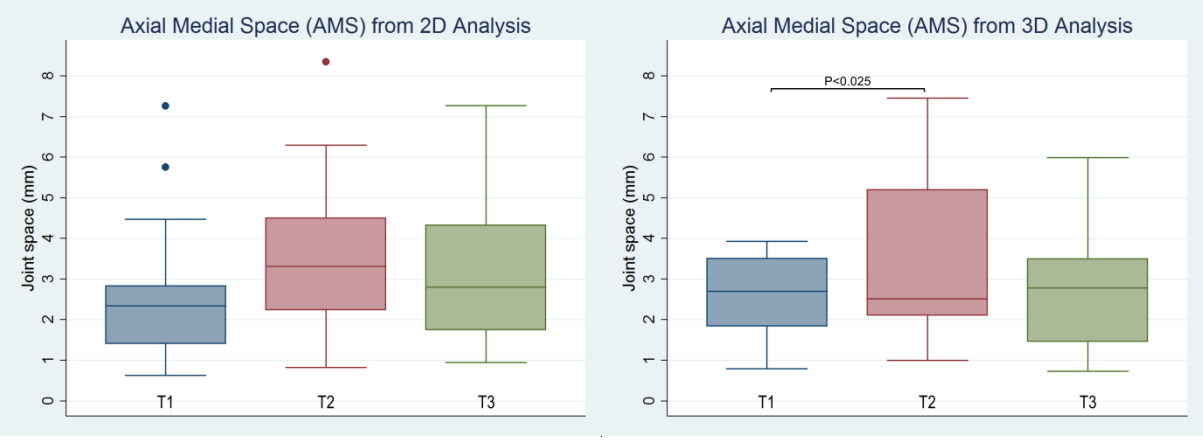


**Figure 56.** Box plots of AMS measurements from 2D (left) and 3D (right) analyses.

# DISCUSSION

## Optimal Patch Density

In establishing the protocol for the novel semi-automated three-dimensional TMJ space analysis using Stratovan Checkpoint, it was necessary to determine which patch density is most effective. Ultimately, optimal patch density should provide sufficient condylar points as well as landmarks on the opposing fossa to capture the changes in joint space and the subtle changes in the condylar shape. Comparing the plot of the fourteen TMJs on PC 1 and PC 2 axes across five groups of different patch densities ranging from 5x5 to 13x13 (Figure 35) suggested that 7x7 patch density (49 condyle landmarks) may be sufficient to capture the shape variations associated with PC 1 and PC 2, since increasing the landmark density to 9x9, 11x11, and 13x13 did not visually change the scatter of the data points. However, when evaluating the pattern on PC 3 and PC 4 axes (Figure 38), both 5x5 and 7x7 groups seemed to differ from the higher density groups, which in turn proposed that patch density of 9x9 (81 condyle landmarks) or higher would be optimal. While reviewing the fourteen TMJs with a range of shape variation and visually assessing the amount of morphological detail of a condyle one could capture with different patch densities, 11x11 (121 condyle landmarks and higher appeared to best represent the actual contour of the condyle, as 5x5 and 7x7 patches often missed concavities present on condylar surfaces, and 9x9 patch did not quite accurately capture the extent of the defect (Figure

57). The illustration demonstrates one such case of a condyle with localized resorption. Since the lowest patch density that effectively captures the joint morphology was desired, 11x11 patch density was selected as the optimal patch density.

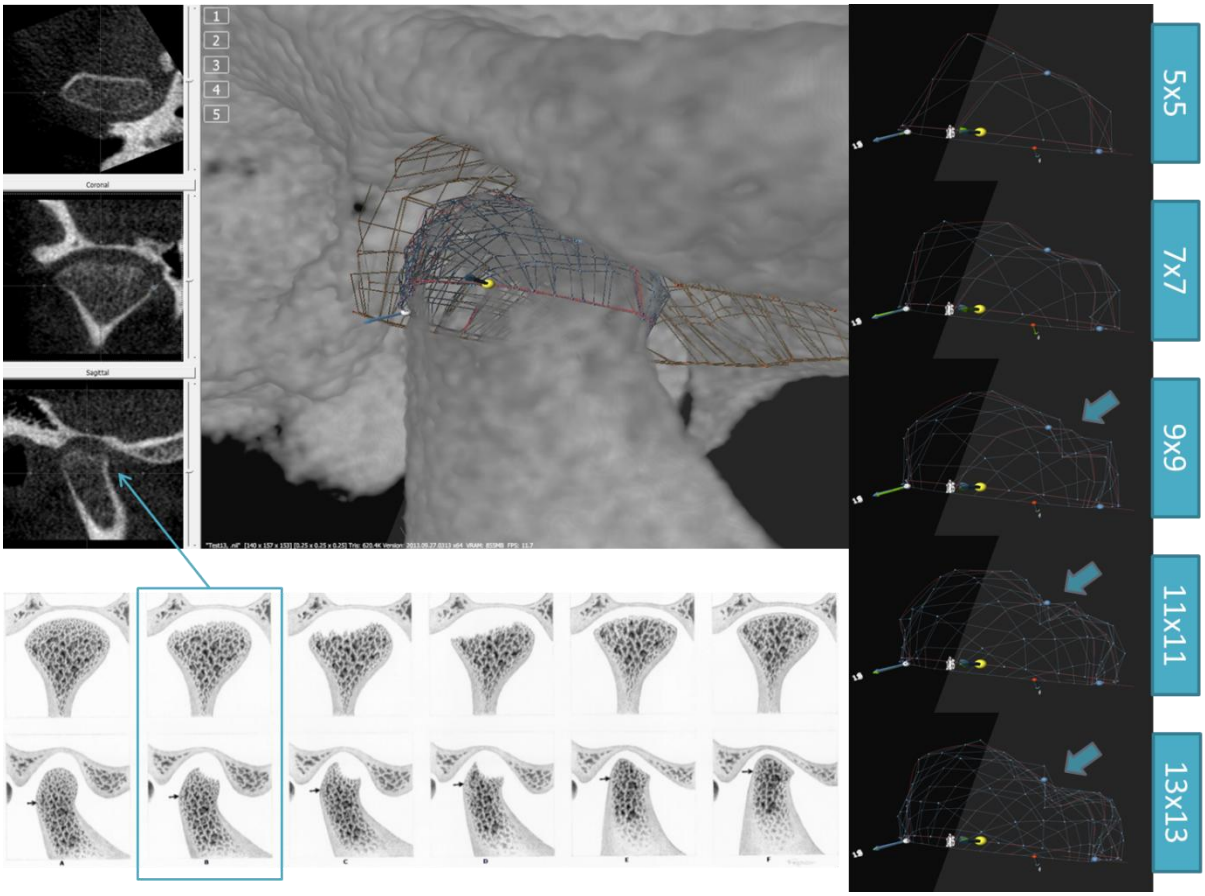


**Figure 57.** Example of a condyle outlined with patches of various densities. The defect caused by localized resorption was not captured at all by the lower density patches, but the lesion and its extent was most effectively captured by 11x11 patch density.

**Reliability**

The novel semi-automated three-dimensional TMJ space analysis demonstrated high intra-observer reliability for all of the 121 condylar landmarks, with average % error not

exceeding 5% (Table 3). Therefore, the landmark protocol using Stratovan Checkpoint software was determined to be a reliable method. The conventional two-dimensional analysis using the multiplanar view was also demonstrated high intra-observer reliability with correlation coefficient of 0.9875 or higher when comparing the measurements from the repeated trials (Table 4, Figure 40).

**TMJ Space Changes in Orthognathic Surgery Patients**

Due to the small sample size, the right and left TMJ data was combined for the two- and three-dimensional analyses. There were noticeable individual variations in the direction and pattern of joint space change from pre-operative (T1), to post-operative (T2), to follow-up (T3), which often averaged out the actual changes to non-significant levels overall. Furthermore, the corresponding joint space measurements from three-dimensional analysis were only an estimate and not directly comparable to those of the two-dimensional analysis since measuring protocol is different between the two analyses. For example, because the joint space is automatically measured between a condylar landmark and an opposing fossa landmark along a pre-determined path in the three-dimensional analysis, the distance may be slightly over-estimated in some cases (Figure 58). Nevertheless, for the majority of joint space data, the two- and three-dimensional analyses gave concurring results.

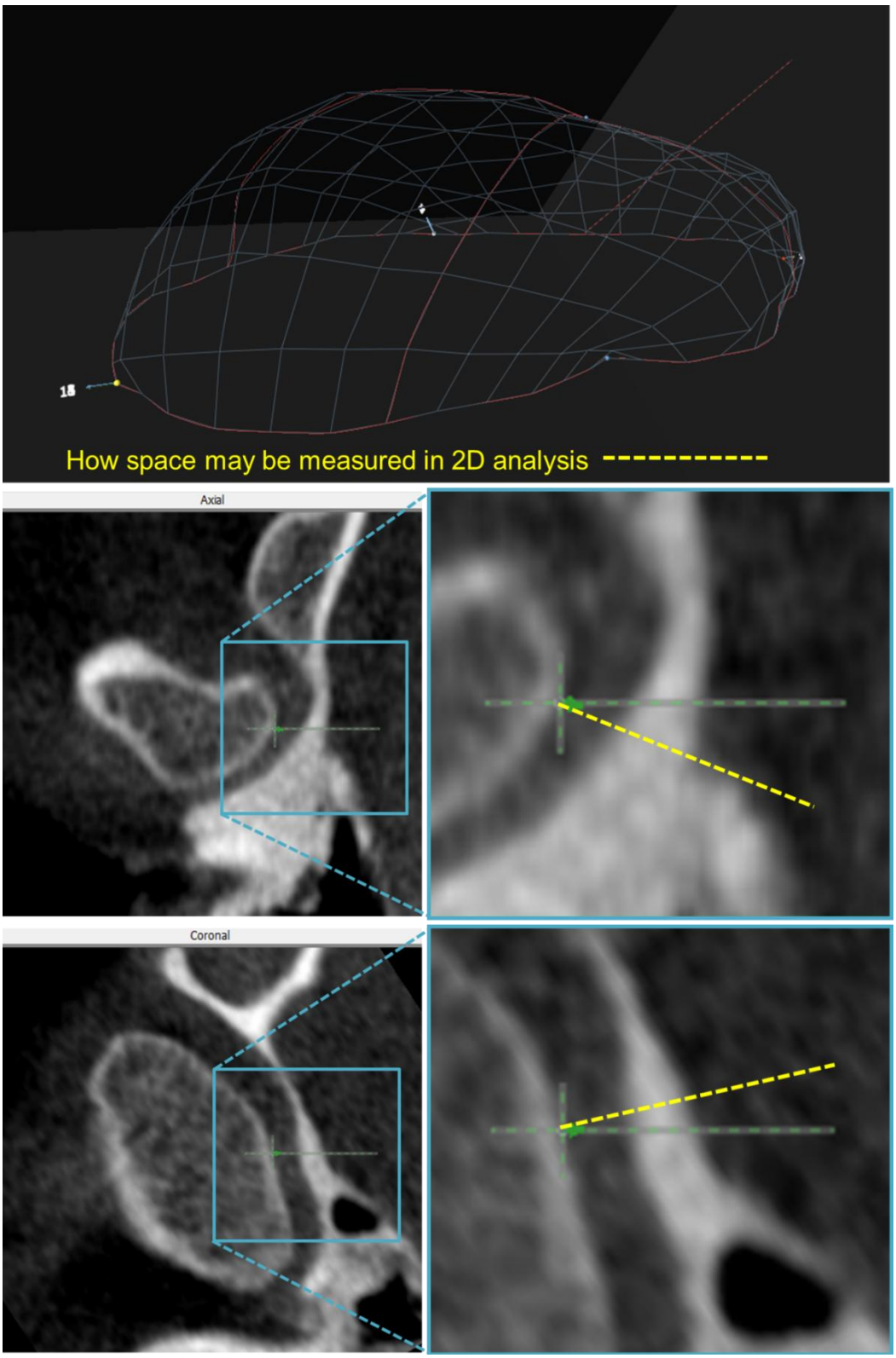


**Figure 58.** Difference between 2D and 3D joint space measurements. While 2D analysis often measures along a line tangent to the condylar surface (yellow), 3D analysis has a pre-determined path along which the measurement is taken.

Both analyses demonstrated a significant increase from T1 to T2 followed by a significant decrease from T2 to T3 in Anterior Space (Table 5, Figures 41-42). Slight increase in Posterior Space from T1 to T2 to T3 was not significant in either of the analysis (Table 7, Figures 45-46). Changes in Coronal Lateral Space over time were also not significant in either of the analysis (Table 8, Figures 47-48). For Coronal Central Space, however, both analyses shows significant increase from T1 to T2, a decrease from T2 to T3—which was significant only in 2D analysis, and a significantly larger space at T3 than T1 (Table 9, Figures 49-50). Both analyses demonstrated a significant increase in Coronal Medial Space from T1 to T2 and a non-significant decrease from T2 to T3 (Table 10, Figures 51-52). Similarly, both analyses showed a non-significant decrease in Axial Lateral Space from T1 to T2, followed by a non-significant increase from T2 to T3 (Table 11, Figures 53-54). For Axial Medial Space, both analyses displayed the same pattern of joint space change—increase from T1 to T2 and a decrease from T2 to T3—with the only difference being that the increase from T1 to T2 in three-dimensional analysis was significant, while others were not (Table 12, Figures 55-56).

The only joint space measurement that differed between two- and three-dimensional analyses was Superior Space (SS). In two-dimensional analysis, SS significantly increased from T1 to T3, but in three-dimensional analysis, SS significantly increased from T1 to T2 and significantly decreased from T2 to T3 (Table 6, Figures 43-44). This could be due to the fact

that the superior aspect of the condylar head has a steep curvature, particularly in the sagittal plane, so if the location of the condylar landmark on the three-dimensional analysis is even slightly different from that of the two-dimensional analysis—which would be the most superior point of the condyle—the space measurement difference could be large (Figure 59).

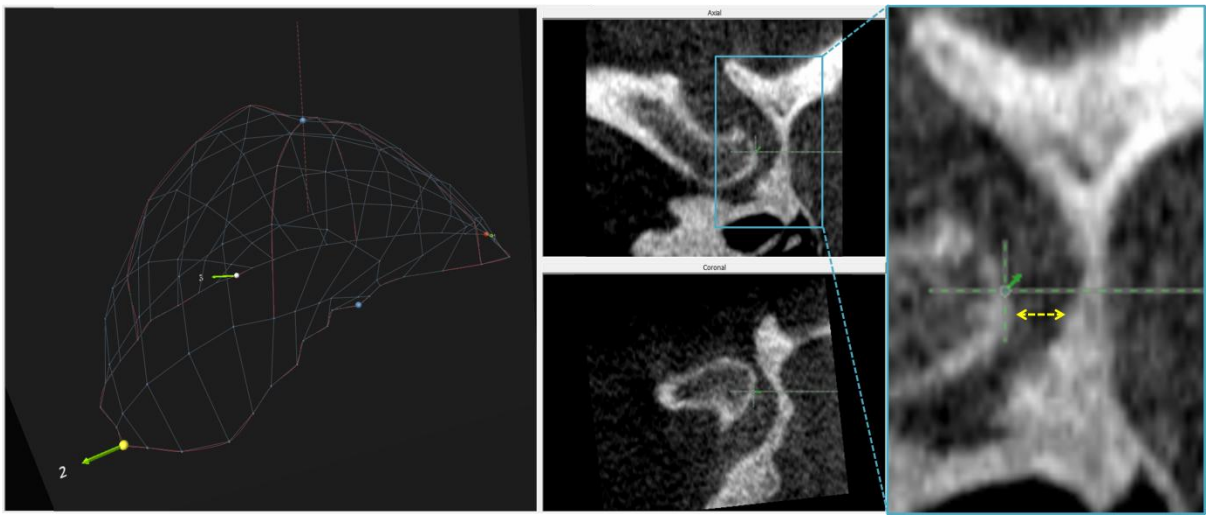


**Figure 59.** Possible reason for the difference between 2D and 3D SS values. In 2D analysis, SS is measured from the point of highest contour on condylar point (yellow), but the condyle landmark in 3D analysis is not guaranteed to be at the exact same location as in 2D, and due to the steep curvature near this area, small difference in the location of the condyle point can lead to a large difference in the space measurement as seen here.

In general, there seems to be an increase in the joint space immediately after surgery, which equates to the condyle being displaced out of the fossa, and a trend for a decrease in the joint space, which implies the return of the condylar position to certain extent. This was a common observation for many of the TMJ analyzed in this study, and such an example is shown

in Figure 60. Such positional change within the joint would clinically manifest itself as typical signs of relapse such as an anterior open bite and increased overjet.

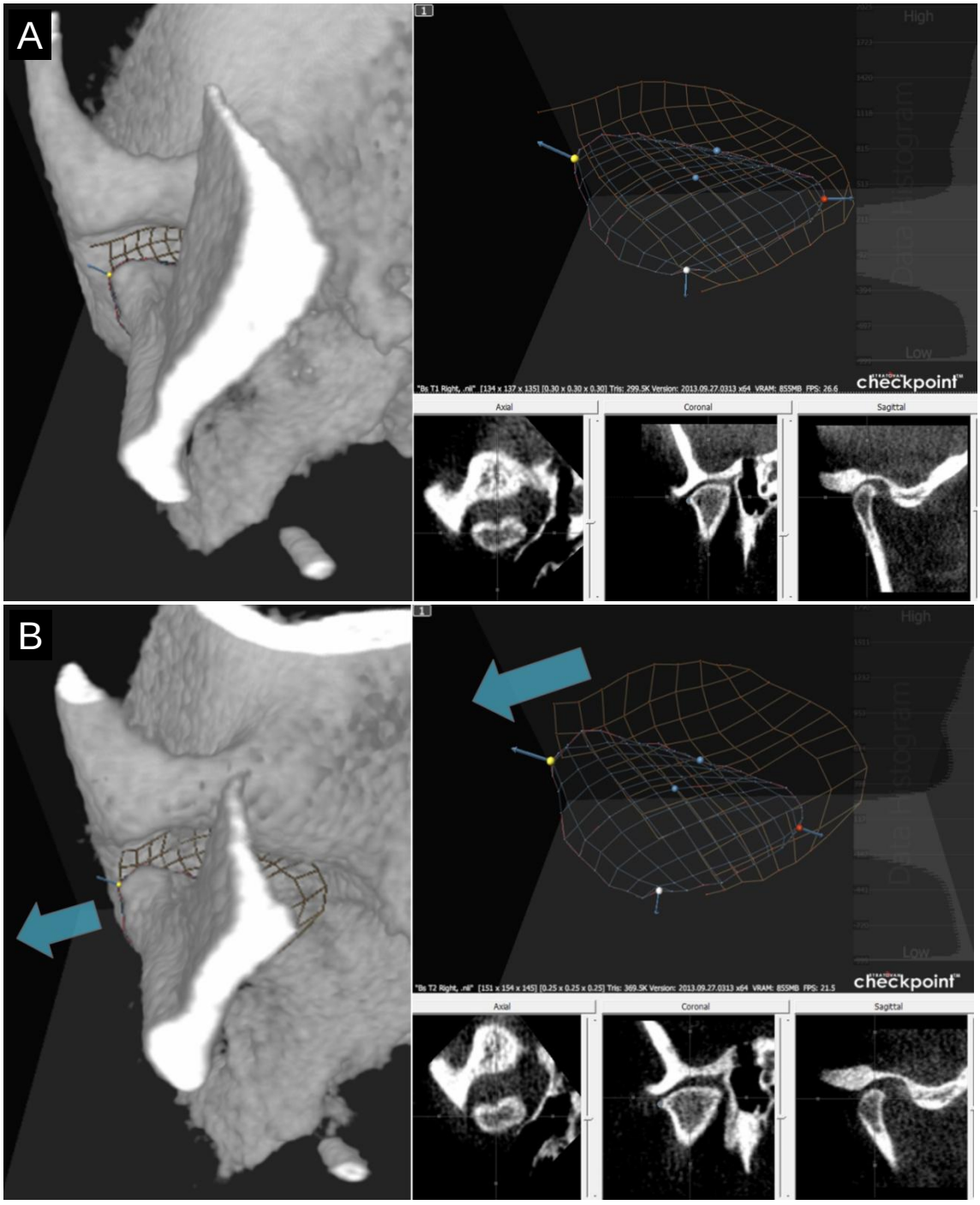


**Figure 60.** Example of the positional and morphological changes over time. (A) One of the sample TMJ at pre-operative. (B) Post-operative imaging showing laterally and posteriorly displaced condyle with increased joint space antero-medially.

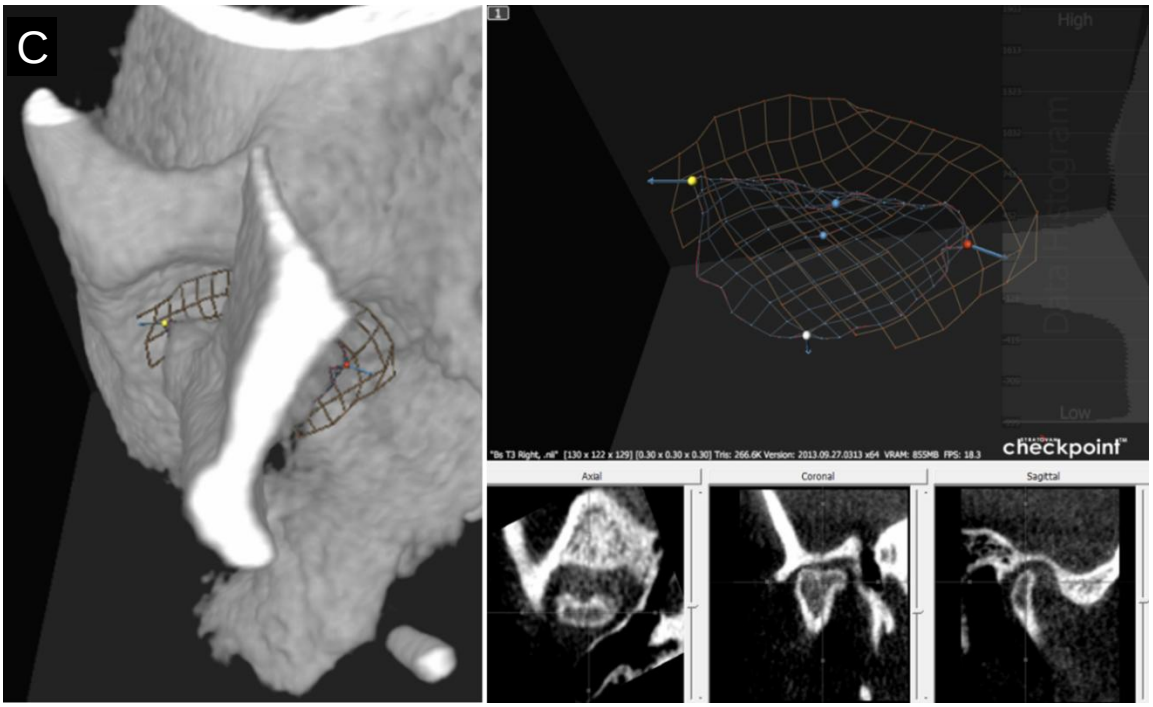


**Figure 60 cont'd.** Example of the positional and morphological changes over time. (C) The same TMJ at follow-up, showing slight return of the condylar position toward its original position, but also obvious morphological changes in the condyle.

In this TMJ, the condyle is visibly displaced laterally and posteriorly when comparing T1 to T2, and slightly returns to its original position from T2 to T3. The accompanying joint space change is detectable in both the two-dimensional analysis (using the multi-planar views at lower right) and the patches from the three-dimensional analysis. However, the three-dimensional analysis offers far more information relating to the joint space changes throughout the articular surfaces of the condyle and fossa and also the post-operative morphological and size changes in the joint, particularly in the condyle (Figure 60-C).

The present study showed that for the majority of the joint spaces, the T1 (pre-operative) and T3 (follow-up) values were not significantly different. Therefore, if there were significant changes in size and shape of the condyles with maintenance of the joint spaces between the pre-surgical and long-term follow-up time points, additional change in mandibular posture and occlusion would be expected.

Joint space dimensions over time are influenced by the shape, size, and spatial relationships of the osseous TMJ components. However, longitudinal analyses limited to the joint space dimensions cannot identify, rule out, or quantify the temporal changes in the size or shape of the TMJ osseous components. The novel three-dimensional analysis of the TMJ space provides the data necessary to evaluate such changes in the size and shape of the TMJ, and future studies on morphological changes in the condyles using the three-dimensional data may present additional benefit of using the three-dimensional analysis.

## CONCLUSIONS

None of the four hypotheses could be rejected. The novel semi-automatic method for three-dimensional evaluation of the TMJ space using CBCT data presented in this thesis is a reliable tool for the three-dimensional analysis of the TMJ space. When compared with the conventional two-dimensional analysis, which also demonstrated high reliability, both analyses were able to evaluate the longitudinal joint space changes after orthognathic surgery and gave concurring results for majority of the joint space measurements. Although not statistically evaluated in this study, the landmark coordinates of the three-dimensional analysis offers additional morphological information that may be clinically valuable.

## REFERENCES

Abdi, H., and Williams, L. J. (2010). Principal component analysis. Wiley Interdiscip Rev Comput Stat *2*, 433-459.

Adams, D. C., Rohlf, F. J., and Slice, D. E. (2004). Geometric morphometrics: ten years of progress following the 'revolution.' Ital J Zool *71*, 5-16.

Alder, M. E., Deahl, S. T., Matteson, S. R., Van Sickels, J.E., Tiner, B. D., and Rugh, J. D. (1999). Short-term changes of condylar position after sagittal split osteotomy for mandibular advancement. Oral Surg Oral Med Oral Pathol Oral Radiol Endod *87*, 159-165.

Angle, A. D., Rebellato, J., and Sheats, R. D. (2007). Transverse displacement of the proximal segment after bilateral sagittal split osteotomy advancement and its effect on relapse. J Oral Maxillofac Surg *65*, 50-59.

Arnett, G. W. (1993). A redefinition of bilateral sagittal osteotomy (BSO) advancement relapse. Am J Orthod Dentofacial Orthop *104*, 506-515.

Athanasiou, A. E. and Mavreas, D. (1991). Tomographic assessment of alterations of the temporomandibular joint after surgical correction of mandibular prognathism. Int J Adult Orthodon Orthognath Surg *6*, 105-112.

Aziz, S. R. (2004). Simon P. Hullihen and the origin of orthognathic surgery. J Oral Maxillofac Surg *62*, 1303-1307.

Baek, S. H., Kim, T. K., and Kim, M. J. (2006). Is there any difference in the condylar position and angulation after asymmetric mandibular setback? Oral Surg Oral Med Oral Pathol Oral Radiol Endod *101*, 155-163.

Barghan, S., Tetradis, S., and Mallya, S. (2012). Application of cone beam computed tomography for assessment of the temporomandibular joints. Aust Dent J *57*, 109-118.

Borstlap, W. A., Stoelinga, P. J., Hoppenreijs, T. J., and van't Hof, M. A. (2004). Stabilisation of sagittal split advancement osteotomies with miniplates: a prospective, multicentre study with two-year follow-up. Part III—condylar remodelling and resorption. Int J Oral Maxillofac Surg *33*, 649-655.

Chen, S., Lei, J., Wang, X., Fu, K. Y., Farzad, P., and Yi, B. (2013). 2013 Short- and long-term changes of condylar position after bilateral sagittal split ramus osteotomy for mandibular advancement in combination with Le Fort I osteotomy evaluated by CBCT. J Oral Maxillofac Surg *71*, 1956-1966.

Cortez, A. L. and Passeri, L. A. (2007). Radiographic assessment of the condylar position after Le Fort I osteotomy in patients with asymptomatic temporomandibular joints: a prospective study. J Oral Maxillofac Surg *65*, 237-241.

Cutbirth, M., Van Sickels, J. E., and Thrash, W. J. (1998) Condylar resorption after bicortical screw fixation of mandibular advancement. J Oral Maxillofax Surg *56*, 178-182.

Eggensperger, N., Smolka, K., Luder, .J, and Iizuka, T. (2006). Short- and long-term skeletal relapse after mandibular advancement surgery. Int J Oral Maxillofac Surg *35*, 36-42.

Ellis, E. and Hinton, R. J. (1991) Histologic examination of the temporomandibular joint after mandibular advancement with and without rigid fixation: an experimental investigation in adult Macaca mulatta. J Oral Maxillofax Surg *49*, 1316-1327.

Ghang, M. H., Kim, H. M., You, J. Y., Kim, B. H., Choi, J. P., Kim, S. H., and Choung, P. H. (2012). Three-dimensional mandibular change after sagittal split ramus osteotomy with a semirigid sliding plate system for fixation of a mandibular setback surgery. Oral Surg Oral Med Oral Pathol Oral Radiol *115*, 157-166.

Harris, M. D., Van Sickels, J. E., and Alder, M. (1999). Factors influencing condylar position after the bilateral sagittal split osteotomy fixed with bicortical screws. J Oral Maxillofax Surg *57*, 650-654.

Honda, K., Larheim, T. A., Johannessen, S., Arai, Y., Shinoda, K., and Westesson, P. L. (2001). Ortho cubic super-high resolution computed tomography: a new radiographic technique with application to the temporomandibular joint. Oral Surg Oral Med Oral Pathol Oral Radiol Endod *91*, 239-243.

Honey, O. B., Scarfe, W. C., Hilgers, M. J., Klueber, K., Silveira, A. M., Haskell, B. S., and Farman, A. G. (2007). Accuracy of cone-beam computed tomography imaging of the temporomandibular joint: comparisons with panoramic radiology and linear tomography. Am J Orthod Dentofacial Orthop *132*, 429-438.

Hoppenreijs, T. J., Freihofer, H. P., Stoelinga, P. J., Tuinzing, D. B., and van't Hof, M. A. (1998). Condylar remodelling and resorption after Le Fort I and bimaxillary osteotomies in patients with anterior open bite. A clinical and radiological study. Int J Oral Maxillofac Surg *27*, 81-91.

Hoppenreijs, T. J., Stoelinga, P. J., Grace, K. L., and Robben, C. M. (1999). Long-term evaluation of patients with progressive condylar resorption following orthognathic surgery. Int J Oral Maxillofac Surg *28*, 411-418.

Huang, Y. L., Pogrel, M. A., and Kaban, L. B. (1997). Diagnosis and management of condylar resorption. J Oral Maxillofax Surg *55*, 114-119.

Hussain, A. M., Packota, G., Major, P. W., and Flores-Mir, C. (2008). Role of different imaging modalities in assessment of temporomandibular joint erosions and osteophytes: a systematic review. Dentomaxillofac Radiol *37*, 63-71.

Hwang, S. J., Haers, P. E., Zimmermann, A, Oechslin, C., Seifert, B., and Sailer, H. F. (2000). Surgical risk factors for condylar resorption after orthognathic surgery. Oral Surg Oral Med Oral Pathol Oral Radiol Endod *89*, 542-552.

Ikeda, K. and Kawamura, A. (2009). Assessment of optimal condylar position with limited cone-beam computed tomography. Am J Orthod Dentofacial Orthop, *135*, 495-501.

Ikeda, K., Kawamura, A., and Ikeda, R. (2011). Assessment of optimal condylar position in the coronal and axial planes with limited cone-beam computed tomography. J Prosthodont *20*, 432-438.

Joss, C. U. and Vassalli, I. M. (2009). Stability after bilateral sagittal split osteotomy advancement surgery with rigid internal fixation: a systematic review. J Oral Maxillofax Surg *67*, 301-313.

Kawamata, A., Fujishita, M., Nagahara, K., Kanematu, N., Niwa, K., and Langlais, R. P. (1998). Three-dimensional computed tomography evaluation of postsurgical condylar displacement after mandibular osteotomy. Oral Surg Oral Med Oral Pathol Oral Radiol Endod *85*, 371-376.

Kim, Y. I., Jung, Y. H., Cho, B. H., Kim, J. R., Kim, S. S., Son, W. S., and Park, S. B. (2010) The assessment of the short- and long-term changes in the condylar position following sagittal split ramus osteotomy (SSRO) with rigid fixation. J Oral Rehabil *37*, 262-270.

Kim, Y. I., Cho, B. H., Jung, Y. H., Son, W. S., and Park, S. B. (2011). Cone-beam computerized tomography evaluation of condylar changes and stability following two-jaw surgery: Le Fort I osteotomy and mandibular setback surgery with rigid fixation. Oral Surg Oral Med Oral Pathol Oral Radiol Endod *111*, 681-687.

Kim, Y. J., Oh, K. M., Hong, J. S., Lee, J. H., Kim, H. M., Reyes, M., Cevidanes, L. H., and Park, S. B., Yang, Y. M., Kim, Y. I., Cho, B. H., Jung, Y. H., and Hwang, D. S. (2012). Effect of bimaxillary surgery on adaptive condylar head remodeling: metric analysis and image interpretation using cone-beam computed tomography volume superimposition. J Oral Maxillofac Surg *70*, 1951-1959.

Klingenberg, C. P. (2011). MorphoJ: an integrated software package for geometric morphometrics. Mol Ecol Resour *11*, 353-357.

Kobayashi, T., Izumi, N., Kojima, T., Sakagami, N., Saito, I., and Saito, C. (2013). Progressive condylar resorption after mandibular advancement. Br J Oral Maxillofac Surg *50*, 176-180.

Lee, W. and Park, J. U. (2002) Three-dimensional evaluation of positional change of the condyle after mandibular setback by means of bilateral sagittal split ramus osteotomy. Oral Surg Oral Med Oral Pathol Oral Radiol Endod *94*, 305-309.

Marmulla, R. and Mühling, J. (2007). Computer-assisted condyle positioning in orthognathic surgery. J Oral Maxillofac Surg *65*, 1963-1968.

Mitteroecker, P. and Gunz, P. (2009). Advances in geometric morphometrics. Evol Biol *36*, 235-247.

Park, Y. H. (2012). Do patients treated with bimaxillary surgery have more stable condylar positions than those who have undergone single-jaw surgery? J Oral Maxillofac Surg *70*, 2143-2152.

Reyneke, J. P. and Ferretti, C. (2002). Intraoperative diagnosis of condylar sag after bilateral sagittal split ramus osteotomy. Br J Oral Maxillofac Surg *40*, 285-292.

Schulze, D., Heiland, M., Thurmann, H., and Adam, G. (2004). Radiation exposure during midfacial imaging using 4- and 16-slice computed tomography, cone beam computed tomography systems and conventional radiography. Dentomaxillofac Radiol *33*, 83-86.

Steinhäuser, E. W. (1996). Historical development of orthognathic surgery. J Craniomaxillofac Surg *24*, 195-204.

Stroster, T. G. and Pangrazio-Kulbersh, V. (1994). Assessment of condylar position following bilateral sagittal split ramus osteotomy with wire fixation or rigid fixation. Int J Adult Orthodon Orthognath Surg *9*, 55-63.

Terhune, C. (2013). How effective are geometric morphometric techniques for assessing functional shape variation? An example from the great ape temporomandibular joint. Anat Rec *296*, 1264-1282.

Tsiklakis, K., Syriopoulos, K., and Stamatakis, H. C. (2004). Radiographic examination of the temporomandibular joint using cone beam computed tomography. Dentomaxillofac Radiol *33*, 196-201.

Ueki, K., Marukawa, K., Shimada, M., Nakagawa, K., and Yamamoto, E. (2005). Change in condylar long axis and skeletal stability following sagittal split ramus osteotomy and intraoral vertical ramus osteotomy for mandibular prognathia. J Oral Maxillofax Surg *63*, 1494-1499.

Ueki, K., Marukawa, K., Shimada, M., Hashiba, Y., Nakagawa, K., and Yamamoto, E. (2007). Condylar and disc positions after sagittal split ramus osteotomy with and without Le Fort I osteotomy. Oral Surg Oral Med Oral Pathol Oral Radiol Endod *103*, 342-348.

Ueki, K., Moroi, A., Sotobori, M., Ishihara, Y., Marukawa, K., Yoshizawa, K., Kato, K., and Kawashiri, S. (2012). Changes in temporomandibular joint and ramus after sagittal split ramus osteotomy in mandibular prognathism patients with and without asymmetry. J Craniomaxillofac Surg *40*, 821-827.

Van Sickels, J. E., Tiner, B. D., Keeling, S. D., Clark, G. M., Bays, R., and Rugh, J. (1999). Condylar position with rigid fixation versus wire osteosynthesis of a sagittal split advancement. J Oral Maxillofac Surg *57*, 31-34.

You, M. S., Yang, H. J., and Hwang, S. J. (2011). Postoperative functional remodeling of preoperative idiopathic condylar resorption: a case report. J Oral Maxillofac Surg *69*, 1056-1063.

Zain-Alabdeen, E. H. and Alsadhan, R. I. (2012). A comparative study of accuracy of detection of surface osseous changes in the temporomandibular joint using multidetector CT and cone beam CT. Dentomaxillofac Radiol *41*, 185-191.

Zhang, Z. L., Cheng, J. G., Li, G., Zhang, J. Z., Zhang, Z. Y., and Ma, X. C. (2012). Measurement accuracy of temporomandibular joint space in Promax 3-dimensional cone-beam computerized tomography images. Oral Surg Oral Med Oral Pathol Oral Radiol *114*, 112-117.

**Publishing Agreement**

It is the policy of the University to encourage the distribution of all theses, dissertations, and manuscripts. Copies of all UCSF theses, dissertations, and manuscripts will be routed to the library via the Graduate Division. The library will make all theses, dissertations, and manuscripts accessible to the public and will preserve these to the best of their abilities, in perpetuity.

I hereby grant permission to the Graduate Division of the University of California, San Francisco to release copies of my thesis, dissertation, or manuscript to the Campus Library to provide access and preservation, in whole or in part, in perpetuity.

Author Signature 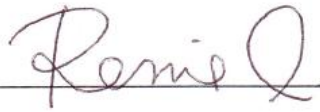 Date 6/11/2014